

SURFACE TREATMENT OF STEEL WITH ION BEAM
IMPLANTATION USING PLASMA FOCUS

TEH THIAM OUN

FACULTY OF ENGINEERING AND QUANTITY SURVEYING
INTI INTERNATIONAL UNIVERSITY

2019

SURFACE TREATMENT OF STEEL WITH ION BEAM
IMPLANTATION USING PLASMA FOCUS

By

TEH THIAM OUN

Being a thesis submitted to
INTI International University
in candidature for the degree of
Doctor of Philosophy (Applied Physics)

FACULTY OF ENGINEERING AND QUANTITY SURVEYING
INTI INTERNATIONAL UNIVERSITY

2019

POSTGRADUATE PROGRAMME
CERTIFICATION OF DOCTORAL THESIS

Author's Full Name : Teh Thiam Oun

Student's Registration No: I15009501

Thesis Title : Surface treatment of steel with ion beam implantation using plasma focus

Academic Session :

With regard to Clause 4.2 of the INTI Student Intellectual Property Policy (Supplementary), the thesis is the student's property. Thereby declare this thesis as:

CONFIDENTIAL

Consisting of classified information under the OFFICIAL SECRETS ACT 1972.

RESTRICTED

Consisting of RESTRICTED information which has been determined by the organisation/body where the research was conducted.

OPEN ACCESS/NON-RESTRICTED

I allow this thesis to be published through open access, full text or copied for study, learning and research purposes only.

For the Open Access/Non-Restricted category, I allow this (Master's/Doctoral) thesis to be kept in the INTI International University (INTI) Library with the following usage conditions:

1. INTI Library has the right to reproduce the thesis for study, learning and research purposes only.
2. INTI Library is allowed to make one (1) copy of this thesis for exchange purpose among higher education institutions and any government body/agency, subject to terms and conditions.

VERIFIED BY:

STUDENT SIGNATURE

SUPERVISOR'S
SIGNATURE

(IDENTITY CARD/PASSPORT
NO.)

Date :

SUPERVISOR'S NAME

Date:

COPYRIGHT

The copyright of this thesis belongs to the author under the terms of the Copyright Act 1987 as qualified by Section 4 of INTI International University Intellectual Property Policy. Due acknowledgement shall always be made of the use of any material contained in, or derived from, this thesis.

© Teh Thiam Oun, 2019

All rights reserved

DECLARATION

I hereby declare that the work has been done by myself and no portion of the work contained in this thesis has been submitted in support of any application for any other degree or qualification of this or any university or institute of learning.

Teh Thiam Oun

ACKNOWLEDGEMENT

I firstly wish to express my deepest gratitude and thanks to both my supervisors Associate Professor Dr Arwinder Singh and Professor Dr Jalil Ali for their gracious supervision and dedicated guidance throughout this PhD course. Without their helpful encouragement, I would have great difficulty in completing this thesis.

I am sincerely thankful to my mentors Professor Dr Lee Sing and Professor Dr Saw Sor Heoh who have provided me with many insights on the plasma focus concepts. Their invaluable advice and support has greatly contributed to my knowledge.

I am deeply indebted to my wife Eileen Chu Pek Yoke and my son Bryan Teh Cheng Wei for all their support and understanding.

I acknowledge research grants INT-CPR-01-02-2013 and FRGS/2/2013/SG02/INTI/01/1 in the research and preparation of this thesis.

DEDICATION

My effort as a researcher builds upon the work of others who have toiled before me and graciously shared their knowledge. This thesis is dedicated to all beings, who have in one way or another, contributed to the knowledge that I have so freely inherited.

ABSTRACT

Plasma nitriding by using a Mather-type plasma focus device is a technique that is not very well explored but it can be used to increase the surface hardness of low carbon steel and to enhance its wear resistance for application as a cutting and machining tool. A column of hot and dense plasma made out of nitrogen ions bombarded on the target surface creates a nitride layer by embedding nitrogen ions on the target surface. It results in modified surface hardness and structure.

In this thesis, a study on the nitriding effects of a 3 kJ Mather-type dense plasma focus (DPF) device in a low-pressure nitrogen atmosphere is carried out using the INTI International University plasma focus machine. Experiments were repeated multiple times by keeping nitrogen gas pressure constant at 0.5, 1, 1.5 and 2 Torr and placing properly cut and polished low carbon steel samples at fixed distances of 40, 60, 80, 100 and 120 mm from anode. It was found that if the INTI International University plasma focus machine is to be used for material hardening, the best results will be obtained at 1 Torr with the target placed at a distance of 40 mm from the anode. It correlates with the prediction made by Lee Model Code which predicts the production of highest energy beam at Nitrogen pressure of 1 Torr in numerical experiments of an earlier study by A. Singh [62]. The central region where the ion beam was concentrated was the region where the hardness was most noticeably improved.

The dense plasma focus device delivered a surface texture of overlapping dimples on the surface of the target. This surface texture can be employed as a base for the application of lubricant in the making of a textured cutting tool for the purpose of dry machining. One of the hardened (nitrided) sample was tested on an aluminium work piece. Cutting was easy and there was no visual indication of aluminium sticking to the rake face of the tool which are prominent indicators of improved hardness and effectiveness of surface patterns produced by DPF during the nitriding process.

Results from our experiments conclude that the DPF machine can be utilized for localized surface nitriding with an additional advantage of surface patterning. The best hardening can be achieved at nitrogen gas pressure of 1 Torr when the sample is placed at 40mm from the anode. Such a hardened steel has great potential as an efficient cutting and machining tool.

TABLE OF CONTENTS

| | |
|-------------------------------------|------|
| Title page | i |
| Certification of Doctoral Thesis | ii |
| Copyright | iii |
| Declaration | iv |
| Acknowledgement | v |
| Dedication | vi |
| Abstract | vii |
| TABLE OF CONTENTS | viii |
| LIST OF FIGURES | xi |
| LIST OF TABLES | xiv |
| LIST OF ABBREVIATIONS | xv |
| NOMENCLATURE | xvi |
| | |
| CHAPTER 1 INTRODUCTION | 1 |
| 1.1 Background | 1 |
| 1.2 Problem Statement | 2 |
| 1.3 Objectives of the Research | 3 |
| 1.4 Scope of the Research | 3 |
| 1.5 Thesis Organization | 4 |
| | |
| CHAPTER 2 LITERATURE REVIEW | 5 |
| 2.1 Nitriding Technology | 5 |
| 2.1.1 Gas Nitriding | 5 |
| 2.1.2 Salt Bath Nitriding | 6 |
| 2.1.3 Glow Nitriding | 6 |
| 2.1.4 Dense plasma focus nitriding | 8 |
| 2.2 Surface texturing | 8 |
| 2.3 Dense Plasma Focus | 10 |
| 2.3.1 Definition of plasma | 10 |
| 2.3.2 The Dense Plasma Focus Device | 12 |
| 2.3.3 Lee Model Code | 14 |

| | | |
|-----------|--|----|
| CHAPTER 3 | METHODOLOGY | 16 |
| 3.1 | Introduction | 16 |
| 3.2 | Preparation of steel samples | 16 |
| 3.2.1 | Material Properties of AISI 1020 Low Carbon Steel | 17 |
| 3.2.2 | Cutting to size | 19 |
| 3.2.3 | Milling | 20 |
| 3.2.4 | Annealing | 21 |
| 3.2.5 | Polishing | 24 |
| 3.2.6 | Using Vickers Microhardness Testing | 27 |
| 3.2.7 | Vickers Hardness Test procedure | 29 |
| 3.3 | Plasma Nitriding with DPF | 30 |
| 3.4 | Ion beam analysis through the Lee Model Code | 34 |
| 3.4.1 | The 5 phases of the Lee Model | 34 |
| 3.4.2 | Computation of ion beam | 36 |
| 3.4.3 | Numerical Fitting of Lee Model Code | 41 |
| 3.4.4 | Use of Lee Code in this research | 42 |
| CHAPTER 4 | RESULTS AND DISCUSSION | 43 |
| 4.1 | Hardness of steel samples before nitriding | 43 |
| 4.2 | Appearance of steel samples after nitriding | 43 |
| 4.3 | Energy-dispersive X-Ray spectroscopy (EDX) of steel samples | 49 |
| 4.4 | Scanning Electron Microscopy (SEM) | 51 |
| 4.5 | Hardness variation graphical comparison | 52 |
| 4.6 | Hardness variation among samples of the same operating pressures | 62 |
| 4.7 | Hardness variation with both pressure and anode distance | 67 |
| 4.8 | Average hardness variation at central spot | 68 |
| 4.9 | Other observations | 69 |
| 4.10 | Application in machining aluminium | 71 |
| 4.11 | Ion Beam analysis using the Lee Model Code | 74 |
| CHAPTER 5 | CONCLUSIONS AND FUTURE WORK | 77 |

| | | |
|------|---|-----|
| 5.1 | Conclusions | 77 |
| 5.2 | Recommendations | 78 |
| 5.3. | Future work | 79 |
| | REFERENCES | 80 |
| | LIST OF PUBLICATIONS | 90 |
| | APPENDIX A: SURFACE HARDNESS READINGS | 92 |
| | APPENDIX B: STANDARD OPERATING PROCEDURES FOR DPF | 133 |
| B.1 | Standard Operating Procedure prior to firing | 133 |
| B.2 | Standard Operating Procedure for firing | 133 |
| B.3 | Standard Operating Procedure for waveform capture | 134 |

LIST OF FIGURES

| | | |
|-------------|---|----|
| Figure 2.1 | Absorption of N ₂ by Steel | 6 |
| Figure 2.2 | Glow nitriding process | 7 |
| Figure 2.3 | Types of surface texture. | 9 |
| Figure 2.4 | The structure of the DPF device | 12 |
| Figure 2.5 | Operation Stages of the DPF device | 13 |
| Figure 2.6 | Lee Model Code waveform | 15 |
| Figure 3.1 | Flow Chart of methodology | 16 |
| Figure 3.2 | Flow Chart for preparation of Test Samples | 17 |
| Figure 3.3 | The iron-carbon phase diagram | 18 |
| Figure 3.4 | Cutting off the steel samples from bar stock by a horizontal band saw | 20 |
| Figure 3.5 | Milling process for steel samples | 21 |
| Figure 3.6 | Heating Temperature versus Time | 22 |
| Figure 3.7 | Annealing Oven | 23 |
| Figure 3.8 | Duration for Heating | 23 |
| Figure 3.9 | Annealing Temperature | 24 |
| Figure 3.10 | Time setting to maintain constant annealing temperature | 24 |
| Figure 3.11 | Steel surface before polishing | 25 |
| Figure 3.12 | Polishing process | 25 |
| Figure 3.13 | Steel surface after the first polishing | 26 |
| Figure 3.14 | Steel surface with improved finish | 27 |
| Figure 3.15 | Indenter and Diagonal Lengths in Vickers Hardness Test | 28 |
| Figure 3.16 | Zero position located visually for Vickers Hardness Measurement | 29 |
| Figure 3.17 | 3 kJ Mather Type Dense Plasma Focus Device | 30 |
| Figure 3.18 | Arrangement of Anode and Cathode in DPF Device | 31 |
| Figure 3.19 | Substrate Holder in Dense Plasma Focus Device | 31 |
| Figure 3.20 | Rate of change of current waveform (top yellow trace) dI/dt and voltage waveform(bottom green trace) V at 1.0 Torr | 32 |
| Figure 3.21 | No pinch at 4.0 Torr | 33 |
| Figure 3.22 | The 5-point Fitting of Computed Current Trace to Measured (reference) Current Trace | 42 |

| | | |
|-------------|---|----|
| Figure 4.1 | Rings around the centre spot with an example from Sample 20 | 48 |
| Figure 4.2 | Samples arranged according to pressure and distance above anode for convenient visual comparison | 49 |
| Figure 4.3 | EDX spectroscopy of the steel before undergoing nitriding. | 50 |
| Figure 4.4 | EDX spectroscopy of the steel after nitriding showing the presence of nitrogen (after 30 shots, 1 Torr, 40 mm anode distance) | 50 |
| Figure 4.5 | Nitrided white layer with 10 shots | 51 |
| Figure 4.6 | Increased nitrided white layer with 30 shots | 52 |
| Figure 4.7 | Sample 1 before and after nitriding | 53 |
| Figure 4.8 | Sample 2 before and after nitriding | 53 |
| Figure 4.9 | Sample 3 before and after nitriding | 54 |
| Figure 4.10 | Sample 4 before and after nitriding | 54 |
| Figure 4.11 | Sample 5 before and after nitriding | 55 |
| Figure 4.12 | Sample 6 before and after nitriding | 55 |
| Figure 4.13 | Sample 7 before and after nitriding | 56 |
| Figure 4.14 | Sample 8 before and after nitriding | 56 |
| Figure 4.15 | Sample 9 before and after nitriding | 57 |
| Figure 4.16 | Sample 10 before and after nitriding | 57 |
| Figure 4.17 | Sample 11 before and after nitriding | 58 |
| Figure 4.18 | Sample 12 before and after nitriding | 58 |
| Figure 4.19 | Sample 13 before and after nitriding | 59 |
| Figure 4.20 | Sample 14 before and after nitriding | 59 |
| Figure 4.21 | Sample 15 before and after nitriding | 60 |
| Figure 4.22 | Sample 16 before and after nitriding | 60 |
| Figure 4.23 | Sample 17 before and after nitriding | 61 |
| Figure 4.24 | Sample 18 before and after nitriding | 61 |
| Figure 4.25 | Sample 19 before and after nitriding | 62 |
| Figure 4.26 | Sample 20 before and after nitriding | 62 |
| Figure 4.27 | Comparison of hardness profile with irradiation distance at pressure 0.5 Torr | 63 |
| Figure 4.28 | Comparison of hardness profile with irradiation distance at pressure 1.0 Torr | 64 |

| | | |
|-------------|--|----|
| Figure 4.29 | Comparison of hardness profile with irradiation distance at pressure 1.5 Torr | 65 |
| Figure 4.30 | Comparison of hardness profile with irradiation distance at pressure 2.0 Torr | 66 |
| Figure 4.31 | Variation of hardness with pressure and anode distance | 68 |
| Figure 4.32 | Average hardness at the central spot | 69 |
| Figure 4.33 | Textured cutting tool shape | 72 |
| Figure 4.34 | Nitrided test sample used as cutting tool | 72 |
| Figure 4.35 | Tool fixed in the tool holder and ready for cutting | 73 |
| Figure 4.36 | Cutting in progress | 73 |
| Figure 4.37 | Turned aluminium workpiece | 74 |
| Figure 4.38 | Number of ions vs pressure. | 75 |
| Figure 4.39 | Beam energy vs pressure. | 76 |

LIST OF TABLES

| | | |
|------------|--|-----|
| Table 1 | Detailed Various Stages of Plasma Focusing | 13 |
| Table 2 | Parameters Used in Lee Model Code | 14 |
| Table 3.1 | Composition of AISI 1020 Steel | 18 |
| Table 3.2 | Parameters for fitting | 41 |
| Table 4.1 | The Appearance of the nitrided steel samples | 44 |
| Table A.1 | Hardness readings for Sample 1 | 93 |
| Table A.2 | Hardness readings for Sample 2 | 95 |
| Table A.3 | Hardness readings for Sample 3 | 97 |
| Table A.4 | Hardness readings for Sample 4 | 99 |
| Table A.5 | Hardness readings for Sample 5 | 101 |
| Table A.6 | Hardness readings for Sample 6 | 103 |
| Table A.7 | Hardness readings for Sample 7 | 105 |
| Table A.8 | Hardness readings for Sample 8 | 107 |
| Table A.9 | Hardness readings for Sample 9 | 109 |
| Table A.10 | Hardness readings for Sample 10 | 111 |
| Table A.11 | Hardness readings for Sample 11 | 113 |
| Table A.12 | Hardness readings for Sample 12 | 115 |
| Table A.13 | Hardness readings for Sample 13 | 117 |
| Table A.14 | Hardness readings for Sample 14 | 119 |
| Table A.15 | Hardness readings for Sample 15 | 121 |
| Table A.16 | Hardness readings for Sample 16 | 123 |
| Table A.17 | Hardness readings for Sample 17 | 125 |
| Table A.18 | Hardness readings for Sample 18 | 127 |
| Table A.19 | Hardness readings for Sample 19 | 129 |
| Table A.20 | Hardness readings for Sample 20 | 131 |

LIST OF ABBREVIATIONS

| | |
|------|--------------------------------------|
| AISI | American Iron and Steel Institute |
| DPF | Dense Plasma Focus |
| SEM | Scanning Electron Microscopy |
| EDX | Energy-dispersive X-Ray spectroscopy |
| UV | Ultraviolet |

NOMENCLATURE

| <u>Symbol</u> | <u>Definition</u> |
|---------------|--|
| d_1 | first diagonal length of the mark of indentation |
| d_2 | second diagonal length of the mark of indentation perpendicular to d_1 |
| f_m | axial mass swept-up factor |
| f_c | axial current factor |
| f_{mr} | radial mass swept-up factor |
| f_{cr} | radial plasma current factor |
| HV | unit of measure for Vickers hardness testing |

CHAPTER 1

INTRODUCTION

1.1 Background

The dense plasma focus (DPF) device was developed by J.W. Mather and N.V. Filippov in the early 1960s. The device is an unconventional plasma device that is able to generate, accelerate and pinch plasma for the production of X-rays, neutrons, relativistic electrons and energetic ion beams [1]. Plasma focus can be utilized in surface modification through ion implantation.

In this research, the surface hardness of low carbon steel will be modified by a nitriding process using different pressures of nitrogen gas in a plasma focus device. Nitriding is a process used to harden steel. The act of nitriding deposits nitrides onto the steel surface which then displays a higher hardness than before.

Steel is a very common production material and is used in many applications where it is subjected to stress, such as in cutting tools or mechanical moving parts. This will cause the surface of the steel to undergo wear in such an environment. Thus, surface modification is required to improve hardness and wear resistance.

Many methods of surface modification have been around for centuries. The desire to make steel implements stronger and harder has led mankind to search for various methods to achieve this objective. One of the earliest methods involved the delivering of hammer blows onto steel, in a process known as peening, until the steel surface becomes harder. Today the methods have become much more varied and they include nitriding, carburizing, boriding and various forms of heat treatment.

About a century ago, it was discovered that when steel was heated with ammonia, nitrogen atoms from the ammonia dissolve in the steel surface and formed a hard compound layer. This was the beginning of the gas nitriding surface treatment practice. Later methods to deliver the nitrogen to the steel surface would involve salt baths and glow discharge plasma methods.

The use of the plasma focus device to conduct nitriding is still in its infancy. In this study, a 3kJ Mather type plasma focus device operating with nitrogen gas in its chamber will be used to modify the surface of steel substrate. The surface hardness of the treated steel will then be determined by using the Micro Vickers hardness tester. There is a possibility that the use of the plasma focus device in nitriding may yield some benefit that is unavailable in other nitriding methods and this research attempts to explore such a possibility.

1.2 Problem Statement

Low carbon steel has a high demand in the manufacturing industry due to cost effectiveness, high strength, good formability and thermal conductivity. This steel is easy to manufacture and is therefore very much cheaper than the more exotic specialty steel alloys. Unlike a lot of other steel alloys, low carbon steel is readily available ex-stock in most hardware stores due to its relatively low cost.

Although available in plentiful supply, low carbon steel is not suitable for usage as a tool due to insufficient hardness. A method is needed to be found for it to be suitably hardened for a more robust usage.

Plasma nitriding by using a Mather-type plasma focus device is a technique that is not very well explored but it can be used to increase the surface hardness of low carbon steel. A column of hot and dense plasma made out of nitrogen ions bombarded on the surface of low carbon steel will deposit a thin layer of nitrides on the steel and improve its surface hardness. The nitrided layer is very much harder than the bulk material and occurs only at the material surface.

The performance of plasma nitriding is highly dependent on the nitrogen gas pressure, distance of substrate from anode and number of shots applied. It is hoped that with this study, the optimal conditions for nitriding with a plasma focus device can be found.

1.3 Objectives of the Research

This research focuses on the nitriding of low carbon steel, which is a novel idea because low carbon steel is difficult to nitride and cannot be effectively nitrided by gas and salt bath nitriding methods. The objectives of this research include the following:

- Determine the variation of surface hardness caused by different nitrogen pressure in the plasma focus device.
- Determine the optimal firing distance to achieve maximum hardness.
- Determine the hardness distribution on the substrate after surface modification by the plasma focus device.
- Determine if there is a characteristic of the ion beam that affects the surface hardness the most.

1.4 Scope of the Research

This research was conducted to study the increase in surface hardness of low carbon steel with 3kJ Mather-type plasma focus device only. The effect of different plasma focus devices may well differ from the results presented here as different devices will generate different ion beams of different intensities and therefore the optimal operating parameters for other devices may differ from the results presented here.

The method employed is limited to the altering of the surface hardness of low carbon steel through nitriding with nitrogen gas only without recourse to the use of other extra nitride forming elements apart from those already present in the base metal. This study is designed to focus on the surface hardness values and not the thickness of the nitrided layer before and after surface modification.

The parameters of gas pressure in the chamber and firing distances from the anode to the target are included in this research. Also included in this research is the study on the extent in surface area where hardness improvement occurs.

The comparison of actual surface hardness results with the results from the numerical experiments with the Lee Model Code is carried out to correlate the results from the actual hardness improvement with the ion beam analysis of numerical experiments.

1.5 Thesis Organization

Chapter 1 of this report is the background of the topic regarding the use of nitriding in industry. The problem statement, objectives and scope of research are discussed.

In Chapter 2, the review of literatures is summarized. The more popular methods of nitriding are discussed here. Some plasma theory and the application of the dense plasma focus device are included. The material under investigation, low carbon steel, is also mentioned. This chapter also discusses the use of the Lee Model Code for modelling the dense plasma focus device.

Chapter 3 is about the methodology to carry out experiment on plasma nitriding. The procedures for preparation of low carbon steel pieces are described. The procedures to carry out plasma nitriding are explained.

Chapter 4 contains the results obtained during the experiment as well as the discussion on the results. The results and data that have been obtained are analysed and then presented in the form of tables, graphs and figures to clearly show the main outcome of the experiment.

In Chapter 5, a conclusion for the important outcome of this thesis will be summarized. The conclusion is based on the objectives that are set in Chapter 1. The suggestions and recommendations for future directions of investigation are also proposed in this chapter.

CHAPTER 2

LITERATURE REVIEW

2.1 Nitriding Technology

The nitriding process is a surface hardening heat treatment process where nitrogen ions are diffused into the substrate surface to form nitrides in combination with different alloying elements of the substrate thus forming compound layers that have high wear resistance properties (Bernal [2]). Nitrogen is very soluble in steel. Steel can have several phases such as austenite, pearlite, martensite among others. The nitriding process of steel does not require a phase change from the steel being treated. Thus, for the steel undergoing nitriding, there is an improvement in desirable properties, such as wear resistance, but without any dimensional change, which is good from the point of view of dimensional integrity.

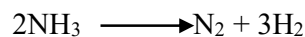
Nitriding of steel is usually practised in the industry to enhance the surface properties of steel surfaces. By employing nitriding, the properties of the nitrided steel will have the following properties:

- High surface hardness and wear strength.
- High resistance to tempering and high-temperature hardness.
- High fatigue strength and low fatigue notch sensitivity.
- Improved corrosion resistance for non-stainless steel.
- High dimensional stability compared to other heat treatment processes.

There are several methods for nitriding as explained in the following sections.

2.1.1 Gas Nitriding

Ammonia is fed into a closed chamber where the substrate to be nitrided is placed and heated to a temperature of about 510°C. The process time may vary according the application and the desired depth of the nitride layer. The ammonia dissociates according to the following chemical equation:



The dissociation of ammonia allows nitrogen to be present and thus can be absorbed by steel as shown in Figure 2.1.

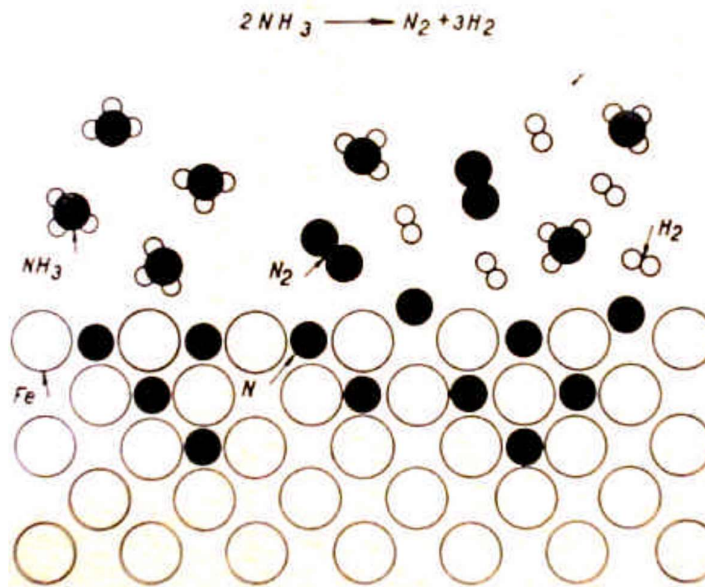


Figure 2.1 Absorption of N_2 by Steel. Source: Bernal [2]

2.1.2 Salt Bath Nitriding

Liquid nitriding (nitriding in a molten salt bath) employs the same temperature range as gas nitriding, that is, around 510 to 580 °C. The substrate to be treated is immersed into a molten, nitrogen-bearing, fused-salt bath containing either cyanides or cyanates. The principle of decomposition of the salt at elevated temperatures results in the liberation of nitrogen within the salt [2].



It is this nitrogen that will diffuse into the steel surface to form nitrides.

2.1.3 Glow Nitriding

Glow nitriding is also categorized as plasma nitriding. The process uses a plasma discharge of a gas due to exposure of electrical potential that enables the filling gas (nitrogen) to ionize and glow. The substrate is connected as the cathode and the furnace walls as the anode.

A voltage in the range of 500 to 1000 volts is applied between the metal part and the chamber wall, resulting in the formation of a plasma through which positive nitrogen ions are accelerated against the negative-biased part to be treated [3]. This ionic bombardment heats the piece to the treatment temperature, cleans the surface by

sputtering, and provides active nitrogen species for the nitriding process. This process must be carried out in a vacuum to increase the mean free path of the accelerated particles. The pressure used in glow nitriding is normally between 100 to 1000 Pa.

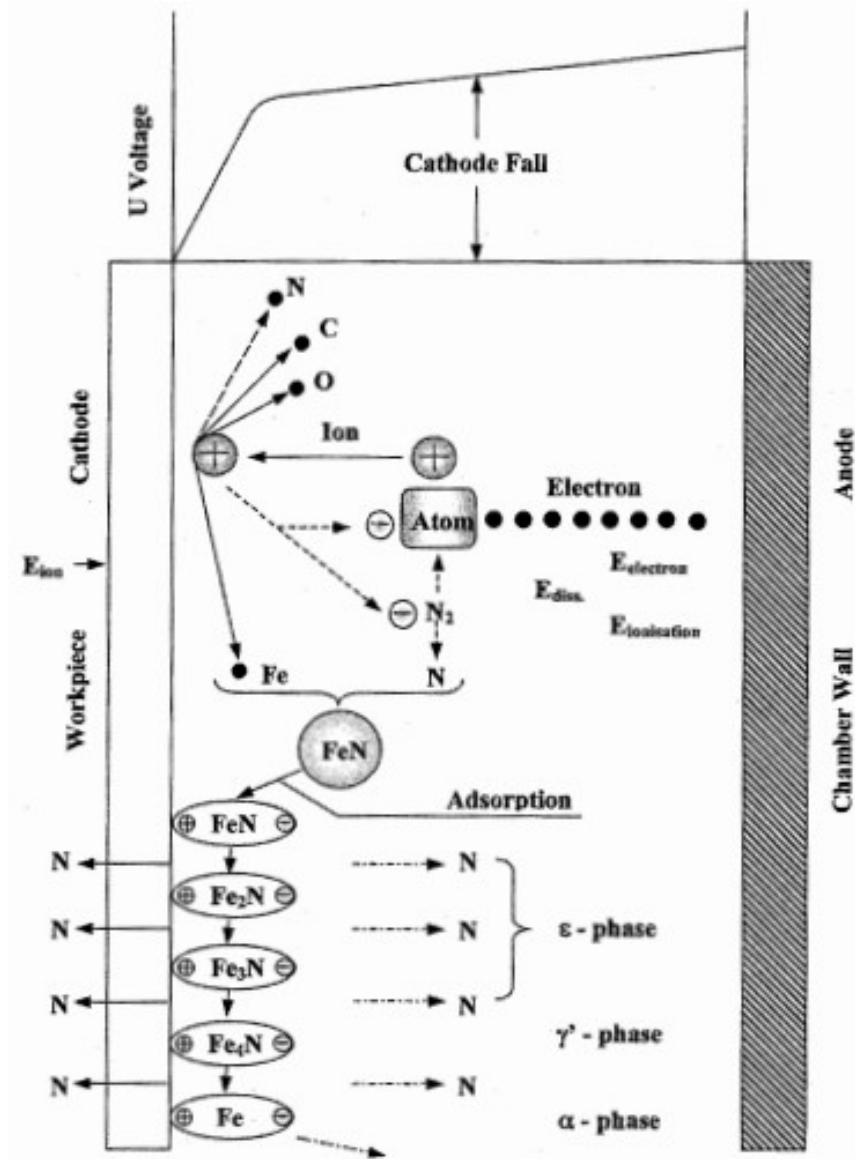


Figure 2.2 Glow nitriding process. Source: Totten & Liang, 2004 [4]

Glow nitriding uses the principle of ions sputtering to achieve successful plasma nitriding. The excited nitrogen will react with the sputtered iron atoms to form iron nitride (FeN) and cause deposition of a thin layer film on the surface of substrate.

The FeN phase may decompose into Fe₂N, Fe₃N and Fe₄N phase due to the bombardment of energetic ion (see Fig 2.2).

This method of nitriding is very common although it does have some shortfall with components with complex geometries and parts with holes.

2.1.4 Dense plasma focus nitriding

The use of the dense plasma focus device for nitriding operations has been largely unexplored. There is very little literature regarding this topic. Nevertheless, some researchers have recently ventured into this area. Borthakur [5] Shafiq [6] and Al-Hawat [7] have done some work on the surface modification of steel using the plasma focus device and they have been able to obtain an increase in surface hardness. This thesis will build on their work and try to investigate the operating conditions for the plasma focus device to obtain the optimal hardness.

2.2 Surface texturing

Surface texturing as a form of surface modification has gained recognition in recent years as a means of improving the performance of cutting tools. Dry machining, without the use of metalworking fluids, is slowly being considered as a viable production approach in industry. Traditionally, the use of metalworking fluids to reduce friction in machining has the benefit of lengthening tool life. During the machining process, heat is generated at the tool-chip interface causing a substantial rise in temperature. This rise in temperature results in greater wear of the tool. Thus cutting fluids are employed to control the temperature and flush away wear debris.

The use of cutting fluids come with a large economic and ecological burden according to G. Singh [8]. In addition, Park [9] added that cutting fluids pollute the environment and also pose a threat to the operator's health. Metalworking fluids can cause adverse health effects through skin contact with contaminated materials, spray, or mist and through inhalation from breathing the metalworking fluid mist. The safe disposal of metalworking fluids (Demirbas [10]) is another issue that needs to be addressed properly in order not to cause pollution in the environment. It is for this reason that the use of cutting fluids is being reviewed (Benedicto [11]) and dry

machining is now being contemplated in order to reduce environmental pollution and health hazards.

Due to the friction between the tool and the work piece, dry machining reduces tool life because of the high heat it generates. Thus, in order to maintain a long tool life without resorting to cutting fluids, new approaches to tool design are required. One approach that has been found to work is to apply micro-texturing to the rake face of the tool thus resulting in a tool having a micro-grooved or micro-dimpled texture. According to Gajrani [12], dry machining with a surface textured tool makes it a viable alternative to the use of cutting fluids.

In the machining of aluminium products, aluminium chips have a tendency to severely adhere to the surface of the cutting tool often leading to tool failure. Aluminium is a soft and is also an easy to machine material but it has a tendency to form a built up edge. Sugihara [13], Rathod [14] and Obikawa [15] found that micro-textured surfaces on the tool improves the anti-adhesive property. To enhance the effectiveness of the textured cutting tool, solid lubricants can be further applied at the chip-tool interface.

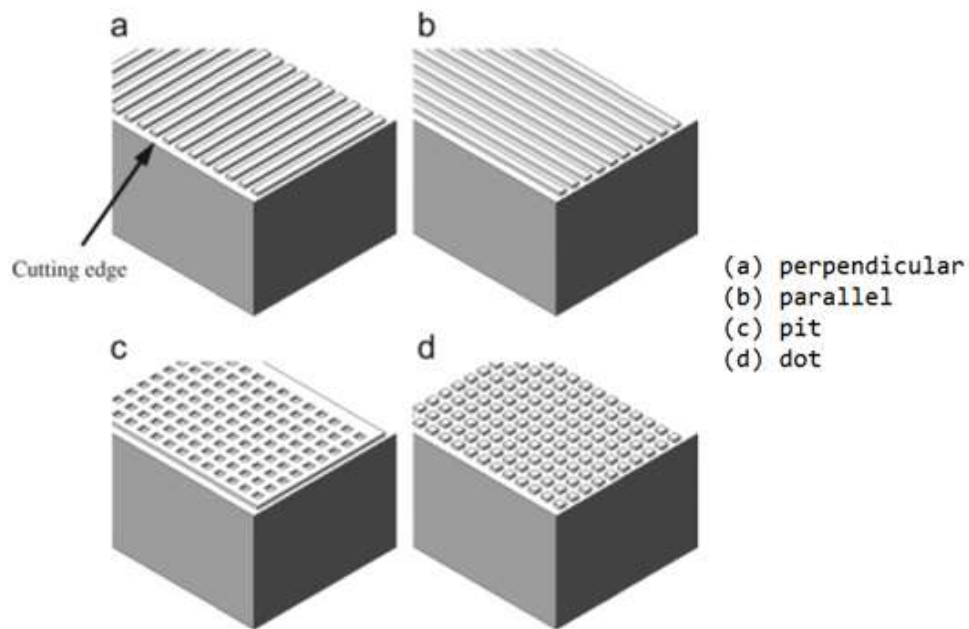


Figure 2.3 Types of surface texture. Source Obikawa [15]

The process for producing a textured tool usually involves the making of the hard tool first and then impressing the surface texture on the tool later. This surface texturing process can be done by pulsed laser (Liu [16] and Sasi [17]), electrochemical machining (Chen[18]), electro discharge machining (Koshy [19]) or even by means of a simple mechanical micro indentation. Tribological testing by Sedlacek [20] showed that there is an influence of the geometry of the surface texture on tool performance. Koshy[19] has proposed that the surface texture of overlapping craters is better than arrayed grooves.

A textured tool is required to have both hardness and texture. The dense plasma focus machine is a source of highly energetic ions. At the same time, the ion beam produces a texture on the surface of the tool due to the high energy with which it impinges onto the tool. The presence of micro textures on the tool surface can reduce the contact length of chip sliding over the tool which in turn reduces sliding friction (Arulkirubakaran [21]). Reduction in contact length leads to less material adhesion resulting in an improved tool life (Kummel [22]). Textured tools are normally used with a lubricant(usually solid) such as molybdenum disulphide (Deng [23]) or calcium difluoride (Sharma [24]). The use of textured tools is not just limited to flat surfaced tools. They have been found to be effective on the curved surfaces of drills as well (Niketh [25]).

This study attempts to take a look in the possibility of the DPF machine in producing a textured tool from low carbon steel for the machining of aluminium.

2.3 Dense plasma focus

2.3.1 Definition of plasma

Plasma is widely known as the “fourth state of matter”, after the other three fundamental states of matter which are more commonly recognized – solid, liquid and gas. Plasma is a highly ionized gas. It consists of positively charged ions, electrons and some other neutrals, such as atoms and molecules that are not electrically charged (Wiesemann [26]).

Unlike solid, liquid and gaseous states, plasmas exist in the environment with sufficient energy condition for producing a large number of ionization processes of

atoms. The ionization processes can be generally categorized as photoionization process by an intense source of ultraviolet (UV) radiation, or as collisional ionization by highly energized electrons.

Impact ionization is the dominant process in the gas discharge processes, due to the sufficient impact collisions between energized electrons and gas atoms. On the other hand, photoionization process comes into place when the plasma densities are low but the environment is enriched with dense UV photons. The latter case is more commonly seen in space plasmas.

Collisional ionization process: $e + A \rightarrow A^+ + 2e$

Photoionization process: $h\nu + A \rightarrow A^+ + e$

The ionization energy of neutral atoms ranges from 3 eV to 25 eV. In order to produce sufficient ionization energy to produce steady state plasmas, a high temperature is required to supply large amount of thermal energy for atoms to get ionized by collisions, while photoionized plasmas require short wavelength UV radiation to sustain the plasma state and resist the recombination processes.

The reciprocal processes of collisional ionization and photoionization process are also known as three-body recombination and two-body recombination process (Piel [27]).

Three-body recombination: $A^+ + 2e \rightarrow A + e$

Two-body recombination: $A^+ + e \rightarrow A$

In neutral gas, the gas particles interact with each other by mean of collision. In most occasions, gas particles move in a straight line independently of other atoms or molecules, and the van der Waals force comes into effect only in close proximity. However, in plasma, the long-range force, the Coulomb force, plays a dominant role in the interaction between charged particles. As a result, each plasma particle simultaneously interacts with other multiple charged particles. When plasma is exposed to an external stimulus, plasma shows collective behaviour, which resembles the cooperative response of many plasma particles, to that stimulus.

2.3.2 The Dense Plasma Focus Device

The plasma pinching phenomena in dense plasma focus (DPF) device was first discovered in the early 1960's. Its primary function was to produce neutron sources of high intensity, and in turn develop DPF device into plasma fusion device. The DPF device is implemented as a source of intense neutrons, high energetic ions, relativistic electrons and X-ray emission of high abundance [1].

The Mather-type DPF device is a structure of coaxial electrode plasma focusing machine that utilizes very high current pulse discharge and compresses the ionized plasma to an extent of high density and temperature (Rawat [28]). The structure of the DPF is as shown in Figure 2.4 .

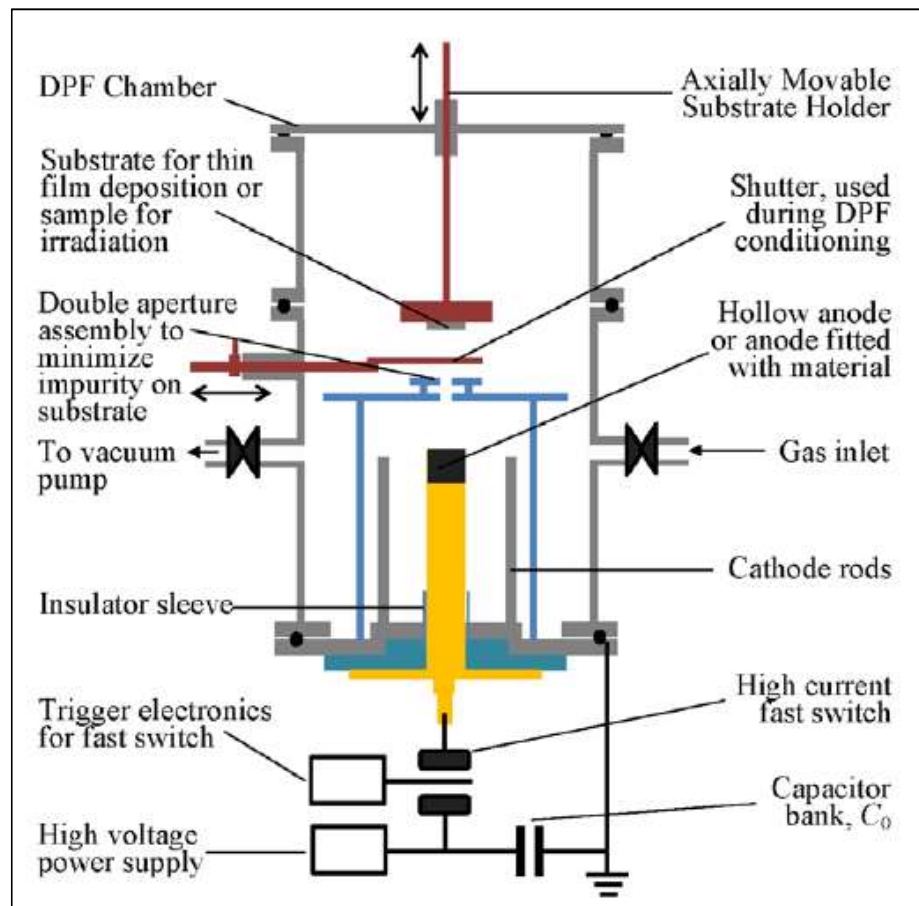


Figure 2.4 The structure of the DPF device. Source: Rawat [28]

The detailed stages of the plasma focusing at different times (Lee & Saw [29]) are illustrated in Figure 2.5.

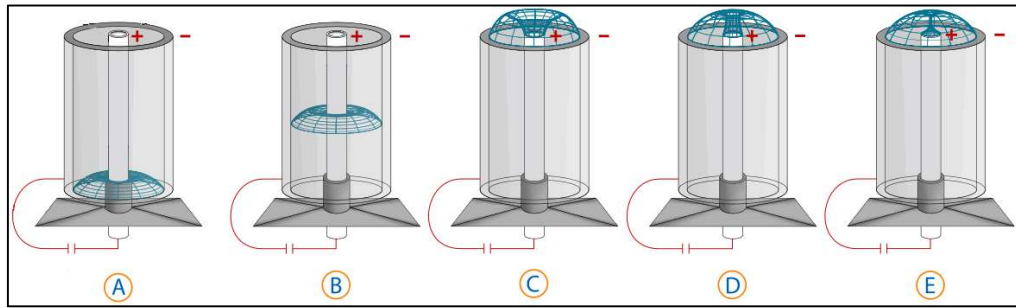


Figure 2.5 Operation Stages of DPF device. Source: Lee & Saw [29]

The description of the stages in Figure 2.5 are described in Table 1.

Table 1 Detailed Various Stages of Plasma Focusing

| Stages | Operations Involved |
|--------|---|
| A | Capacitor bank is charged to high voltages within range 10 kV to 30 kV. As the control switch is triggered, the high amount of electrical energy is transferred from the capacitor bank to the region across the electrode assembly. Thus, a well-defined plasma sheath is initiated near the closed end of electrode assembly. |
| B | This stage is also known as axial acceleration phase, at which the current sheath is driven by Lorentz force (due to the interaction between current sheath and magnetic field produced by itself). As a result, the current sheath accelerates towards the open end of electrode assembly at approximately 4 to 6 cm/ μ s. |
| C | The current sheath reaches the open end of anode and starts to change its acceleration direction. |
| D | This is the radial compression phase, at which the current sheath is accelerating towards the anode axis radially at approximately 2 to 2.5 times of the speed in axial acceleration phase. |
| E | The plasma columns are pinched and disrupted due to $m = 0$ (sausage instability) and $m = 1$ (kink instability) modes. The $m = 0$ mode instabilities accelerate ions of filling gas towards the surface of specimen-to-be-treated and electrons towards the anode (Rawat [28]) |

2.3.3 Lee Model Code

The Lee Model Code also known as Radiative Dense Plasma Focus Computation Package (RADPF) is a tool implemented by Professor Sing Lee in 1984 used to compute the properties of the plasma focus. This implementation helps the researcher to simulate the dense focus properties including the plasma focus dynamics, thermodynamics, and radiation. The code which took into account the five phases was successfully used to simulate and assist numerical experiment with several machines. Professor Sing Lee stated that his methodology for the 5-phase model includes axial phase, radial inward shock phase, radial reflected shock phase, pinch phase and expanded column phase (Saw, Lee, Rawat, & Lee [30] and Lee 2014 [31]). The 5-phase model was later followed by a 6-phase model.

The DPF device discharge current trace is taken by a Rogowski coil. The parameters used in the Lee Model Code can be separated into three different parameters which are bank, tube and operation parameters (Lee & Saw [32]). Table 2 shows the parameters used in the Lee Model Code.

Table 2 Parameters Used in Lee Model Code

| | |
|-----------------------------|-------|
| <i>Bank Parameters</i> | |
| Static Inductance | L_o |
| Capacitance | C_o |
| Stray Resistance | r_o |
| <i>Tube Parameters</i> | |
| Cathode radius | b |
| Anode radius | a |
| Anode Length | Z_o |
| <i>Operation Parameters</i> | |
| Voltage | V_o |
| Pressure | P_o |

The bank parameters include the capacitance, inductance and the resistance in the circuit. The tube parameters represent the size of the tube used in the plasma focus device. Lastly, the operation parameter shows the operating voltage that charged the capacitor and pressure of gas filled to the chamber.

The computational total discharge current waveform can be obtained by adjusting the four model parameters. These four parameters are axial mass swept-up factor (f_m), axial current factor (f_c), radial mass swept-up factor (f_{mr}) and radial plasma

current factor (f_{cr}). The gas parameters used in the input to the Lee Code are described by its atomic number, its molecular weight and whether it is atomic or molecular gas.

For the fitting of total discharge current waveform, the measured total discharge current waveform is taken from the laboratory plasma focus experiment. Then the computed total current waveform is fitted with the measured waveform by changing the 4 model parameters (f_m , f_c , f_{mr} and f_{cr}) one by one until both waveforms fit well and match each other (Lee, 2014 [31]) as shown in Figure 2.6.

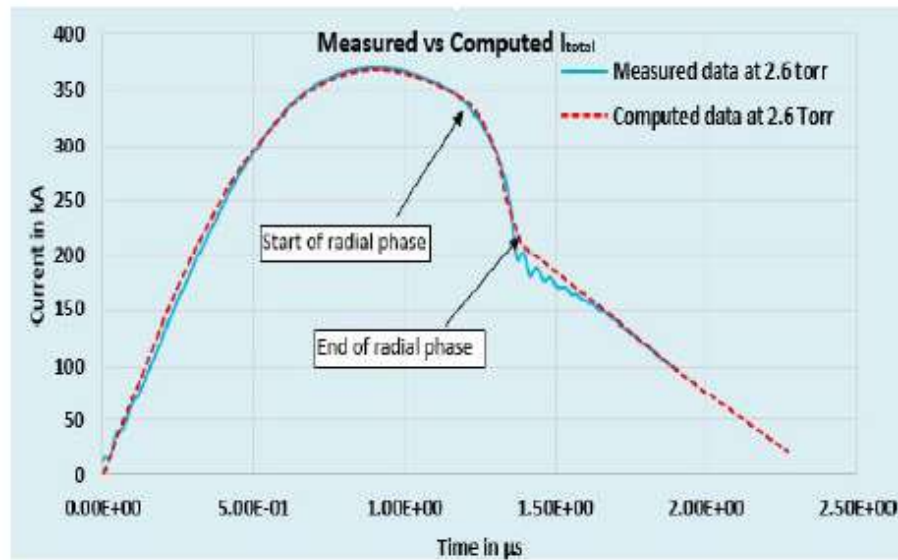


Figure 2.6 Lee Model Code waveform. Source: Lee [31]

CHAPTER 3

METHODOLOGY

3.1 Introduction

The methodology for this research can be categorized into four parts: preparation of steel test samples, firing the samples in a dense plasma focus device, testing for changes in hardness with a micro Vickers hardness tester and the subsequent analysis of the surface. The figure below (Figure 3.1) shows the flow diagram for experiment.

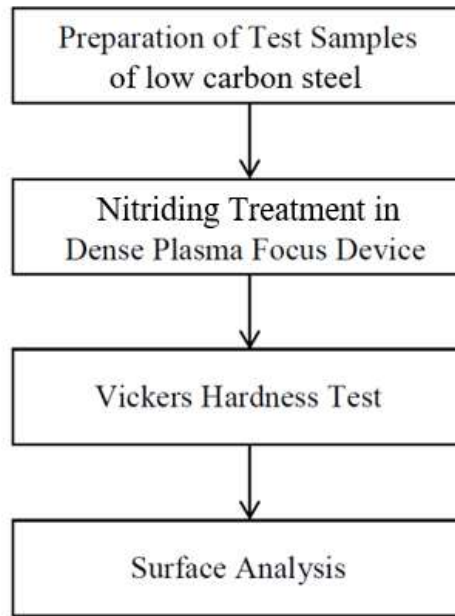


Figure 3. 1 Flow Chart of methodology

3.2 Preparation of steel samples

In this project, it is intended to determine the effect of using the plasma focus device to nitride low carbon steels by varying the distance from the sample to the central anode and also by varying the chamber pressure. For this purpose, steel samples are required to be prepared. The samples are cut to the dimensions of 70 mm × 25 mm × 7 mm from bar stock. The dimensions are chosen such that the samples could fit into the target holder and physically lowered into the chamber easily.

The procedures and sequence for the preparation of the test samples are indicated in the Figure 3.2.

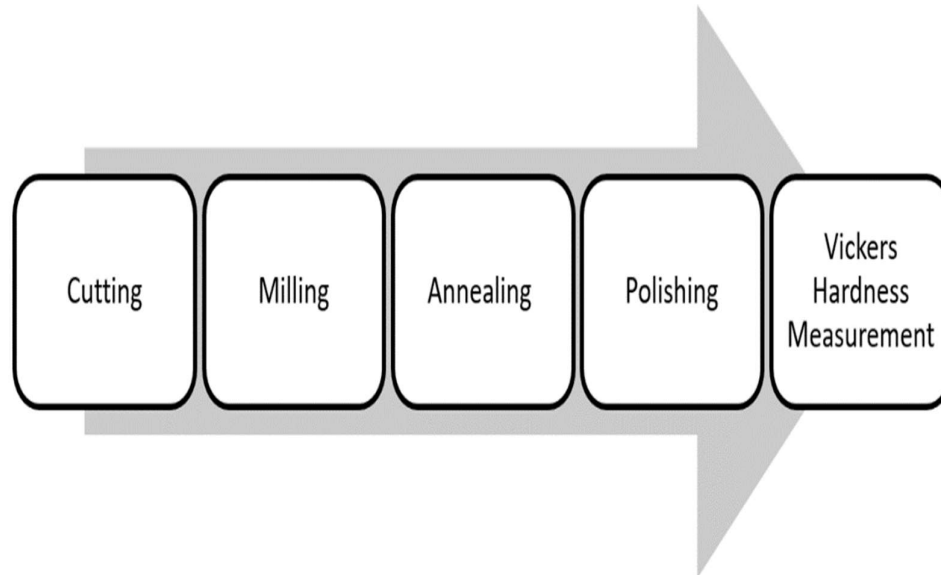


Figure 3.2 Flow Chart for preparation of test samples

The low carbon steel chosen for this research is AISI 1020. It is cheap, easily available and is used in a lot of factories.

3.2.1 Material Properties of AISI 1020 Low Carbon Steel

According to designation systems provided by AISI (American Iron and Steel Institute) and SAE (Society of Automotive Engineers), AISI 1020 is categorized as a type of low tensile carbon steel that has a Vickers hardness in the range of 125 – 247 HV and tensile strength ranging from 410 MPa to 790 MPa. It is usually readily available commercially in a cold drawn condition. In industry, AISI 1020 is a common material for manufacturing because of its easy weldability and machinability.

The five major chemical elements involved in AISI 1020 steel are presented in Table 3.1.

Table 3.1 Composition of AISI 1020 Steel. Source: AZO Materials [33]

| Element | Composition % |
|-----------------|---------------|
| Iron (Fe) | 99.08 – 99.53 |
| Carbon (C) | 0.17 – 0.23 |
| Manganese (Mn) | 0.3 – 0.6 |
| Phosphorous (P) | ≤ 0.040 |
| Sulfur (S) | ≤ 0.050 |

The iron-carbon phase diagram for steel [34] is presented in Figure 3.3. This iron-carbon diagram has to be referred to if there is a requirement to heat-treat the metal.

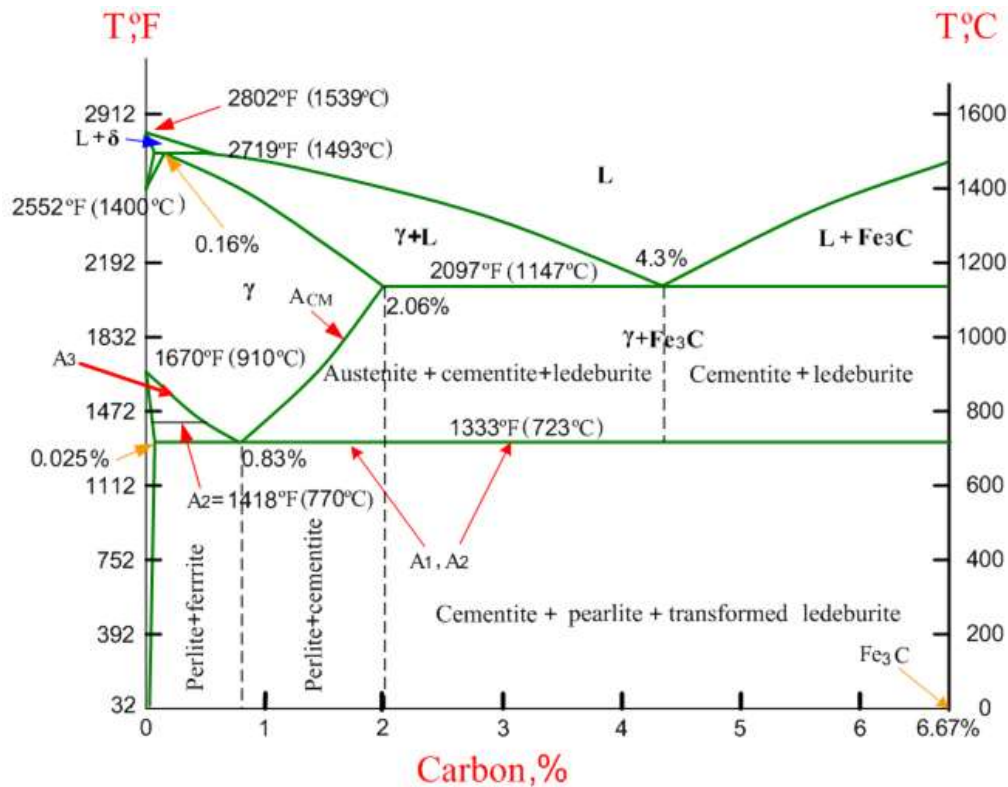


Figure 3.3 The iron-carbon phase diagram. Source: [34]

Annealing is usually implemented on cold-worked steel pieces to eliminate residual stresses without changing its phase fractions established by prior heat treating processes.

For annealing, a step named austenitizing is required to heat steels to produce homogeneous austenite. Austenitizing is conducted about 30 °C above the upper

transformation temperature A_3 , resulting steel consisting 100% austenite. For the case of AISI 1020, the carbon content is around 0.2%. In theory, at the 0.2% carbon level, the A_3 temperature determined from Figure 3.3 is approximately 830 °C, thus providing the suitable austenitizing temperature of $830 + 30 = 860$ °C. In practice, metal workers tend to go a bit higher than 860 °C as an added measure of safety. After the heating process, the temperature should be held constant over a certain amount of time to ensure a constant heating temperature throughout the specimen. After that, the cooling process takes place within the chamber furnace. Slow cooling ensures the annealed steel to have coarse pearlite, providing relatively low strength and good ductility (Askeland, Fulay, & Wright [35]). The general industrial practice to anneal AISI 1020 steel is to heat it to the range of 870 °C to 910 °C followed by a period of slow cooling.

3.2.2 Cutting to size

The steel samples were cut from an AISI 1020 carbon steel flat bar stock purchased from a hardware store. The raw metal bar had already undergone a series of cold rolling processes to arrive in the form of a flat bar. Therefore, it had already undergone work hardening as part and parcel of the manufacturing process. This work hardening would have increased the hardness of the sample inadvertently.

The steel pieces were cut (Figure 3.4) from the center of steel bar by using a horizontal band saw. The steel pieces were measured at 75 mm × 30 mm × 10 mm which were bigger than the desired size of 70 mm × 25 mm × 7 mm as mentioned earlier on in this chapter. This additional material volume was to cater for the milling allowance later on in the milling process.



Figure 3.4 Cutting off the steel samples from bar stock by a horizontal band saw

3.2.3 Milling

Milling was carried out to remove the oxide layer on the surface of steel samples and also to provide a reasonably flat surface. Each surface of the steel pieces was machined (Figure 3.5) until the desired dimensions of 70 mm × 25 mm × 7 mm were reached. The sharp metal edges were smoothed out with a bench grinder. Although great care was taken to feed the milling tool slowly, scratches were inevitable on the surfaces of the samples.



Figure 3.5 Milling process for steel samples

3.2.4 Annealing

Steel taken from bar stock have a higher hardness than steel of the same composition taken from the ingot form. This is because, in the manufacture of bar stock, the steel has to undergo cold rolling processes until the required thickness of the bar stock is achieved. Cold working increases hardness and decreases ductility. Thus this cold rolling process imparts an increase in hardness to the steel bar with each pass of the rolling process. The amount of cold working that the steel had undergone is not even and some parts of the bar stock can be harder than other parts. Testing for the hardness of the steel is also problematic as it cannot be ascertained if the hardness was caused by the dense plasma focus nitriding process or by the cold

working that the steel had received beforehand. For this reason, the steel samples were sent for annealing to remove the effects of the prior cold working of the bar stock.

The steel samples were heated to a temperature of 910 °C (Figure 3.9) in an annealing oven (Figure 3.7). It took one hour for the temperature to rise to 910 °C (Figure 3.8) and this temperature was maintained for an hour (Figure 3.10) as shown in the chart of Figure 3.6. The samples were then allowed to cool slowly in the oven for 16 hours before they were taken out of the oven. By doing so, the Vickers hardness of the samples was later found to have dropped after the work hardening effects on the steel were removed through annealing.

Graph of Temperature Versus Time

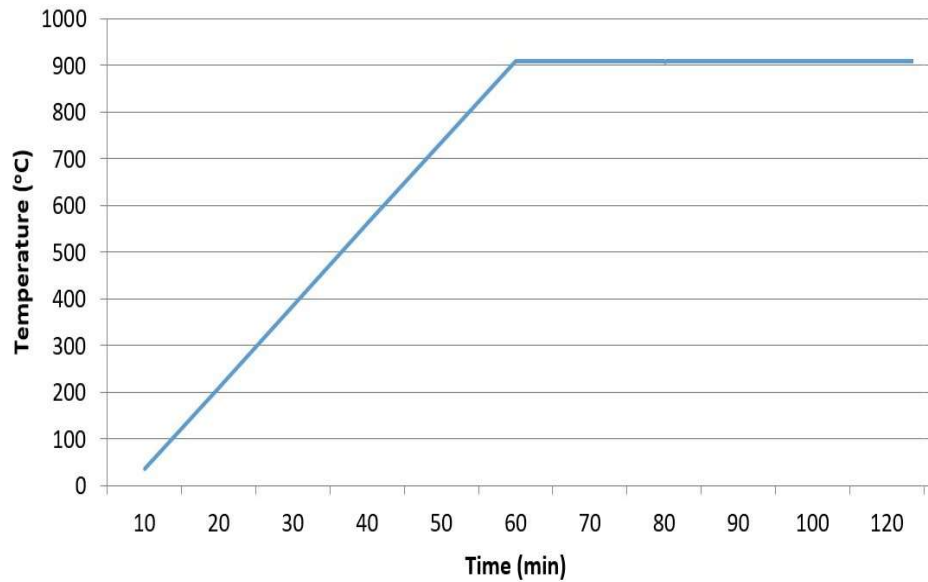


Figure 3.6 Heating Temperature versus Time



Figure 3.7 Annealing Oven

The samples were heated slowly for one hour (Figure 3.8) until they reached the annealing temperature of 910 °C (Figure 3.9). The annealing temperature was then set to hold constant for 1 hour (Figure 3.10).



Figure 3.8 Duration for Heating



Figure 3.9 Annealing Temperature



Figure 3.10 Time setting to maintain constant annealing temperature

3.2.5 Polishing

A piece of steel obtained from bar stock tends to have a layer of oxide on its surface. This has to be removed by using a milling machine. Figure 3.11 shows the microstructure of the steel surface under optical microscopy before it has undergone the polishing process. Very deep tool marks from the milling process are visible in Figure 3.11.

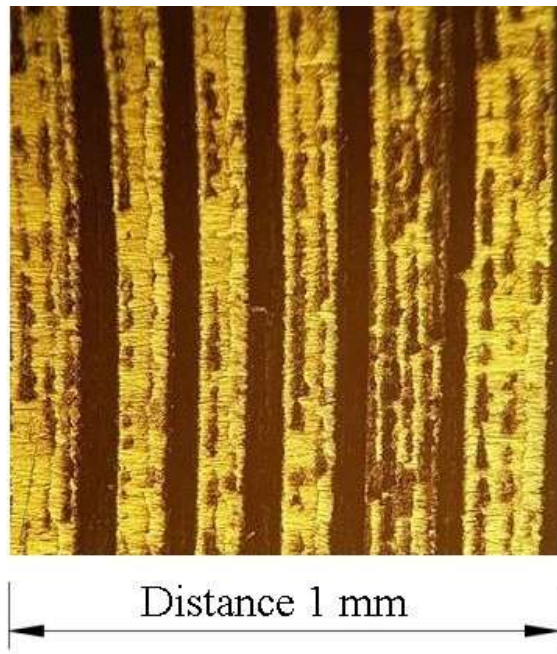


Figure 3.11 Steel surface before polishing

After the samples have been annealed, they are sent to the wet polishing process. During the polishing process, the steel piece is held by hand and forced down onto a rotating silicon carbide abrasive paper. A high rotational speed is used to increase the polishing effectiveness.



Figure 3.12 Polishing process

During the first stage of the polishing process, a rough abrasive paper with grit number of 60 is used to remove the milling scratches and any remaining oxide layer. The rotational speed of abrasive paper is adjusted to 600 rpm and the steel piece is pressed down against the spinning abrasive paper. Figure 3.13 shows the steel surface after polishing with grit number 60 abrasive paper. The milling tool marks have been removed but a lot of scratches still remain on the surface.

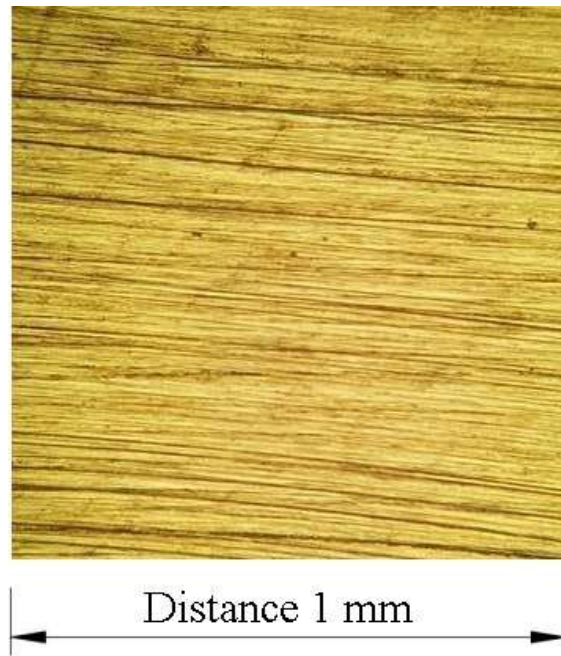


Figure 3.13 Steel surface after the first polishing

The tiny scratches that are still visible after polishing with grit number 60 abrasive paper need to be removed. Further polishing processes are carried out with 240, 400, 800 and 1200 grit numbers to achieve a finer surface finish. The surface roughness of abrasive paper decreases when the grit number increases. Figure 3.14 shows the surface for the steel piece with a much improved and finer surface finish.

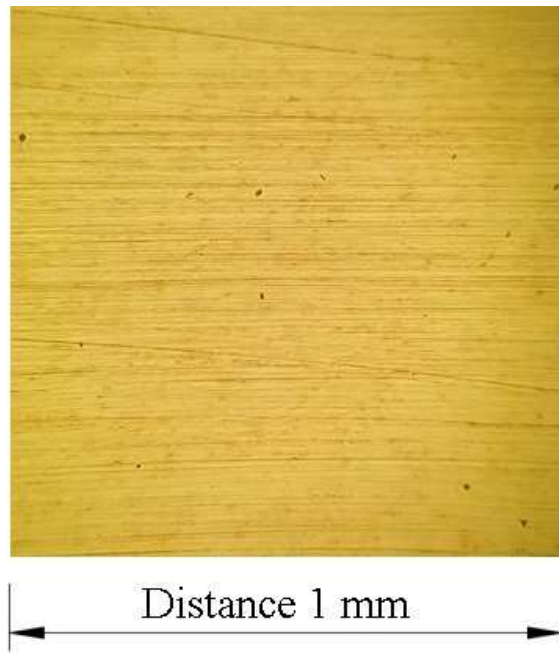


Figure 3.14 Steel surface with improved finish

3.2.6 Using Vickers Microhardness Testing

The hardness test is a method to determine the material resistance to the penetration of its surface by a hard object. It can represent resistance to scratching or indentation, and is a qualitative measure of the material strength. In general, microhardness tests are defined as hardness tests with applied load less than 2N. Microhardness tests are relatively useful in cases where the surface has higher hardness than the bulk materials in which different areas show different levels of hardness, or samples that are not macroscopically flat (Askeland, Fulay, & Wright [35]).

The Vickers microhardness test is a standard procedure to determine the surface hardness of a given metallic surface, governed by International Standard ISO 6507-1:2005. The hardness test is carried out by loading a diamond pyramid indenter into the surface of sample that is to be tested, and followed by the measurement of the diagonal length of the mark of indentation on the surface after the applied indenting force is removed as shown in Figure 3.15.

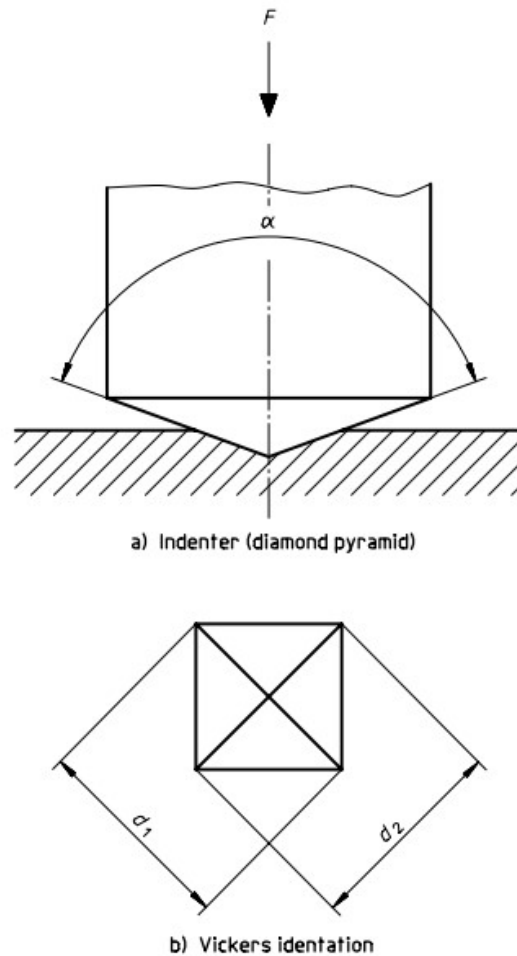


Figure 3.15 Indenter and Diagonal Lengths in Vickers Hardness Test. Source [35]

The arithmetic mean of both the diagonal lengths of indented mark is given by

$$d = \frac{d_1 + d_2}{2}$$

For a given test force F and arithmetic mean length d , the Vickers hardness HV can be calculated by the formula

$$HV = 0.102 \frac{2F \sin \frac{136^\circ}{2}}{d^2} = 0.1891 \frac{F}{d^2}$$

where 136° is the angle α in Figure 3.15 and lies between the opposite faces of the pyramidal indenter.

The Vickers hardness is normally expressed by the symbol HV . It is preceded by the hardness value and test force value in kgf and duration of loading in seconds if the value is out of the range between 10 seconds and 15 seconds.

For example, 640 HV 30 represents a Vickers hardness of 640 which is determined by applying a test force of 30 kgf (294.3 N) for a duration of 10 to 15 seconds.

The Vickers hardness value measured is independent of the applied test force, which makes it more convenient in comparing hardnesses between different works or projects (Herrmann [36]).

3.2.7 Vickers Hardness Test procedure

The hardness of the steel pieces was measured by using a micro Vickers hardness tester. A Vickers hardness test was carried out by using the load of 0.2 kgf (1.961 N) with dwelling time for 10 seconds. A total of 69 readings were measured on the centre line of steel surface at every 1mm interval as shown in Figure 3.16. By taking the hardness value at every 1 mm interval, one can determine the surface hardness distribution on the entire surface. The average Vickers hardness for every steel piece was calculated.

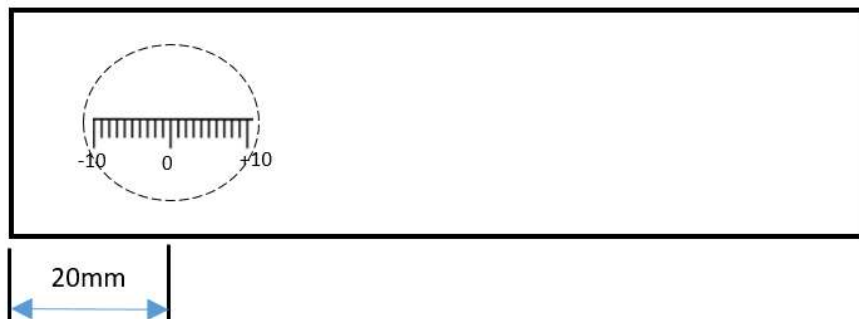


Figure 3.16 Zero position located visually for Vickers Hardness Measurement

The steel sample was mounted in the plasma focus device in such a way that the “zero” position corresponds to the centre of the fired ion beam. This “zero” position, or origin, is approximately 20 mm from the left edge of the steel sample as shown in Figure 3.16.

3.3 Plasma Nitriding with DPF

The machine used in this nitriding experiment is a simple cost-effective plasma focus device based on a 3 kJ single capacitor and a maintenance-free parallel plate spark gap. The system has been designed and operated as a reliable source of plasma shown in Figure 3.17. Saw and Lee [37] have shown that high energy density conditions exist for such simple machines. Thus a 3 kJ Mather type plasma focus device is used to carry out the nitriding process for surface treatment of AISI 1020 carbon steel. The system is powered by a single capacitor of 30 μF and operated at 12 kV. The anode of the plasma focus device is a hollow copper rod of 16 cm length. The anode is surrounded by six copper rods forming a coaxial cathode (Figure 3.18). The filling gas used is nitrogen.

The standard operating procedures for using the DPF machine have been given in great detail in Appendix B of this thesis. These standard operating procedures are rigorously followed for reasons of safety.



Figure 3.17 3 kJ Mather Type Dense Plasma Focus Device



Figure 3.18 Arrangement of Anode and Cathode in DPF Device

Each steel sample is first cleaned with 2-Propanol to remove any dirt and impurities on the surface before fixing it into the holder. The holder (Figure 3.19) was then lowered into the vacuum chamber of the plasma focus device and the distance of steel sample from the anode tip was recorded.



Figure 3.19 Substrate Holder in Dense Plasma Focus Device

The 6 litre chamber was evacuated to a base pressure of 0.01 Torr by a Franklin vacuum pump and subsequently filled with nitrogen gas to about 10 Torr. This step was carried out three times to improve the purity level of the filling gas (nitrogen). The nitrogen gas was then evacuated until the desired pressure was reached. It was left in this state for a while and the pressure gauge was monitored to see if the vacuum chamber leaked. If there was no sign of significant leakage (indicated by the pressure gauge needle showing no movement for one hour), the device was ready for use.

A Digital Phosphor Oscilloscope was used to observe the current waveform during the bombardment of plasma towards the steel target. The voltage waveform was also monitored. The presence of an intense voltage spike indicates the strong focusing (plasma pinch) action. Figure 3.20 shows the voltage waveform at a nitrogen pressure of 1.0 Torr when the pinch occurred. The yellow trace at the top is the rate of change of current waveform dI/dt . The lower green trace shows the voltage waveform.

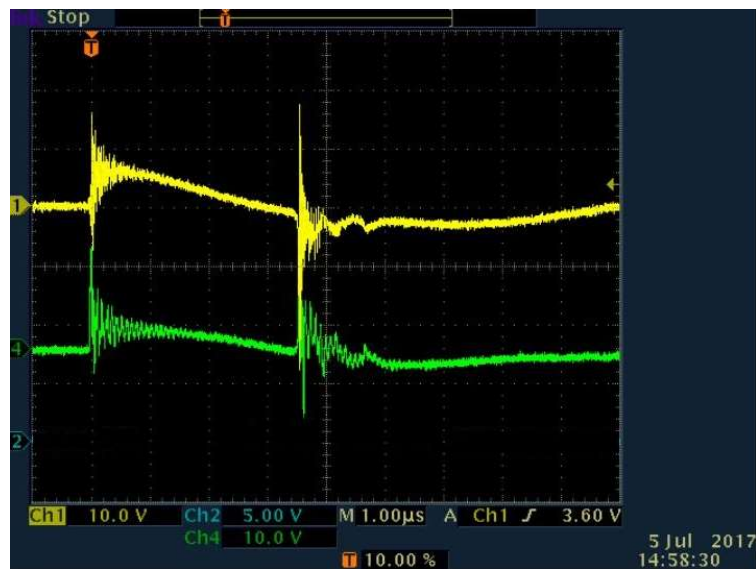


Figure 3.20 Rate of change of current waveform (top yellow trace) dI/dt and voltage waveform (bottom green trace) V at 1.0 Torr

During the preparation stages, the device was fired at 4.0 Torr of nitrogen gas for 2 to 3 times to condition the device. For this conditioning procedure the nitrogen gas pressure must be set above 2.5 Torr to prevent the current pinch from occurring.

Figure 3.21 shows the absence of a pinch in the voltage waveform that was obtained from Digital Phosphor Oscilloscope at 4.0 Torr.

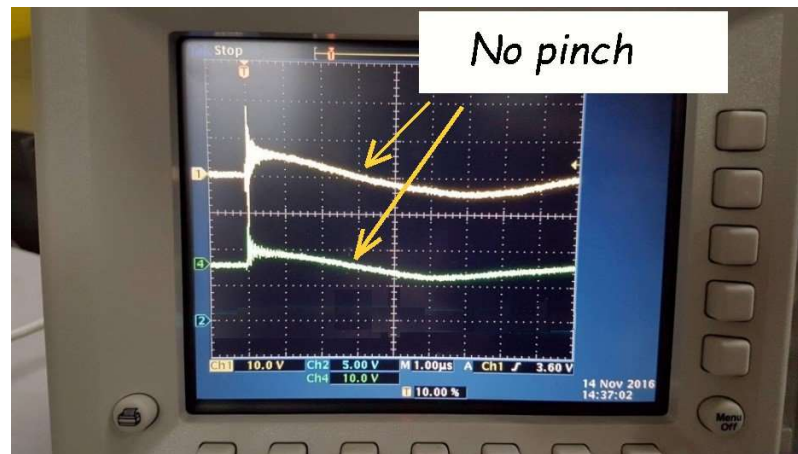


Figure 3.21 No pinch at 4.0 Torr

At 4.0 Torr of nitrogen, the voltage spike and corresponding dI/dt spike are absent in the waveform. Previous experiments showed that there was no nitriding effect in the absence of indications of a pinch. It was initially thought that there would be some level of nitriding achieved in the slow focus mode of the dense plasma focus machine. After some experimentation, it became evident that there was no presence of a white layer that would have indicated nitriding success. Surface hardness improvement occurred only when there was a current pinch.

After firing a couple of conditioning shots, the chamber was evacuated and fresh nitrogen was introduced into the vacuum chamber to the desired pressure. The DPF was then fired at pressures suitable to form current pinches (as in Figure 3.20) in order to get nitriding effects.

The experiment was conducted by using different nitrogen pressures of 0.5, 1.0, 1.5 and 2.0 Torr. In each pressure regime, the experiment was repeated with different distances of test pieces from the anode tip at 4 cm, 6 cm, 8 cm, 10 cm and 12 cm. Each steel piece was exposed to 30 shots of plasma firing.

3.4 Ion beam analysis through the Lee Model Code

The Lee Model Code has been used in the design and interpretation of Mather-type PF experiments (Lee [38]) as a complementary facility to provide diagnostics. It provides a realistic simulation regarding plasma focus properties of any Mather-type plasma focus device. It couples the electrical circuit with plasma focus dynamics, thermodynamics, radiation and signal delay slug to simulate the properties of the plasma column. The numerical data from the simulation of plasma dynamics helps to obtain greater insight and fostering deeper understanding of fundamental physical processes in plasma focus device (Shakonah [39]).

The Lee Model is used to compute the focus pinch current from the measured discharge current waveform. Plasma focus ion beam fluence and flux has been investigated by Lee [40]. The Lee Model is used to estimate ion beam properties by identifying the energy, flux, fluence, number of ions of ion beam of any gas [41].

3.4.1 The 5 phases of the Lee Model

The 5-phase Lee Model classifies plasma dynamics into five different phases [38].

(a) Axial Phase

This phase is described by a snow-plow model with an equation of motion coupled to a circuit equation. The equation of motion includes the axial phase model parameters:

(i) Mass swept-up factor (f_m)

f_m accounts for the porosity of the current sheet, inclination of the moving current sheet shock front structure, boundary layer effects and other unspecified effects which can affect the amount of mass in the moving structure during axial phase.

(ii) Current factor (f_c)

f_c accounts for the fraction of the current effectively driving the structure during axial phase.

(b) Radial Inward Shock Phase

A communication delay between shock front and current sheath due to the finite small disturbance speed is crucially implemented in this phase. All three radial phases incorporate the same radial phase model parameter:

(i) Radial mass swept up factor (f_{mr})

It accounts for the effects on the amount of mass in the moving slug during radial phase.

(ii) Radial current factor (f_{cr})

It accounts for the fraction of the current effectively driving the radial slug.

The radial inward shock phase is described by four equations in the code [32].

(c) Radial Reflected Shock (RS) Phase

A reflected shock which moves radially outwards will develop when the shock front hits the axis, whilst the radial current sheath piston continues to move inwards. Similar to the inward shock phase, four equations are used to compute this phase.

(d) Slow Compression (Quiescent) or Pinch Phase

When the out-going reflected shock hits the inward moving piston, the compression enters a radiative phase. Radiation power and Joule heating are included in the equation of motion. The emission of the radiation, neutron, ion beam and electron beam occur in this phase. The duration of the slow compression phase is the time of transit of small disturbances across the pinched plasma column.

(e) Expanded Column Phase

This phase occurs after the focus pinch. As in phase (a) above two equations are used to describe this phase. The computation of this phase is done primarily to obtain the extension of the computed current trace for more complete fitting of the computed to the measured current trace. Experimentally it has been observed that the pinch phase breaks up rapidly transitioning into

a low density expanded column. This behaviour is captured in the equations which continue to follow the elongation of this expanded column in the post-pinch dynamics.

3.4.2 Computation of ion beam

A brief description of the Lee Model 5-phase and extended 6-phase model (RADPFV6.1b) is explained below [42-54]. The 6-phase model is essentially the 5-phase model with the added modelling of the unstable region between the pinch phase and the expanded column phase.

a. Axial Phase: According to Lee, the equation of motion in this phase combines the axial phase model parameters: mass and current factors f_m and f_c [55, 56]. The mass swept-up factor f_m accounts for not only the porosity of the current sheet but also for the inclination of the moving current sheet-shock front structure, boundary layer effects, and all other unspecified effects which have effects equivalent to increasing or reducing the amount of mass in the moving structure, during the axial phase. The current factor f_c accounts for the fraction of current effectively flowing in the moving structure (due to all effects such as current shedding at or near the back-wall, and current sheet inclination). This defines the fraction of current effectively driving the structure, during the axial phase. Equations 1 and 2 describe this phase [38].

$$\frac{d^2z}{dt^2} = \left[\frac{f_c^2}{f_m} \frac{\mu(\ln c)}{4\pi^2\rho_0(c^2-1)} \left(\frac{I}{a} \right)^2 - \left(\frac{dz}{dt} \right)^2 \right] / z \quad (1)$$

$$\frac{dI}{dt} = \left[V_0 - \frac{\int Idt}{C_0} - r_0 I - I f_c \frac{\mu}{2\pi} (\ln c) \frac{dz}{dt} \right] / \left[L_0 + \frac{f_c \mu}{2\pi} (\ln c) z \right] \quad (2)$$

The terms f_m is the fraction of mass swept down the tube in the axial direction; f_c is the fraction of current flowing in piston (or current sheet CS); $c = b/a =$ cathode radius/anode radius, $\rho_0 =$ ambient density, $I =$ time varying circuit current, $\mu =$ permeability and $r_0 =$ circuit stray resistance.

The equation of motion is affected by the electric current I . The circuit equation is affected by the current sheath motion dz/dt and position z [38].

b. Radial Inward Shock Phase: According to Lee, the equation of motion in this phase takes into consideration the thermodynamic effects due to ionization and excitation. The model parameters, radial phase mass swept-up f_{mr} and radial current factor f_{cr} are combined in this radial phases. The radial mass swept-up factor f_{mr} takes into account all mechanisms which increase or reduce the amount of mass in the moving slug, during the radial phase. The current factor f_{cr} is the fraction of current effectively flowing in the moving piston forming the back of the slug (due to all effects). This defines the fraction of current effectively driving the radial slug. Equations 3 to 6 describe this phase [38].

$$\frac{dr_s}{dt} = - \left[\frac{\mu(\gamma+1)}{\rho_0} \right]^{\frac{1}{2}} \frac{f_c}{\sqrt{f_{mr}}} \frac{I}{4\pi r_p} \quad (3)$$

$$\frac{dz_f}{dt} = - \left(\frac{2}{\gamma+1} \right) \frac{dr_s}{dt} \quad (4)$$

$$\frac{dr_p}{dt} = \frac{\frac{2}{\gamma+1} \frac{r_s}{r_p} \frac{dr_s}{dt} - \frac{r_p}{\gamma I} \left(1 - \frac{r_s^2}{r_p^2} \right) \frac{dI}{dt} - \frac{r_p}{z_f} \left(1 - \frac{r_s^2}{r_p^2} \right) \frac{dz_f}{dt}}{\frac{\gamma-1}{\gamma} + \frac{1}{\gamma} \frac{r_s^2}{r_p^2}} \quad (5)$$

$$\frac{dI}{dt} = \frac{V_o - \frac{\int I dt}{C_0} - r_0 I - f_c \frac{\mu}{2\pi} \left(\ln \frac{b}{r_p} \right) I \frac{dz_f}{dt} + f_c \frac{\mu}{2\pi} \frac{z_f}{r_p} I \frac{dr_p}{dt}}{L_0 + f_c \frac{\mu}{2\pi} (\ln c) z_0 + f_c \frac{\mu}{2\pi} \left(\ln \frac{b}{r_p} \right) z_f} \quad (6)$$

where γ is the specific heat ratio of the gas, z_f is the position of the axial current sheet, z_0 is the length of the anode, r_s is the position of the radial shock front and r_p is the position of the radial current sheet

The four generating equations (3, 4, 5, 6) form a closed set of equations which is integrated for r_s , r_p , z_f and I .

c. Radial Reflected Shock (RS) Phase: When the shock front hits the axis, because the focus plasma is collisional, a reflected shock develops which moves radially outwards, whilst the radial current sheath piston continues to move inwards. The model parameters f_{mr} and f_{cr} are also used in this phase. Equations 7 to 10 describe this phase [58].

$$\frac{dr_r}{dt} = -0.3 \left(\frac{dr_s}{dt} \right)_{on-axis} \quad (7)$$

$$\frac{dr_p}{dt} = \frac{-\frac{r_p}{\gamma I} \left(1 - \frac{r_s^2}{r_p^2} \right) \frac{dI}{dt} - \frac{r_p}{z_f} \left(1 - \frac{r_s^2}{r_p^2} \right) \frac{dz_f}{dt}}{\frac{\gamma - 1}{\gamma} + \frac{1}{\gamma} \frac{r_s^2}{r_p^2}} \quad (8)$$

$$\frac{dz_f}{dt} = - \left(\frac{2}{\gamma + 1} \right) \left(\frac{dr_s}{dt} \right)_{on-axis} \quad (9)$$

$$\frac{dI}{dt} = \frac{V_o - \frac{\int I dt}{C_0} - r_0 I - f_c \frac{\mu}{2\pi} \left(\ln \frac{b}{r_p} \right) I \frac{dz_f}{dt} + f_c \frac{\mu}{2\pi} \frac{z_f}{r_p} I \frac{dr_p}{dt}}{L_0 + f_c \frac{\mu}{2\pi} (\ln c) z_0 + f_c \frac{\mu}{2\pi} \left(\ln \frac{b}{r_p} \right) z_f} \quad (10)$$

The integration of these 4 coupled generating equations 7-10 is carried out step-by-step as in the radial inward shock phase [38].

d. Pinch Phase: When the out-going reflected shock hits the inward moving piston, the compression enters a radiative phase. This phase is described by equation 11.

$$\frac{dr_p}{dt} = \frac{-\frac{r_p}{\gamma I} \frac{dI}{dt} - \frac{1}{\gamma + 1} \frac{r_p}{z_f} \frac{dz_f}{dt} + \frac{4\pi(\gamma - 1)}{\mu \gamma z_f} \frac{r_p}{f_c^2 I^2} \frac{dQ}{dt}}{\frac{\gamma - 1}{\gamma}} \quad (11)$$

It should be noted that an energy loss/gain terms (dQ / dt) has been added into the equation of motion [38]. The plasma gains energy from Joule heating; and loses energy through Bremsstrahlung and line radiation

e. Unstable region: At the end of the pinch phase the system becomes unstable, develops a high “anomalous” resistivity [38] and breaks up. This phase is described by equations 12 and 13.

$$\frac{dz_f}{dt} = \left[\frac{\mu}{4\pi^2(\gamma+1)\rho_0} \right]^{1/2} \frac{If_c}{r_p} \quad (12)$$

$$\frac{dI}{dt} = \frac{V_0 - \frac{\int Idt}{C_0} - \frac{\mu}{2\pi} \left(\ln \frac{b}{r_p} \right) \frac{dz_f}{dt} If_c + \frac{\mu}{2\pi} \frac{z_f}{r_p} \frac{dr_p}{dt} If_c - I(Rf_c + r_0)}{L_0 + \frac{\mu}{2\pi} f_c \left((\ln c)z_0 + \left(\ln \frac{b}{r_p} \right) z_f \right)} \quad (13)$$

In equation 13, the term R is the plasma resistance. It should be noted that step-by-step integration was terminated at the end of a period related to the transit time of small disturbance speed across the plasma pinch column [38].

f. Expanded Column Phase: As in phase (a) above, two equations are used to describe this phase. Experimentally it has been observed that the pinch (phase d above) breaks up rapidly (phase e above) transitioning into a low density expanded column. This behaviour is captured in the equations which continue to follow the elongation of this expanded column in the post-pinch dynamics.

Using the four model parameters f_c , f_m , f_{mr} , f_{cr} good fitting can be obtained between the computed total current waveform to the measured total current waveform since Lee Model code combines the energy and mass balances equivalent, at least in the gross sense, to all the processes which are not even specifically modelled.

Hence the computed gross features such as speeds, trajectories and integrated neutron and soft x-ray yields can be obtained; and are found to be comparable with measured values.

The neutron yield in the Lee Model is computed using a phenomenological beam-target neutron generating mechanism described by V A Gribkov *et al* [57] and adapted to yield the following equation:

$$Y_{b-t} = C_n n_i I_{\text{pinch}}^2 z_p^2 \ln(b/r_p) \sigma / U^{0.5} \quad (14)$$

The ion density is n_i , b is the cathode radius, r_p is the radius of the plasma pinch with length z_p , σ the cross-section of the D-D fusion reaction, and U is the beam energy. C_n is treated as a calibration constant combining various constants in the derivation process [48]. Since the neutron yield equation (14) depends on a mechanism in which an ion beam interacts with the plasma target, information on the number of ions is implicit in the formulation of this equation [40]. The code has therefore been extended [40, 41] to compute the number and properties of the ions for various gases. This extended code is used in our work to compute the number of ions and the energy in the ion beam in each shot in order to determine how these properties vary with pressure of operation. It was hoped that this could result in a correlation between the hardness of the irradiated sample and these properties of the ion beam. This correlation is made in Section 4.11.

The code also computes line radiation Q_L which is calculated as

$$\frac{dQ_L}{dt} = -4.6 \times 10^{-31} n_i^2 Z Z_n^4 (\pi r_p^2) z_f / T \quad (15)$$

The SXR energy generated within the plasma pinch depends on the properties: number density n_i , effective ion number density Z , the atomic number Z_n , pinch radius r_p , pinch length z_f and temperature T . It also depends on the pinch duration since in the Lee Model code the Q_L is obtained by integrating over the pinch duration.

3.4.3 Numerical Fitting of Lee Model Code

The Lee Model Code computes the plasma properties from a measured current waveform to modelling for diagnostics. This Lee Model Code is configured to work on any plasma focus by providing the following appropriate parameters:

- (i) **Tube Parameters:** Radius of Anode (a), Radius of Cathode (b) and Effective Length of Anode (z_0)
- (ii) **Capacitor Bank Parameters:** Inductance of Discharge Circuit (L_0), Bank Capacitance (C_0) and Short Circuited Resistance of the Discharge Circuit (r_0)
- (iii) **Operational Parameters:** Bank Charging Voltage (V_0), Operating Pressure (P_0)
- (iv) **Information of Filling Gas:** Molecular Mass (MW), Atomic Number (A), and Number of Atoms ($At-1\ mol-2$).

The gross performance of the plasma focus device is best indicated by the current trace. The parameters of the machine (Table 3.2) are required for the code. The computed total current waveform is fitted onto the measured waveform [32] during the experiment by adjusting the four model parameters f_m , f_c , f_{mr} , and f_{cr} , until the computed waveform matches the measured waveform as shown in Figure 3.22. First, the axial model factors f_m and f_c are adjusted. Then, the radial model factors f_{mr} and f_{cr} , are adjusted until the two waveforms are fitted together.

Table 3.2 Parameters for fitting

| Parameters | Value |
|-----------------|----------------------------|
| L_0 | 114 nH |
| C_0 | 30 μ F |
| b | 3.2 cm |
| a | 0.95 cm |
| z_0 | 16 cm |
| r_0 | 13 m Ω |
| V_0 | 12 kV |
| p_0 | 0.5 / 1.0 / 1.5 / 2.0 Torr |
| MW | 28 g/mol |
| Atomic Number | 7 |
| Atom / Molecule | 2 (Molecule) |

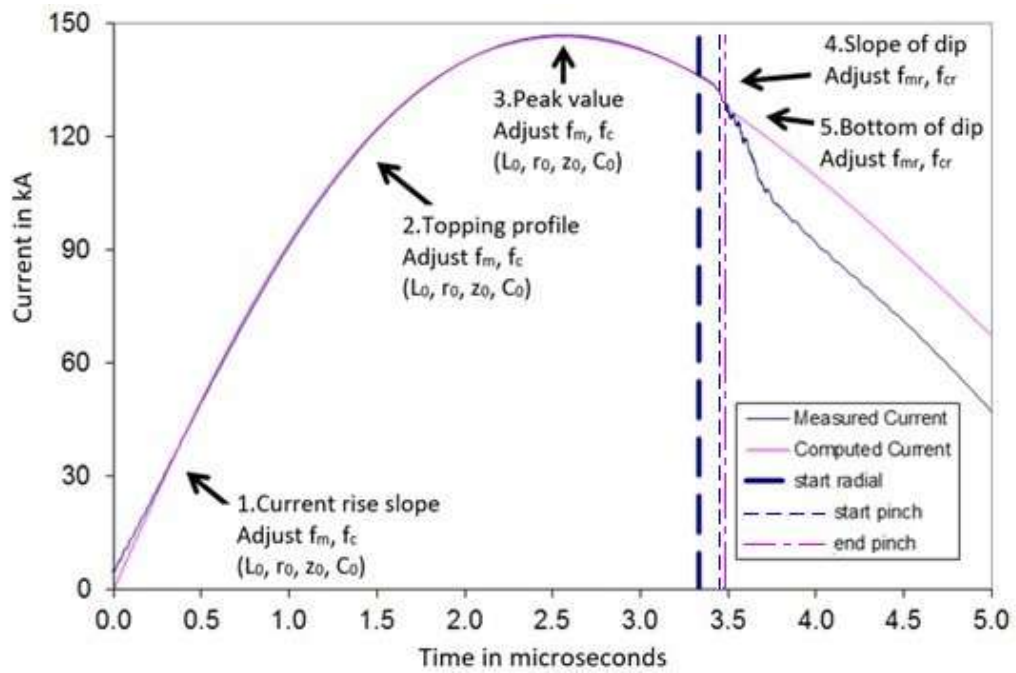


Figure 3.22 The 5-point Fitting of Computed Current Trace to Measured (reference) Current Trace. Source: Arwinder Singh et al [59]

The following is the description of the 5 points in Figure 3.22:

- Point 1:** The rising slope of the total current trace. (Adjust f_m and f_c)
- Point 2:** The rounding off of the peak current. (Adjust f_m and f_c)
- Point 3:** The peak value of the current. (Adjust f_m and f_c)
- Point 4:** The slope of the current dip. (Adjust f_{mr} and f_{cr})
- Point 5:** The depth of the current dip. (Adjust f_{mr} and f_{cr})

3.4.4 Use of Lee Code in this research

In each shot that is fired to irradiate a sample, a current trace is measured using the oscilloscope described elsewhere in this thesis. The code is configured as this plasma focus. The code is run and the computed current waveform is fitted to the measured current waveform. The plasma parameters for this shot are obtained. In particular the beam ion parameters are noted for correlation with the effects of the irradiation. This aspect of the work is described in greater detail in section 4.11.

CHAPTER 4

RESULTS AND DISCUSSION






4.1 Hardness of steel samples before nitriding




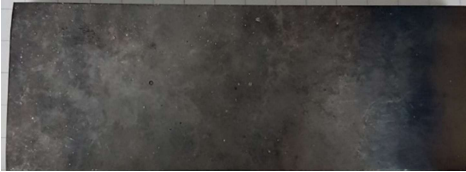

Before the steel samples were nitrided, their surface hardness was measured after the annealing process. The hardness of steel tends to occur in a range rather than appearing as a single figure when measured with the Micro Vickers hardness tester. The hardness is not entirely homogenous throughout the steel but primarily fluctuates within a tight range of between 170 to 190 HV. This is a typical steel behaviour that the researcher has to work with.






4.2 Appearance of steel samples after nitriding






After the plasma focus nitriding procedures were completed, the samples were examined visually. Discolouration was detected and that provided a clue that some change had taken place. However, the amount of discolouration is not able to tell us to what degree the surface hardness has changed. Nevertheless, it is still useful in helping to determine the beam centre of the plasma focus shot. Table 4.1 below shows the appearance of the samples after they had undergone nitriding in the plasma focus device.

Table 4.1: The Appearance of the nitrated steel samples

| Nitrogen Pressure | Anode Firing Distance | Picture of the Samples |
|-------------------|-----------------------|--|
| 0.5 Torr | 40 mm |  <p data-bbox="1008 583 1114 617">Sample 1</p> |
| | 60 mm |  <p data-bbox="1008 852 1114 886">Sample 2</p> |
| | 80 mm |  <p data-bbox="1008 1125 1114 1159">Sample 3</p> |
| | 100 mm |  <p data-bbox="1008 1392 1114 1425">Sample 4</p> |
| | 120 mm |  <p data-bbox="1008 1650 1114 1684">Sample 5</p> |

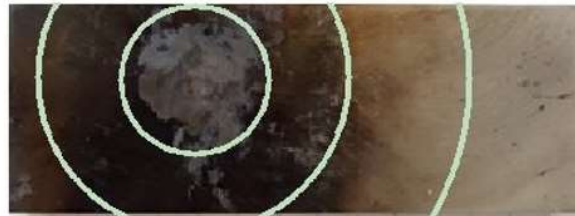
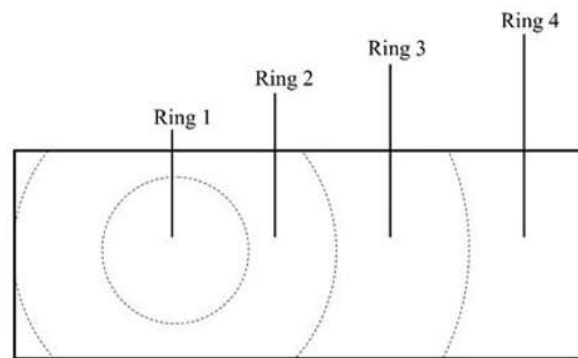
| | | |
|--------|--------|---|
| 1 Torr | 40 mm |  <p>Sample 6</p> |
| | 60 mm |  <p>Sample 7</p> |
| | 80 mm |  <p>Sample 8</p> |
| | 100 mm |  <p>Sample 9</p> |
| | 120 mm |  <p>Sample 10</p> |

| | | |
|----------|--------|--|
| 1.5 Torr | 40 mm |  <p data-bbox="998 388 1120 420">Sample 11</p> |
| | 60 mm |  <p data-bbox="998 714 1120 745">Sample 12</p> |
| | 80 mm |  <p data-bbox="998 1039 1120 1071">Sample 13</p> |
| | 100 mm |  <p data-bbox="998 1375 1120 1407">Sample 14</p> |
| | 120 mm |  <p data-bbox="998 1701 1120 1732">Sample 15</p> |

| | | |
|--------|--------|---|
| 2 Torr | 40 mm |  <p data-bbox="1003 380 1118 411">Sample 16</p> |
| | 60 mm |  <p data-bbox="1003 709 1118 741">Sample 17</p> |
| | 80 mm |  <p data-bbox="1003 1003 1118 1035">Sample 18</p> |
| | 100 mm |  <p data-bbox="1003 1308 1118 1339">Sample 19</p> |
| | 120 mm |  <p data-bbox="1003 1617 1118 1648">Sample 20</p> |

The pictures of the samples shown in Table 4.1 show that after the plasma focus nitriding, there is a white sheen on the steel surface. This whitish layer is typical of nitrided steel and is commonly known in industry as the “white layer”. This layer contains nitrides that are formed during the nitriding process.

From visual inspection, it can be seen that the ion beam produces a rough circular spot of approximately 1 cm radius on the steel surface. This spot has very rough surface texture compared to the rest of the metal surface. Rings of discolouration radiate from this circular spot and can be represented in the drawing of Figure 4.1



Rings drawn on Sample 20 as an example

Figure 4.1 Rings around the centre spot with an example from Sample 20

Ring 1 is the spot that receives most of the ion beam bombardment. It will be shown later that Ring 1 also has the greatest surface hardness improvement. For the purpose of making a visual comparison of textures with the variation in pressure, the samples are arranged according to the two parameters of chamber pressure and the firing distance above the anode as shown in Figure 4.2.

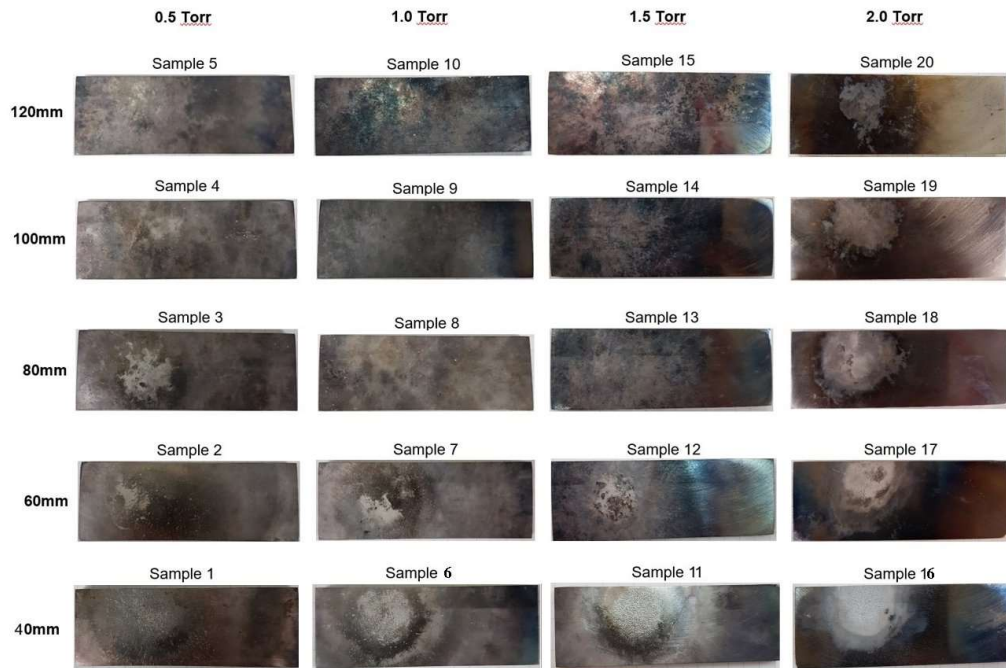


Figure 4.2 Samples arranged according to pressure and distance above anode for convenient visual comparison

The variation of pressure and distance above the anode does not present much information that can be detected visually. The only effect that we can see is that the closer the sample is to the anode, the central ring is more pronounced and the surface texture is more evident. This was evident in all the pressures used. The effect of the ion beam is more dispersed at further distances from the anode.

4.3 Energy-dispersive X-Ray spectroscopy (EDX) of steel samples

By using the Energy-dispersive X-Ray Spectroscopy, the composition of the nitrated AISI 1020 low carbon steel can be determined. Figure 4.3 shows the EDX spectroscopy of the steel sample before undergoing nitriding.

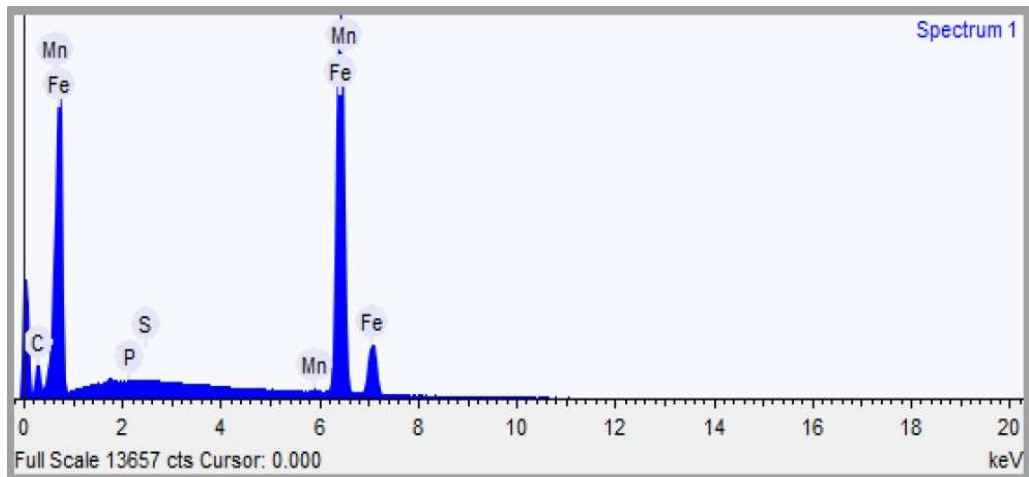


Figure 4.3 EDX spectroscopy of the steel before undergoing nitriding.

After the steel has undergone 30 plasma shots at 1 Torr at a distance of 40 mm from the anode, the EDX spectroscopy was taken again and Figure 4.4 shows that the nitrogen element has crept into the result.

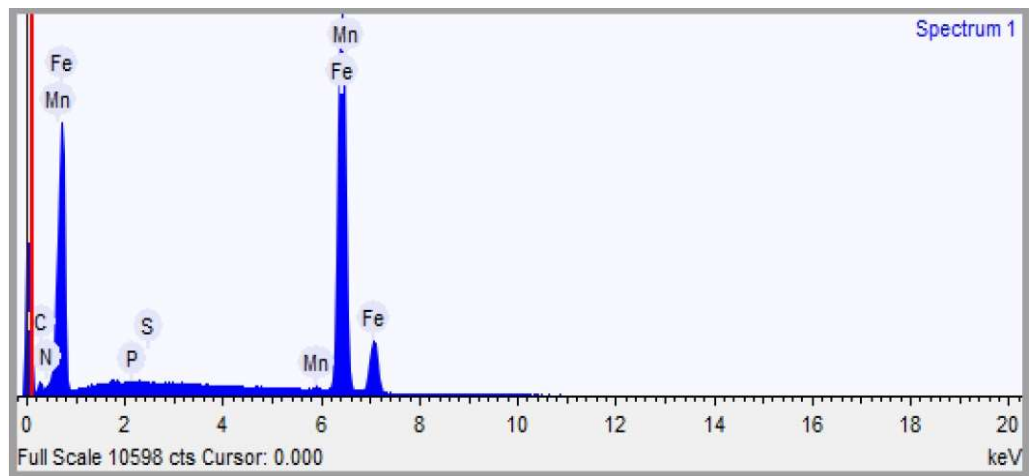


Figure 4.4 EDX spectroscopy of the steel after nitriding showing the presence of nitrogen (after 30 shots, 1 Torr, 40 mm anode distance)

The presence of nitrogen would imply that the steel has formed nitrides after the nitriding operation.

4.4 Scanning Electron Microscopy (SEM)

Upon examination of the cross section of the nitrated steel sample with an SEM machine, the nitrated white layer, which is typical of nitrated steels, can be readily observed in Figure 4.5.

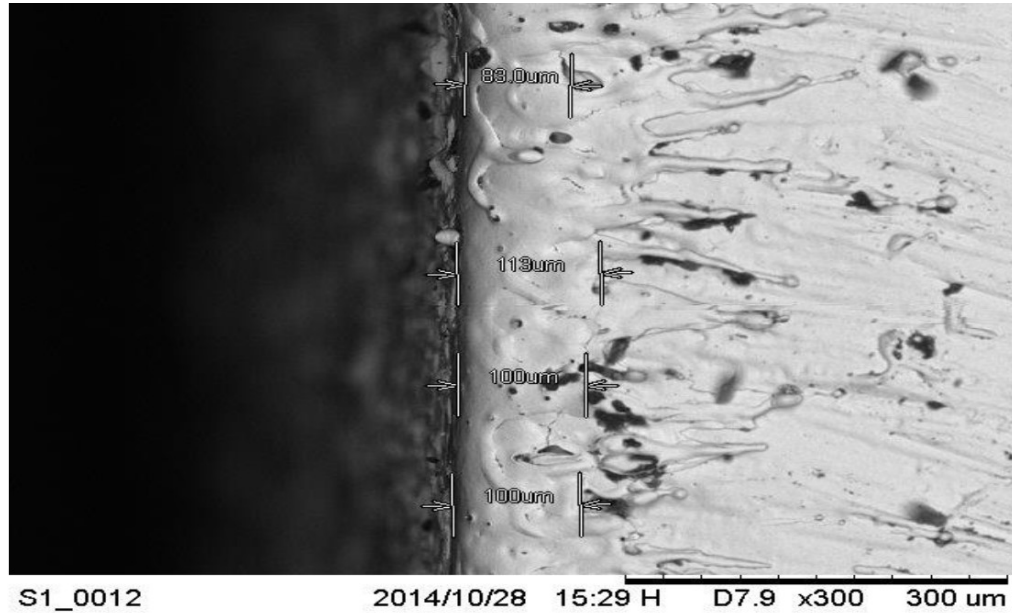


Figure 4.5 Nitrated white layer with 10 shots

The sample in Figure 4.5 has been placed 40 mm above the anode and bombarded with 10 shots of nitrogen ion beam at 1 Torr. It was also noted that the white layer was not very thick but only in the region of slightly more than a 100 microns where the ion beam hit the target. It would be logical to think that this was roughly related to the depth of penetration of the ion beam into the metal.

Figure 4.6 shows a steel sample that has been placed 40 mm above the anode and treated with 30 shots of plasma at 1 Torr. Although the number of shots has been tripled, the white layer thickness increased only slightly to around 130 microns. The depth of penetration of nitrides increases with the number of shots but this increase is not correspondingly proportional.

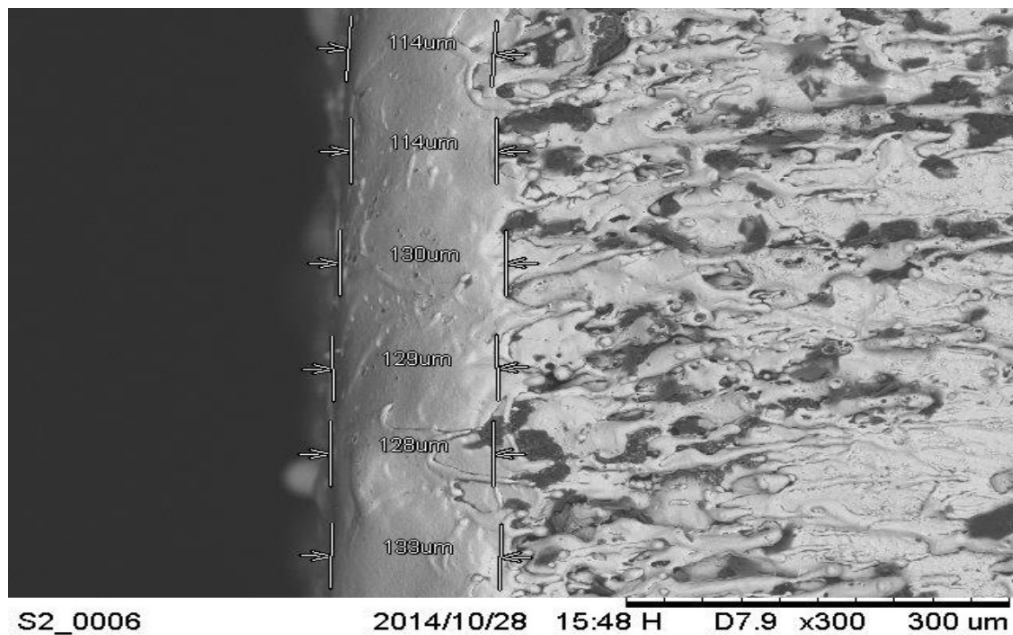


Figure 4.6 Increased nitrided white layer with 30 shots

The depth of penetration is only one of the factors contributing to the increase in hardness and it is not possible to predict how hard a material can get by just looking at the depth of penetration. Figure 4.4 and Figure 4.6, when read together, serve to indicate that nitriding has taken place. Figure 4.5 and Figure 4.6 imply that a greater number of shots will give a greater nitriding effect. The EDX and SEM readings have shown that surface modification by using this method is valid. Beyond that, they will not yield much more information. Therefore, direct hardness measurements will be the primary focus of this experiment.

4.5 Hardness variation graphical comparison

The hardness readings of all the samples are tabulated in Appendix A of this thesis. For each sample, the values of the hardness are plotted on a graph for ease of visualization of the change in hardness as shown in Figures 4.7 to 4.26. The origin, or '0' position, in the graphs corresponds to the centre position of the ion beam shot. The graphs show that the hardness has increased in some of the samples.

Sample 1 (0.5 Torr Nitrogen, 40mm from Anode)

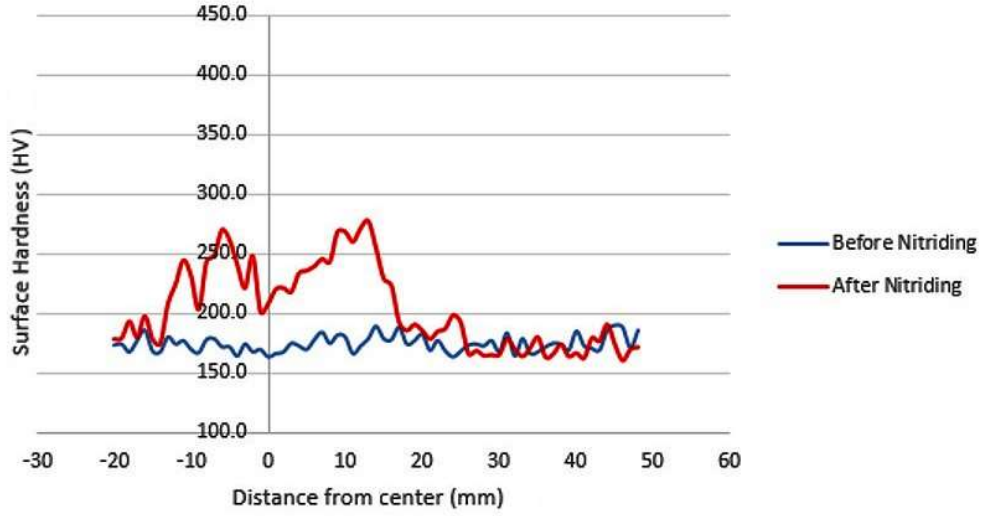


Figure 4.7 Sample 1 before and after nitriding

Sample 2 (0.5 Torr Nitrogen, 60mm from Anode)

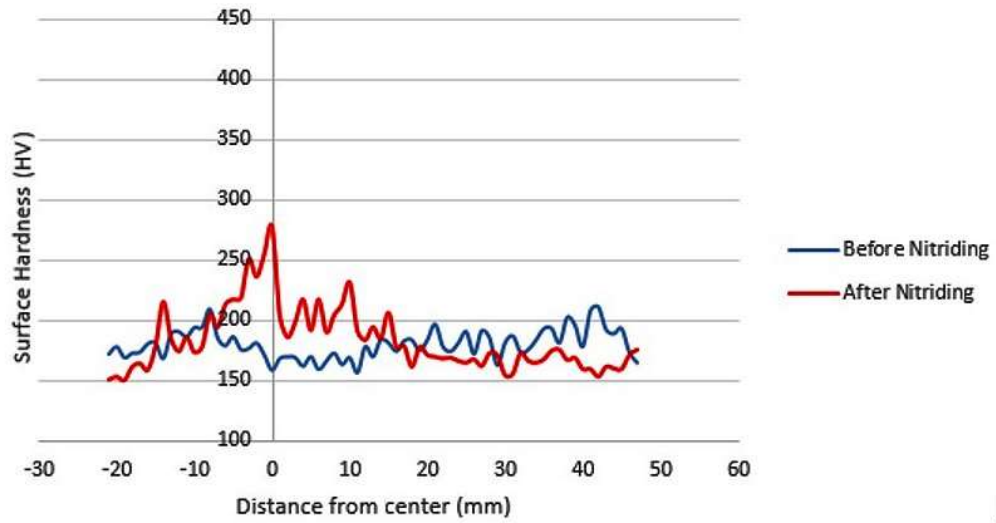


Figure 4.8 Sample 2 before and after nitriding

Sample 3 (0.5 Torr Nitrogen, 80mm from Anode)

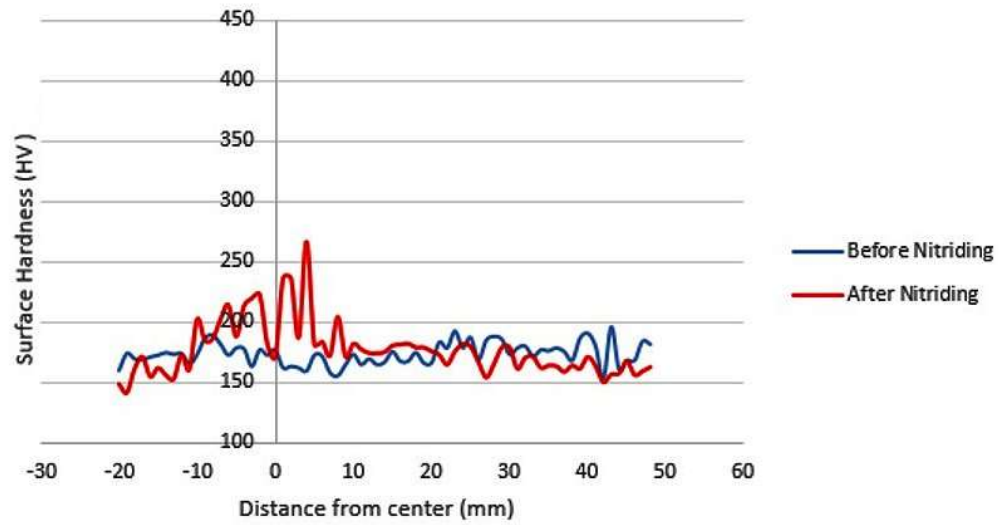


Figure 4.9 Sample 3 before and after nitriding

Sample 4 (0.5 Torr Nitrogen, 100mm from Anode)

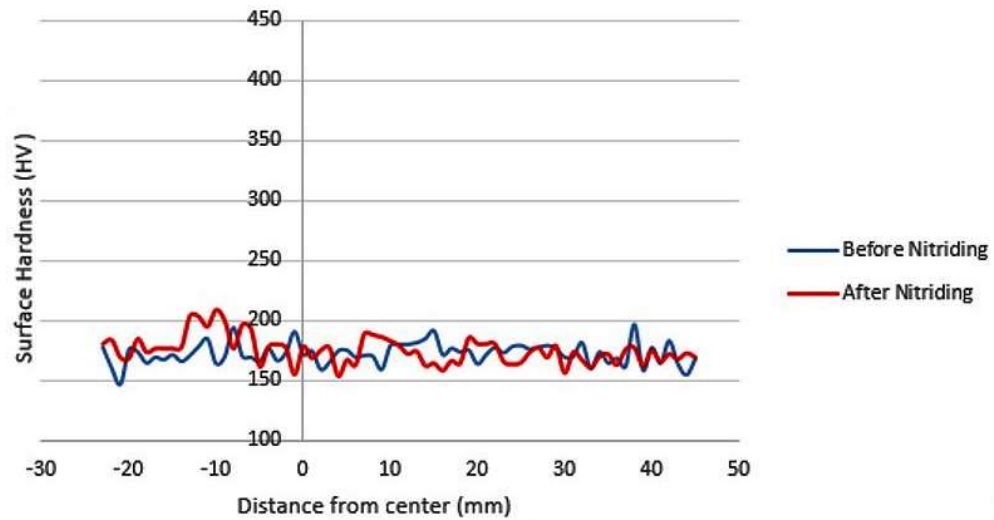


Figure 4.10 Sample 4 before and after nitriding

Sample 5 (0.5 Torr Nitrogen, 120mm from Anode)

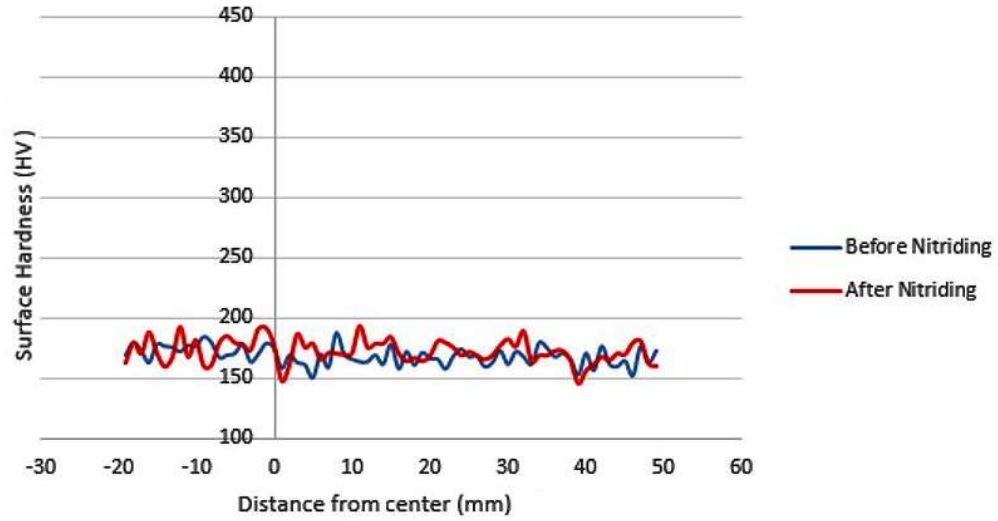


Figure 4.11 Sample 5 before and after nitriding

Sample 6 (1.0 Torr Nitrogen, 40mm from Anode)

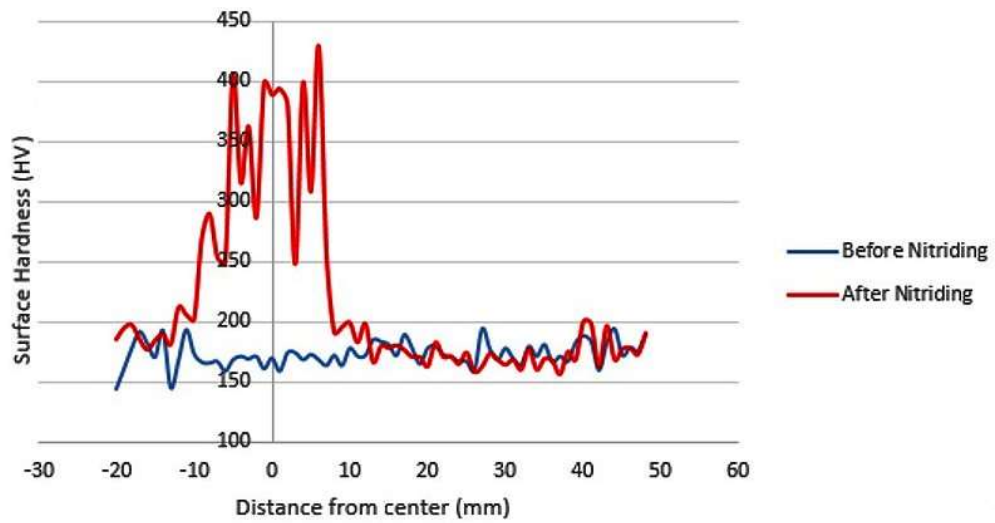


Figure 4.12 Sample 6 before and after nitriding

Sample 7 (1.0 Torr Nitrogen, 60mm from Anode)

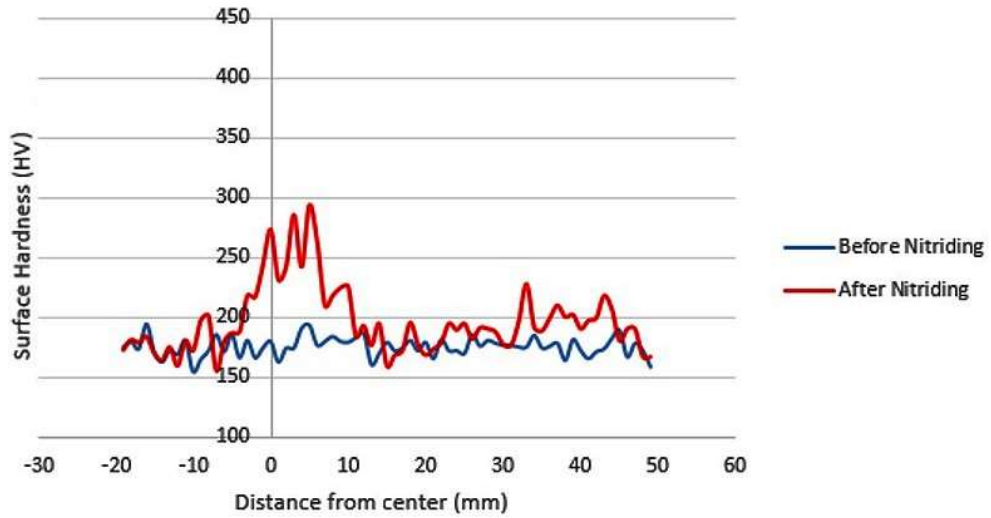


Figure 4.13 Sample 7 before and after nitriding

Sample 8 (1.0 Torr Nitrogen, 80mm from Anode)

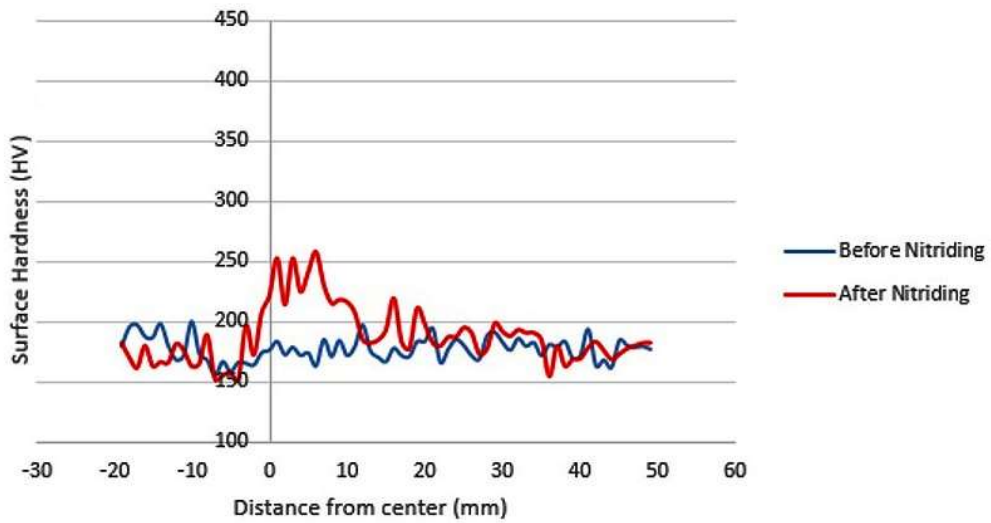


Figure 4.14 Sample 8 before and after nitriding

Sample 9 (1.0 Torr Nitrogen, 100mm from Anode)

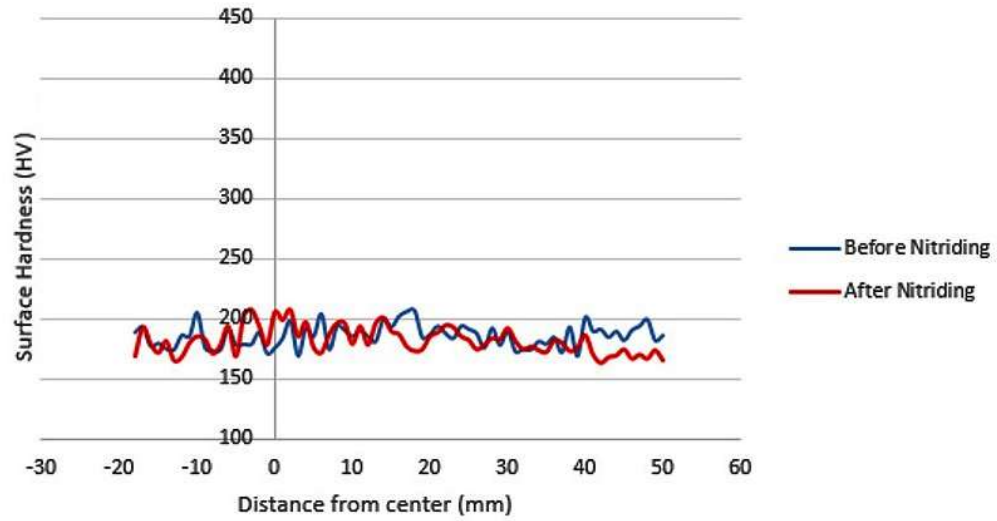


Figure 4.15 Sample 9 before and after nitriding

Sample 10 (1.0 Torr Nitrogen, 120mm from Anode)

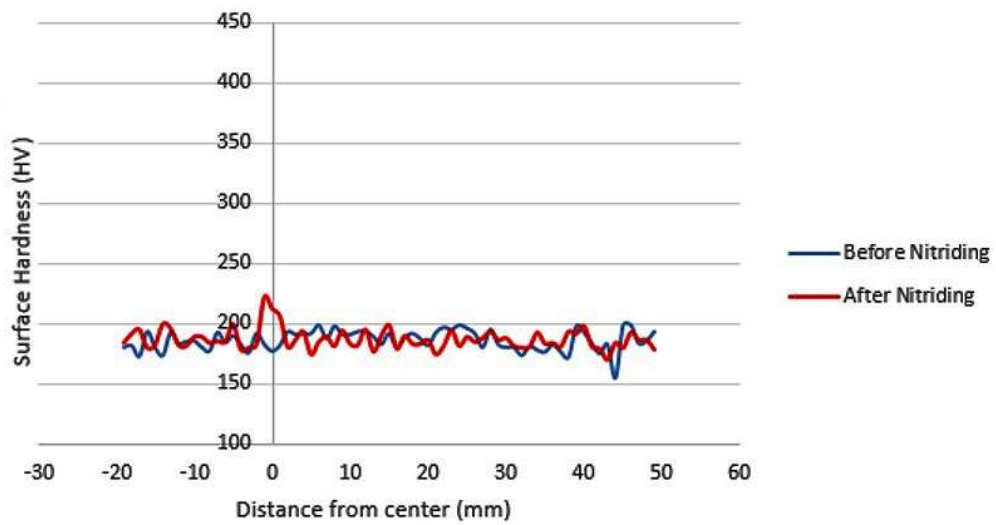


Figure 4.16 Sample 10 before and after nitriding

Sample 11 (1.5 Torr Nitrogen, 40mm from Anode)

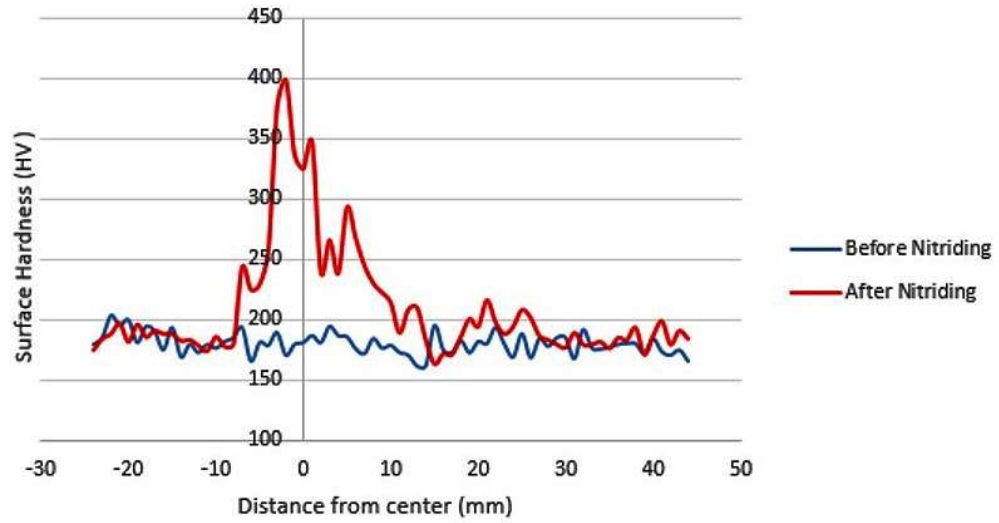


Figure 4.17 Sample 11 before and after nitriding

Sample 12 (1.5 Torr Nitrogen, 60mm from Anode)

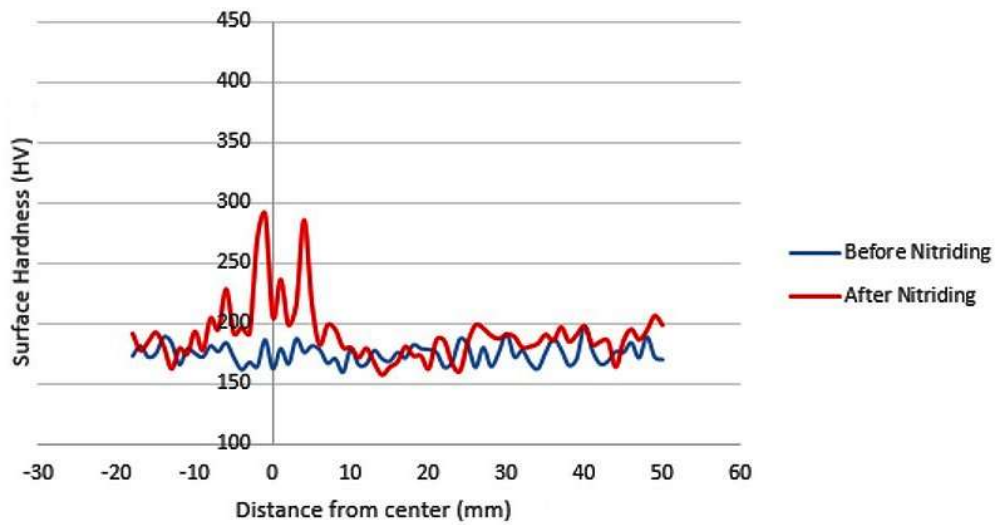


Figure 4.18 Sample 12 before and after nitriding

Sample 13 (1.5 Torr Nitrogen, 80mm from Anode)

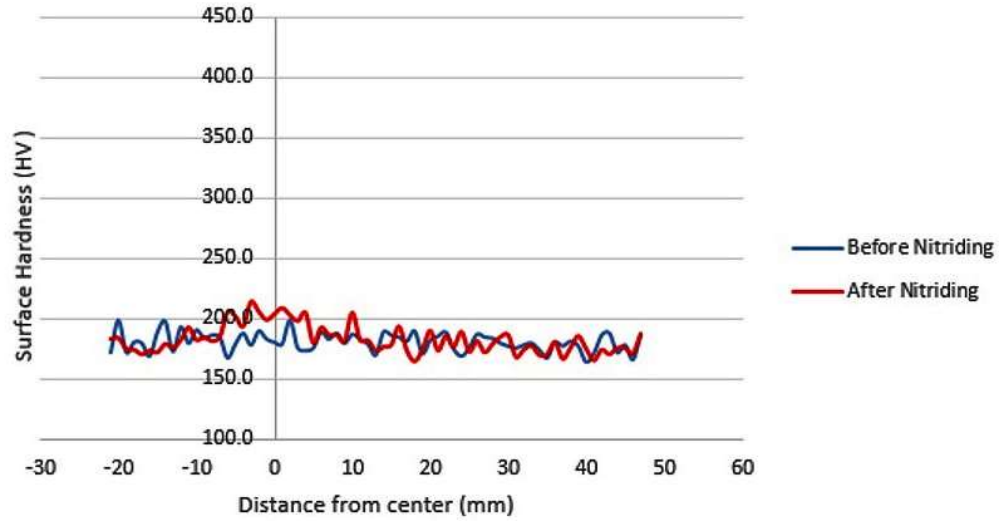


Figure 4.19 Sample 13 before and after nitriding

Sample 14 (1.5 Torr Nitrogen, 100mm from Anode)

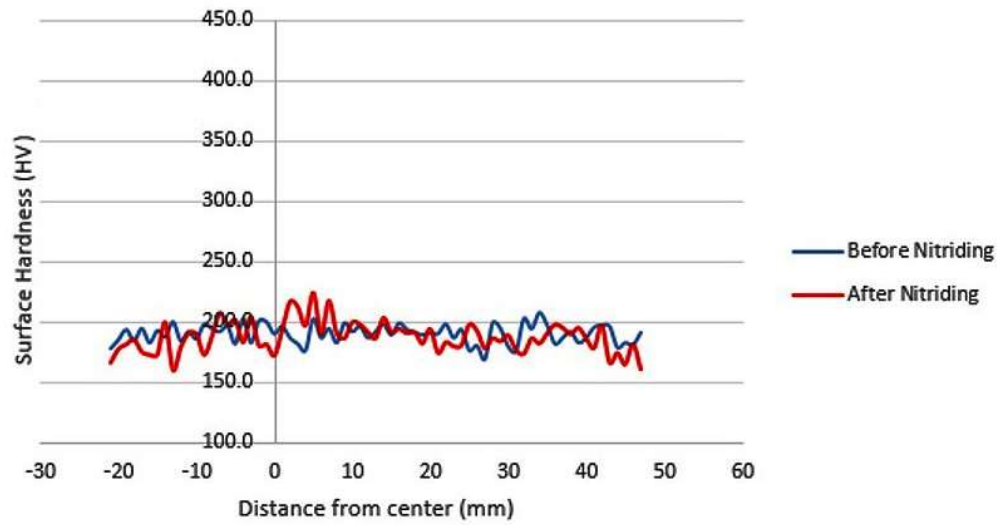


Figure 4.20 Sample 14 before and after nitriding

Sample 15 (1.5 Torr Nitrogen, 120mm from Anode)

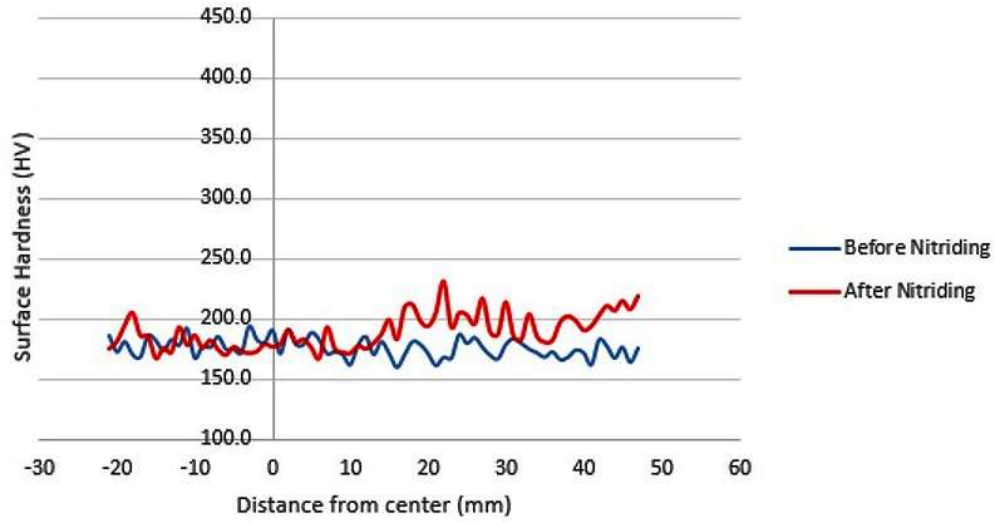


Figure 4.21 Sample 15 before and after nitriding

Sample 16 (2.0 Torr Nitrogen, 40mm from Anode)

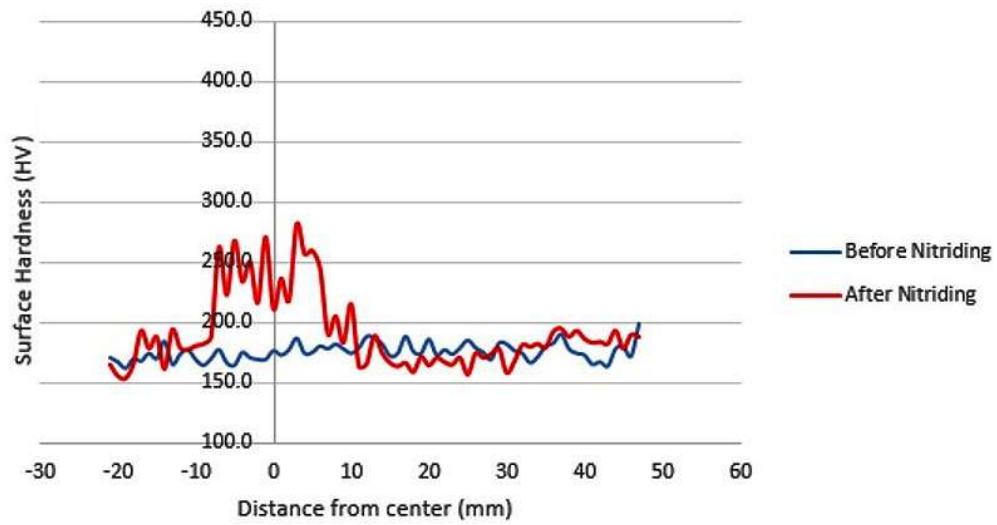


Figure 4.22 Sample 16 before and after nitriding

Sample 17 (2.0 Torr Nitrogen, 60mm from Anode)

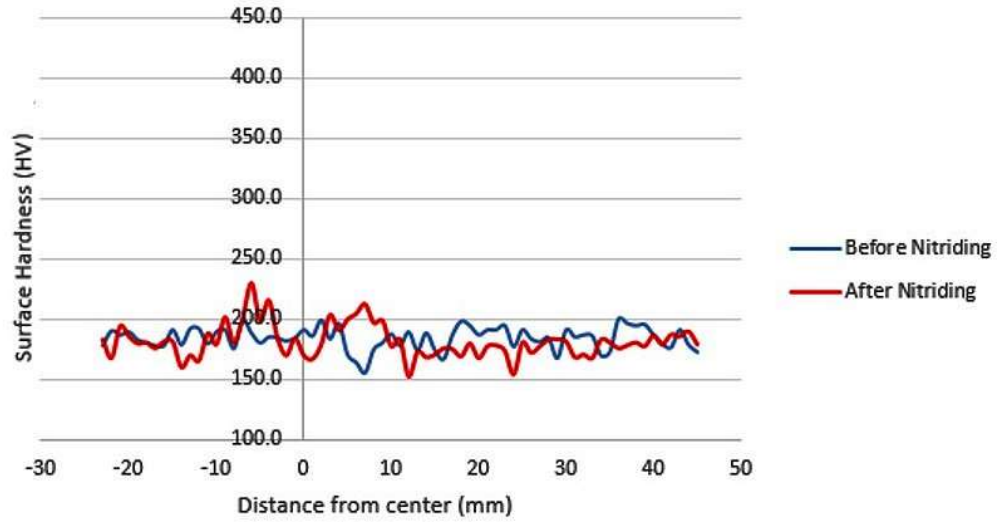


Figure 4.23 Sample 17 before and after nitriding

Sample 18 (2.0 Torr Nitrogen, 80mm from Anode)

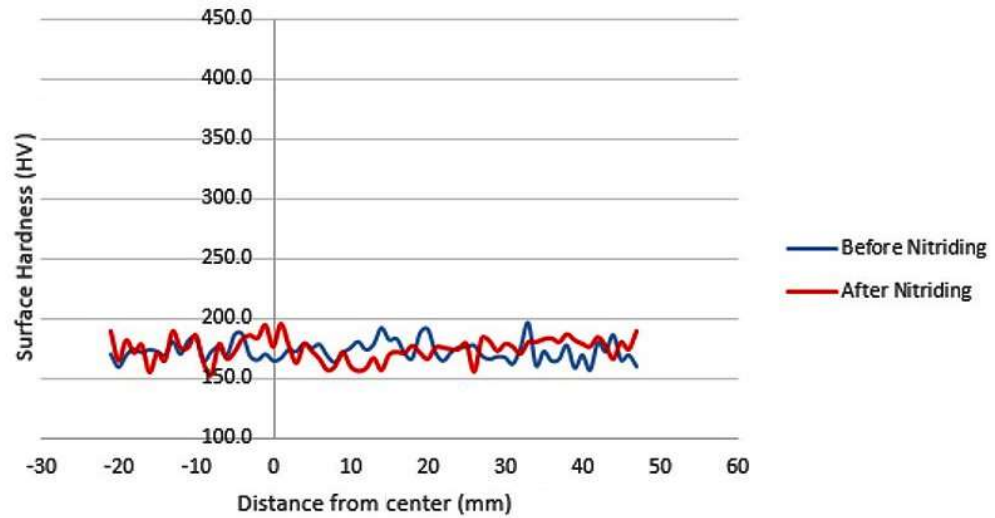


Figure 4.24 Sample 18 before and after nitriding

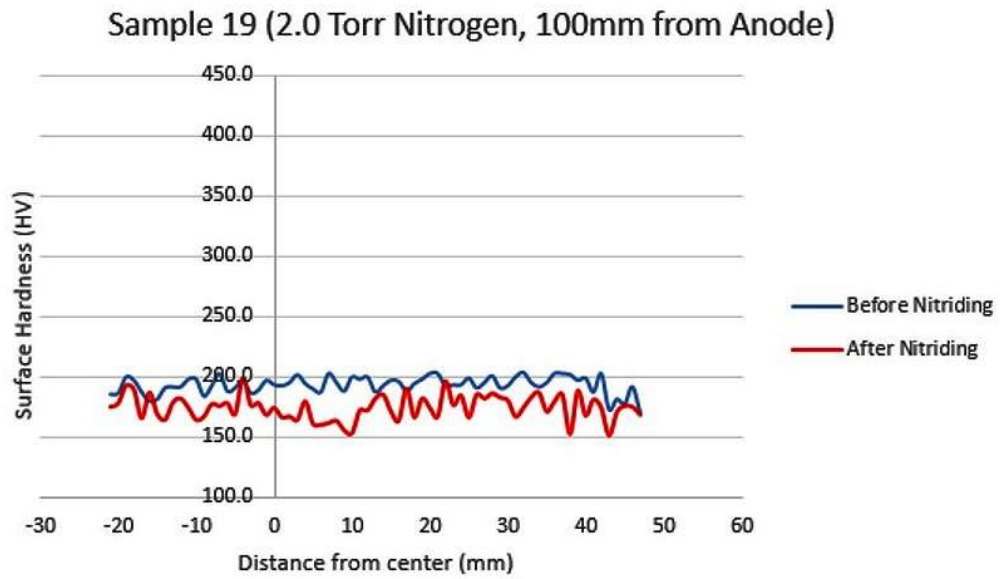


Figure 4.25 Sample 19 before and after nitriding

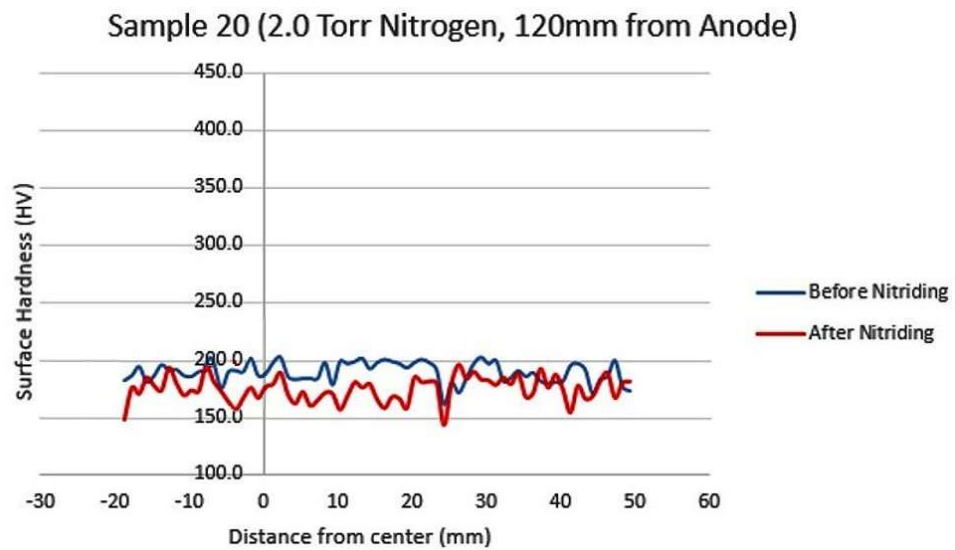


Figure 4.26 Sample 20 before and after nitriding

4.6 Hardness variation among samples of the same operating pressures

By comparing the samples of the same operating pressures and plotting their hardness on the same graph, it can be easily seen that the anode distance has a profound effect on the hardness (Figures 4.27 to 4.30).

Comparison of Hardness data with Pressure, 0.5 Torr

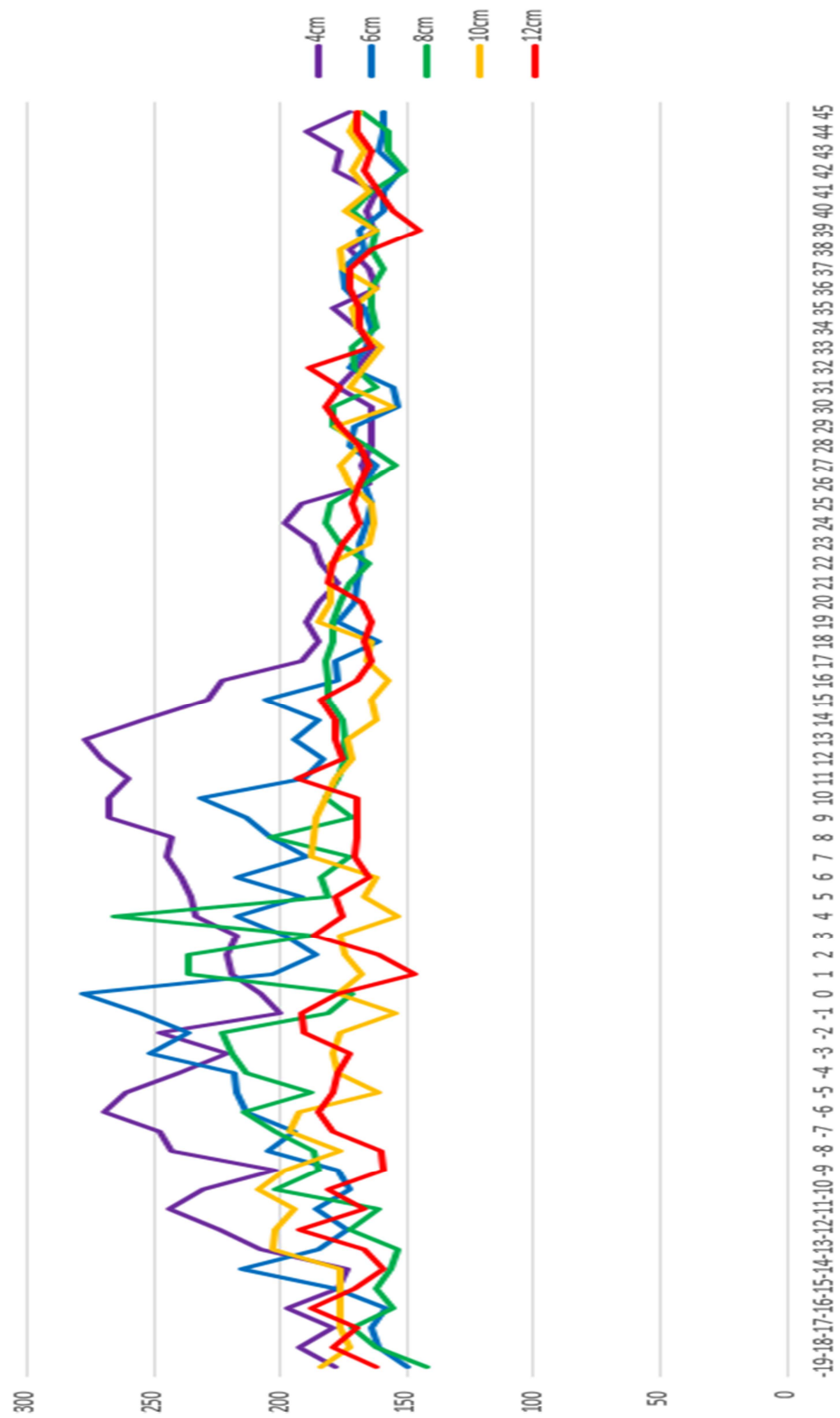


Figure 4.27 Comparison of hardness profile with irradiation distance at pressure 0.5 Torr

Comparison of Hardness data with Pressure, 1 Torr

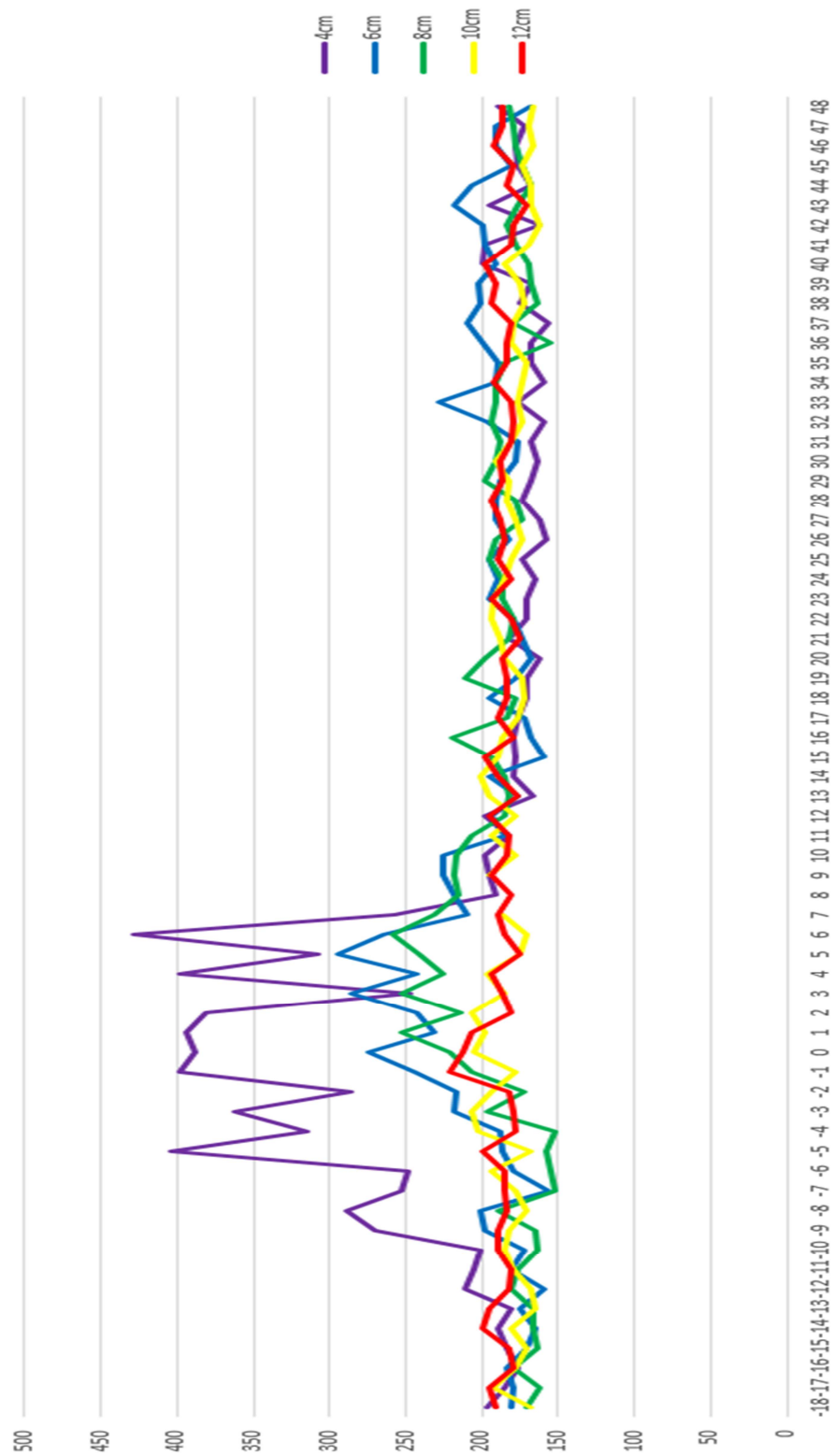


Figure 4.28 Comparison of hardness profile with irradiation distance at pressure 1.0 Torr

Comparison of Hardness data with Pressure, 1.5 Torr

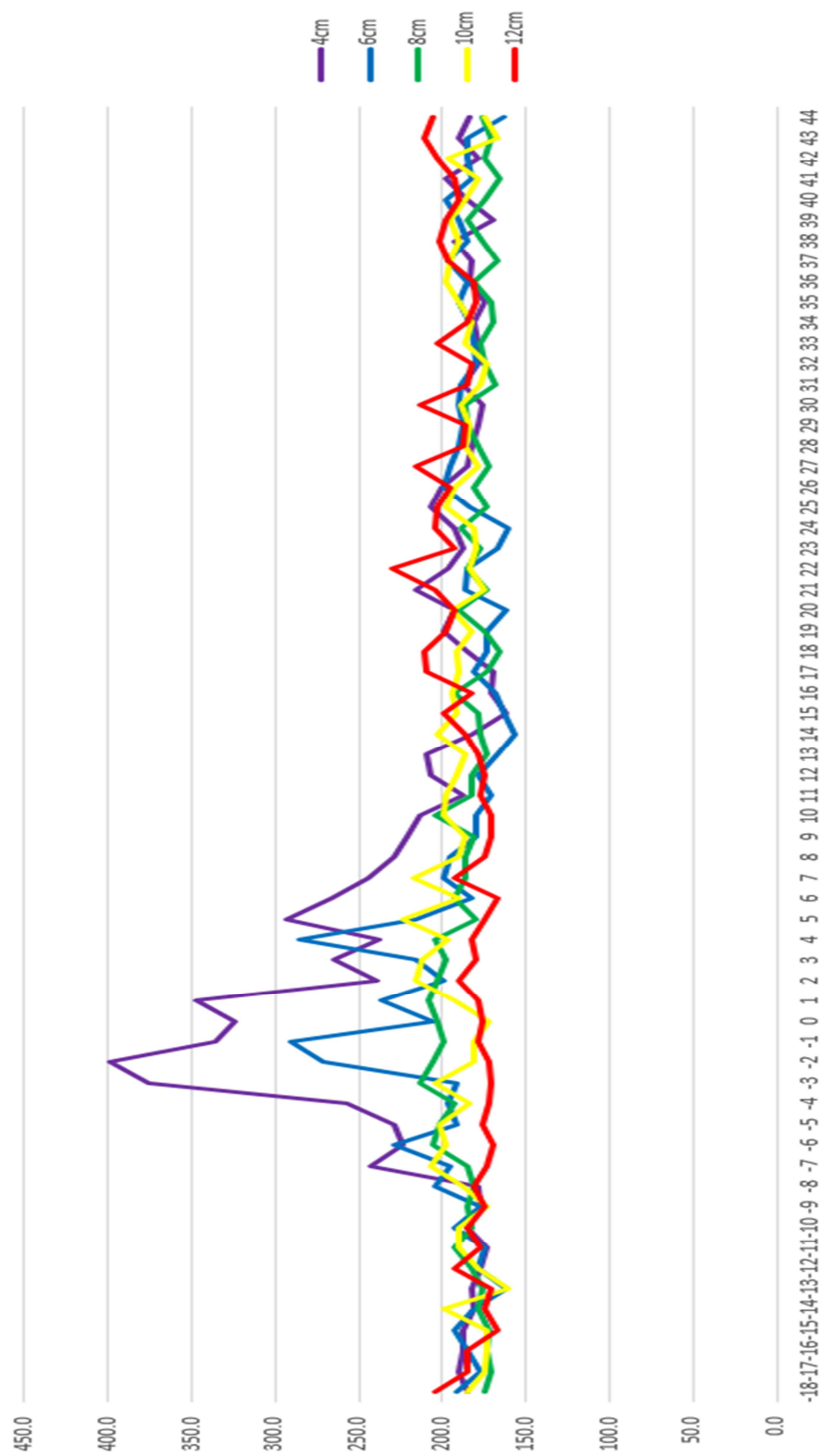


Figure 4.29 Comparison of hardness profile with irradiation distance at pressure 1.5 Torr

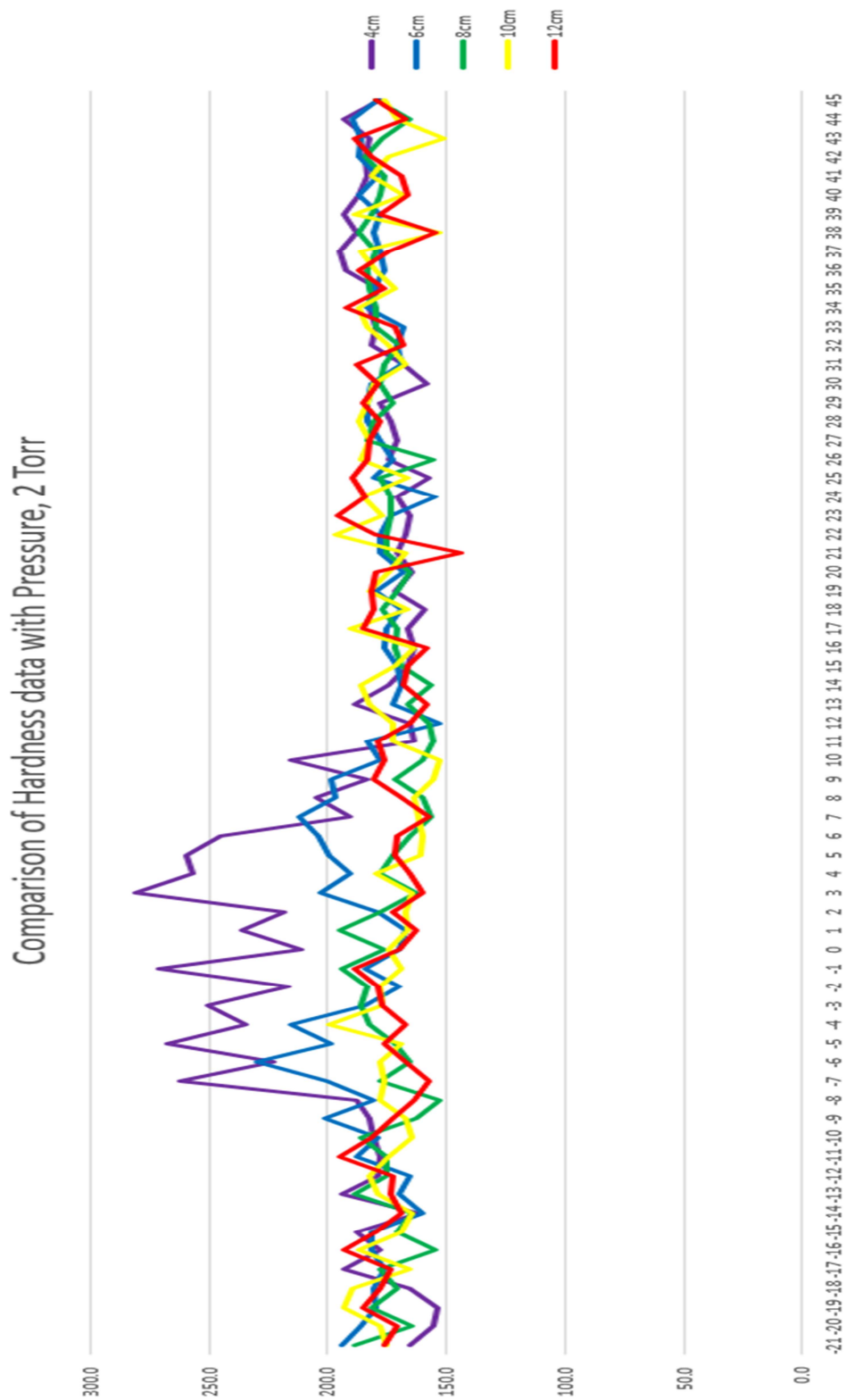


Figure 4.30 Comparison of hardness profile with irradiation distance at pressure 2.0 Torr

The graphs for Figure 4.27 to Figure 4.30 show that the hardening effect by the plasma focus nitriding tend to be strongest around the positional range -7 to +7 mm from the centre '0' position. Once out of this range, the hardening effect tapers off rapidly. Thus, the hardening effect is felt only in an area about the size of a small coin. This method of nitriding can therefore be considered a "spot nitriding" process. The higher hardness value at this circular spot is due to the ion beam focusing onto the spot due to the current pinch and this has led to the spot receiving most of the plasma ion beam energy. This circular region of the spot roughly corresponds to visually observed Ring 1 of Figure 4.1. This circular region will be referred to as the "central spot" in this thesis even though it is not the centre of the test sample. However, it is the location of the centre of the ion beam shot.

Another observation that can be made is that the anode distance has an effect on the surface hardening. Generally, the graphs 4.27 to 4.30 show that the closer, the anode distance, the better is the hardening effect.

4.7 Hardness variation with both pressure and anode distance

Twenty steel samples have been nitrided by the dense plasma focus machine where the distance of the anode to the steel target was varied. The distances were set at 40, 60, 80, 100 and 120 mm. In addition to that, the nitrogen pressure in the chamber was also varied with different pressure nitrogen settings of 0.5, 1.0, 1.5 and 2.0 Torr. Then the hardness readings were taken along the length of the sample at 1 mm intervals.

One way to show the effect of all three variables is to create a colour coded hardness contour diagram. This is shown in Figure 4.31 which expressed the variation of hardness with pressure and anode distance.

The arrangement of the contour diagram is such that the vertical axis denotes the vertical distance of the test sample from the anode. The horizontal axis denotes the nitrogen pressure at which the ion beam was fired. The hardness is read by noting the colour and comparing it to the hardness colour strip on the right edge of the diagram.

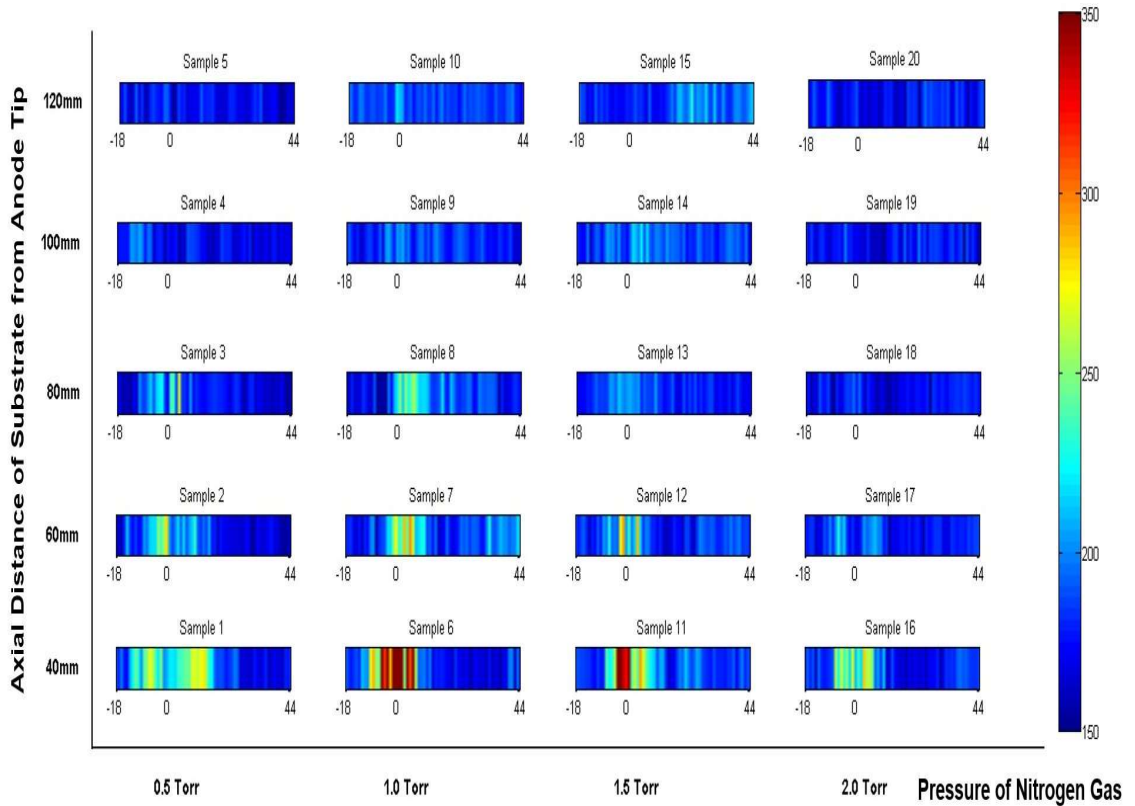


Figure 4.31 Variation of hardness with pressure and anode distance

From the colour contour diagram of Figure 4.31, the greatest hardness found in the samples tend to hover around the ‘0’ position where the ion beam struck the sample. Looking at the colour contours, it is obvious that the greatest improvement in hardness is found in the sample placed 40 mm from the anode and nitrided at 1.0 Torr.

Comparing the results row by row, the most promising results were displayed by the row of samples placed 40 mm from the anode. The hardness diminished as the distance from the anode was increased.

Again, looking at Figure 4.31 and comparing the results column by column, the samples operated at 1 Torr (second column of samples from the left) appear to do better than the samples operated at other pressures.

4.8 Average hardness variation at central spot

The colour contour hardness diagram of Figure 4.31 compares the hardness across the length of the sample. It is also useful to compare the results at the central

spot where most of the hardening takes place. For this purpose, the hardness readings for 15 positions for each sample, from the position -7 mm to +7 mm at 1 mm intervals, were taken and then averaged out. This is shown in Figure 4.32.

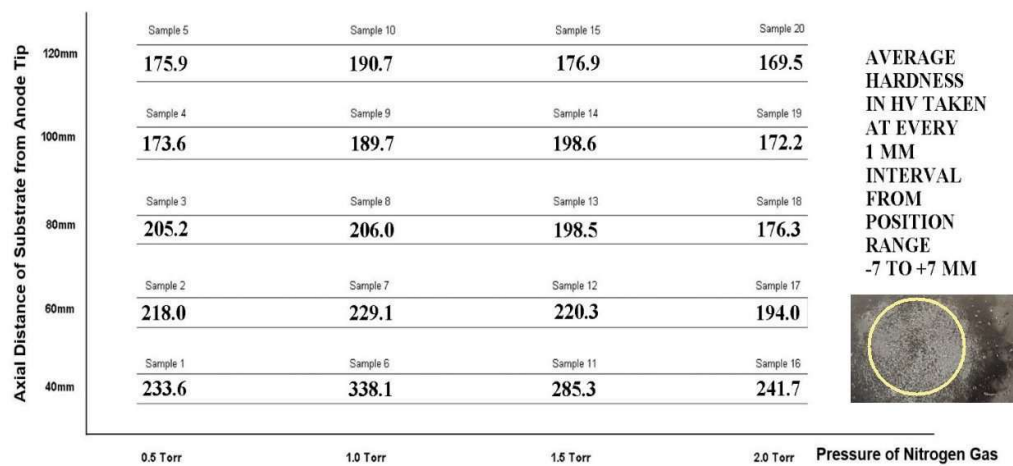


Figure 4.32 Average hardness at the central spot

It was mentioned before that the hardness prior to nitriding was in the range of 170 to 190 HV. Looking at Figure 4.32, at an anode distance of 60 mm (2nd row from the bottom), there was slight increase in hardness but that could hardly be called a significant increase. The only significant increase in hardness came from the bottom row of 40 mm anode distance. Again, it was the 1.0 Torr pressure that delivered the best results among all the pressures used.

4.9 Other observations

In the chamber of the plasma focus device, the ion beam impinges onto the mild steel target with great energy. When a steel target is hit with an energetic beam, it undergoes heating because the energy is dissipated as heat. The steel target cools in the vacuum chamber slowly as it is not taken out of the chamber while waiting for the next ion beam shot. Essentially, this process whereby the steel is subjected to heating and slow cooling is akin to heat treatment. A solid metal is composed of tiny little crystallites or grains. The grains are randomly oriented and contact each other at surfaces called the grain boundaries. High temperatures will cause an increase in size of grains in a metal. The grain size increases and is accompanied by a reduction in the

number of grains per volume. The larger the grain size, the softer the metal becomes. This is widely known as the Hall–Petch relationship.

In the plasma focus device, two processes are going on at the same time: nitriding and heat treatment. The effect of nitriding will cause the metal to become harder while the effect of heat treatment will cause the metal to become softer. If the effect of the nitriding is greater than the effect of the heat treatment, then the net effect is that the metal undergoes an increase in hardness. However, if the effect of the nitriding is less than the effect of heat treatment, the metal will undergo a reduction in hardness.

In Figures 4.25 and 4.26 (samples 19 and 20), the hardness of the samples appears to have reduced after nitriding. These two samples were fired at 2 Torr and at a far anode distance of 100 and 120 mm respectively. In section 4.7, we have seen that hardness diminished as the anode distance is increased. In addition, the samples fired at 2 Torr appear to have less hardening than that of other three pressures in Figure 4.31. It will be shown later in section 4.11 that the ion beam at 2 Torr has the lowest beam energy of all. With the disadvantage of high anode distance and a 2 Torr pressure, there is a likelihood that the effect of the nitriding is less than the effect of heat treatment. Thus it is not surprising to observe that the samples in Figures 4.25 and 4.26 have undergone a reduction in hardness.

In Figure 4.21 (sample 15 at 1.5 Torr, 120 mm anode distance) there appears to be an anomaly. The hardness improvement is not at the usual central spot but appear to be away from the centre. For this particular sample, a visual inspection of the surface (sample 15 in Table 4.1) yields an interesting observation. Not only is the central spot not as well defined as that of other samples, the beam centre position appears to have shifted to the right. Out of the 30 shots, a fair number of shots could have landed on the far right. There is always an expectation that the beam will naturally aim in a direction axial to the anode and thus move centrally upwards. However, there is no beam guiding mechanism in the plasma focus machine so this expectation of a perfect aim may not always be accurate. If the aim is off by a little bit, the effect is magnified with a greater anode distance. Generally, a shot of moving particles is subjected to the phenomena of shot dispersion and I think the ion beam will also be no different. The further the anode distance, the more the beam particles

become dispersed. The two factors of an imperfect aim accompanied by a shot dispersion will be more much evident at 120 mm than at 40 mm anode distance. The visual inspection appears to indicate that this was what happened to sample 15. The lesson to be learned from this experience is that one should not attempt nitriding at a 120 mm anode distance.

4.10 Application in machining aluminium

An application of this method may be possible in the production of cutting tools for dry machining in the aluminium machining industry. Machining of aluminium products does not require a cutting tool that is very hard because aluminium has a hardness of around 110 to 120 HV only. Any sharp metal tool that is harder than aluminium should be capable of cutting it. In fact, a tool of several hundred HV (Vickers hardness value) should be sufficient to carry out the cutting operation as it is several times harder. This required hardness value is easily achievable using the plasma focus machine to nitride cheap low carbon steel.

Machining aluminium does however pose a problem that is not found in the machining of many other materials. Aluminium chips may adhere strongly to the cutting edge of the tool, leading to tool breakage. If the surface of the cutting tool is textured, this adhesion is considerably reduced. The surface of the tool is textured in the form of micro dimples or linear grooves and has been found to decrease cutting forces, coefficient of friction and cutting temperature. Textured surface improved the crater wear resistance by serving as (i) a micro-reservoir for a cutting fluid and (ii) a micro-trap for wear debris [60]. If the surface of the tool is smooth, then grooves can be cut into the surface using laser technology in order to produce a textured surface.

The dense plasma focus machine can harden a steel tool and at the same time impart a surface texture to it in the same setup (Teh [61]). The ion beam introduces nitrides into the steel target and at the same time it erodes the surface to produce tiny grooves on the surface. This is what is required to produce a textured cutting tool. The advantage is that both effects are achieved in one setup and using only one piece of equipment.

Thus, this method is highly suitable for producing a textured cutting tool such as that shown in Figure 4.33. Cutting tools come in all shapes and sizes and the tool need not be limited to the shape shown in Figure 4.33.

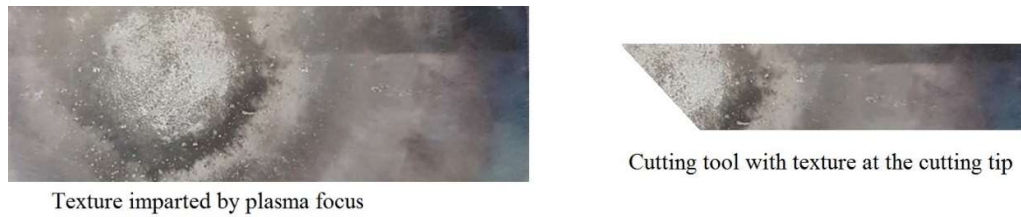


Figure 4.33 Textured cutting tool shape

Using this method, a mild steel bar has its end shaped into a desired cutting edge and then placed in a plasma focus machine for nitriding. The advantage of this method is that the ion beam can impart a hardness increase as well as a surface texture onto the cutting edge in one setup.

A test cut was carried out using one of the nitrided steel samples as a cutting tool as shown in Figure 4.34. The textured surface was coated with a bit of oil for lubrication.

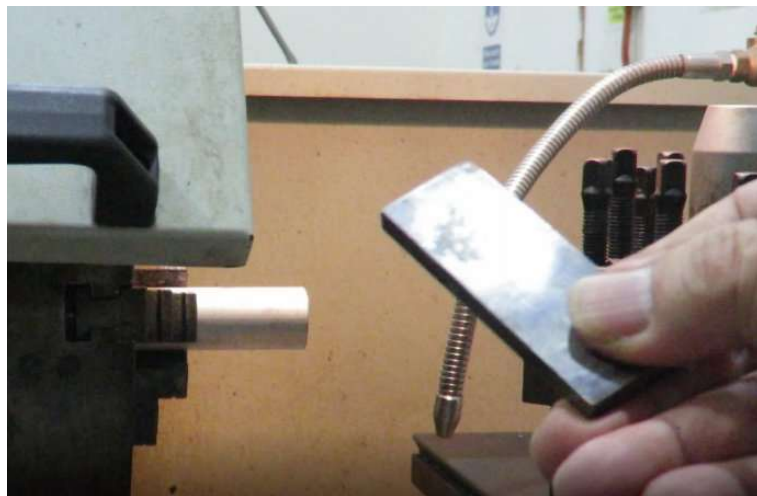


Figure 4.34 Nitrided test sample used as cutting tool

It was then clamped into the tool holder of a lathe machine so that it can be used as a cutting tool as shown in Figure 4.35. An aluminium rod was fixed into the lathe spindle and used as a work piece.

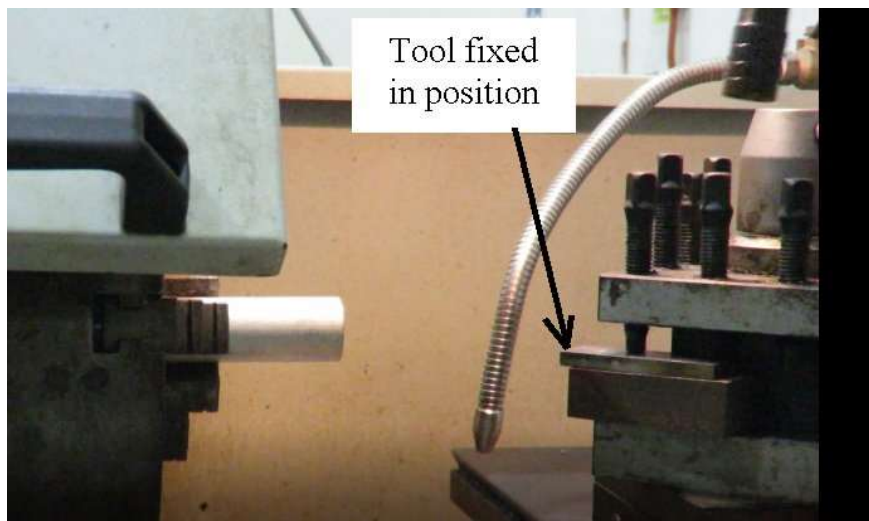


Figure 4.35 Tool fixed in the tool holder and ready for cutting

The spindle was turned on and the tool was fed into the aluminium work piece. Figure 4.36 shows the cutting in progress.

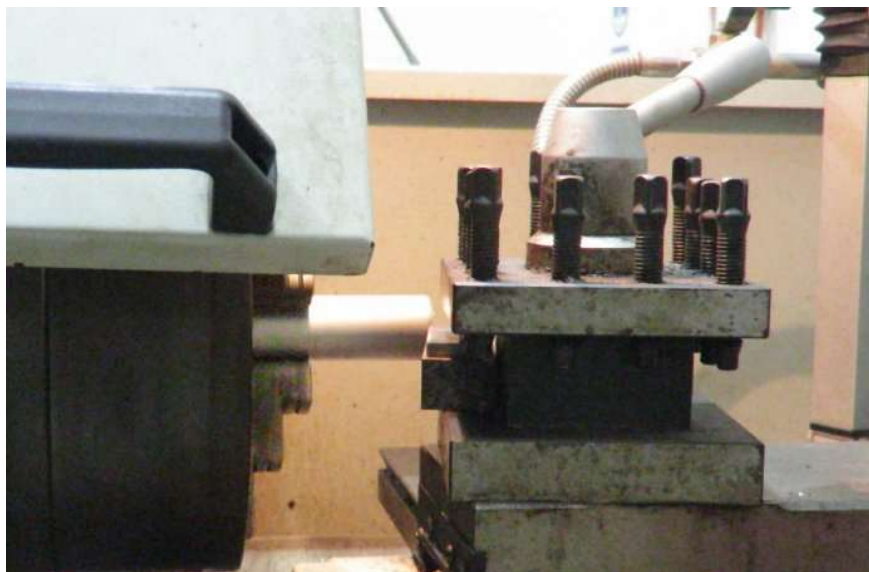


Figure 4.36 Cutting in progress

The result of the cutting is shown in Figure 4.37



Figure 4.37 Turned aluminium workpiece

The cutting was easy and there was no evidence of aluminium sticking to the rake face of the tool. Thus it is demonstrated that the dense plasma focus machine is capable of turning out a textured tool.

4.11 Ion Beam analysis using the Lee Model Code

In a numerical study done jointly with A. Singh [62], the Lee model code was used to perform numerical experiments [62-69] in an attempt to correlate the beam energy with the physical hardness results. This is possible when the capacitor bank parameters are determined [70] and then fed into the Lee code together with the other operating parameters. In conjunction with this work we note that [73] in parallel with the laboratory work there has been extensive theoretical, analytical and numerical work on the plasma focus which could be traced back to the original one-fluid formulation of piston-like ‘snowplow’ model of Rosenbluth [72-76] to 2-D two-fluid magnetohydrodynamic models [77] and three-fluid magnetohydrodynamic models [78,79]. Kinetic models were extended to fully kinetic simulations [80-83] giving perhaps the most advanced simulations of the plasma focus at the expense of considerable theoretical sophistication and computing resources. On the other hand, simpler methods with varying degrees of utility had been used by others [84-91]. The Lee code [92-94, 44] uses a relatively simple approach and yet is able to achieve the widest range of applications in plasma focus computations.

The machine used in this project is a conventional Mather type machine known as the UNU/ICTP PFF (United Nations University/International Centre for Theoretical Physics Plasma Fusion Facility) [95]. It has a capacitance of 30 μF , static inductance of 114 nH, a circuit resistance of 13 m Ω and an anode length of 16 cm with a radius of 0.95 cm. The anode is surrounded by cathodes arranged in a circle having a radius of 3.2 cm measured from its centre.

The 6 phase model of the Lee Code (version RADPFV6.1) is configured as the INTI PF by entering the capacitor bank, tube and operational parameters. The computed total current waveform is fitted to the measured waveform by adjusting the model factors f_m , f_c , f_{mr} and f_{cr} one by one, till the computed waveform agrees with the measured waveform [55-56, 95-97]. With the variation in operating pressure, the following results shown Figure 4.38 and 4.39 with regards to the number of ions and the beam energy with each shot are obtained.

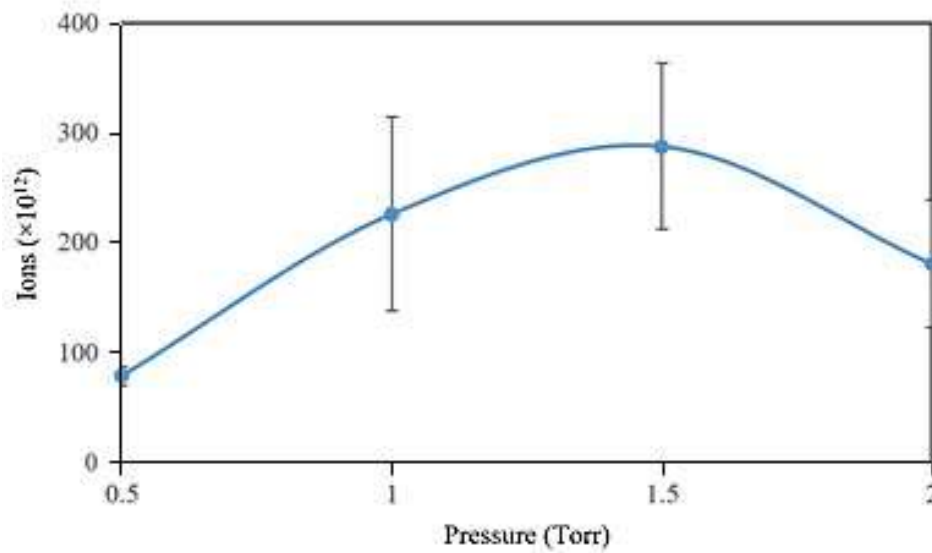


Figure 4.38 Number of ions vs pressure. Source [61]

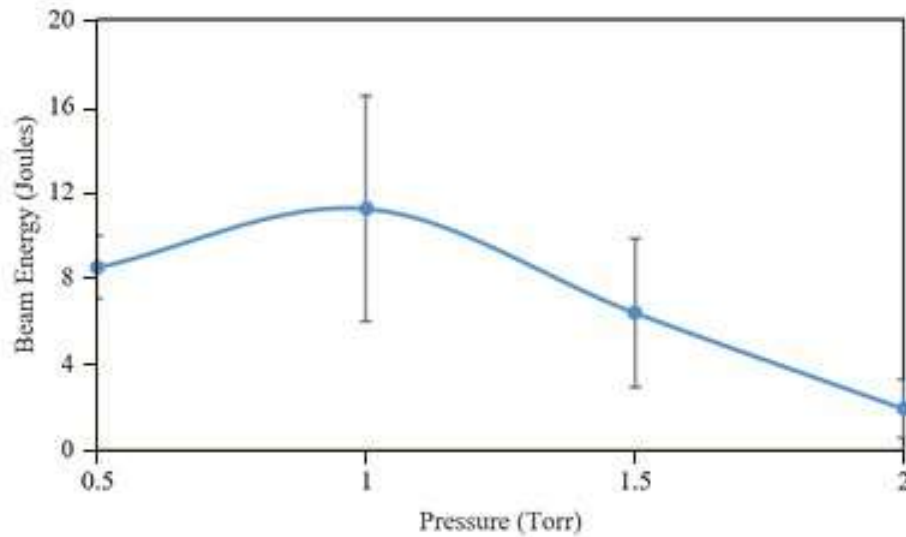


Figure 4.39 Beam energy vs pressure. Source [61]

From figures 4.38 and 4.39, it can be seen that the number of ions per shot reached a peak at 1.5 Torr while the beam energy reached at peak at 1 Torr. From figure 4.31, it is noted that surface hardness peaked at 1 Torr, which is coincidentally at the same pressure reading as the peak of beam energy. The observation that the peak of beam energy coincides with the peak of hardness can be explained by the idea that greater beam energy makes it easier to implant nitrides into the steel which thus resulted in greater surface hardness. Thus the fact that the hardness of the samples treated at 2.0 Torr is less than those treated at 1 and 1.5 Torr can be explained by the fact that the beam energy available at 2.0 Torr is less than the beam energy available at 1 and 1.5 Torr.

If the beam energy was the sole determinant of hardness, then the hardness at 0.5 Torr will be greater than the hardness at 1.5 Torr. However, this is not the case because the hardness at 1.5 Torr is greater. This indicates that the beam energy is not the sole determinant for hardness and therefore we can conclude that the number of ions is also a factor for hardness. This is acceptable and does not negate the observed fact that the pressure for peak hardness coincides with the pressure where the greatest beam energy is obtained.

CHAPTER 5

CONCLUSIONS AND FUTURE WORK

5.1 Conclusions

The surface treatment experiment was executed using a Mather-type dense plasma focus machine which successfully modified the properties of AISI 1020 low carbon steel. The plasma focus nitriding experiment was done by using different nitrogen pressures, different anode firing distances and a fixed number of plasma shots for each sample. There were a total 20 steel samples being nitrided for this project. The nitrogen pressures used were 0.5 Torr, 1 Torr, 1.5 Torr and 2 Torr. The firing distances were set at 40 mm, 60 mm, 80 mm, 100 mm and 120 mm. The nitrided steels were tested with a Micro Vickers hardness tester to study the variation of pressure and anode firing distances on the hardness value. This approach has been found to yield results to allow one to conclude that there is indeed a relationship between the chamber pressure and anode firing distances on the hardness value of the steel targets.

The first objective of this research is to determine the variation of surface hardness caused by different nitrogen pressure in the plasma focus device. Among the nitrided steel samples, the maximum hardness reading is obtained from Sample 6 at 429.1 HV. The hardness value obtained after nitriding is more than double that before nitriding. We can conclude that for best results, the nitrogen pressure in the chamber must be kept at 1 Torr which appears to be the optimum pressure. When the pressure is decreased or increased from this 1 Torr optimum pressure, the hardening effect is decreased.

The second objective is to determine the optimal firing distance to achieve maximum hardness. The best results are obtained at the firing distance of 40 mm from the anode. When the distance is increased, the hardening effect tapers off. This is hardly surprising as the ion beam will become more dispersed as it travels further away from the anode.

The third objective is to determine the hardness distribution on the substrate after surface modification by the plasma focus device. It has been found that, after nitriding, the hardest area on the steel samples are found within the central spot which

is roughly circular in shape with a radius of 9 mm. Once out of this central spot, the hardness effect tapers off rapidly.

The last objective is to determine if there is a characteristic of the ion beam that affects the surface hardness the most. The Lee Model Code is utilized to determine if there is a relationship between the ion beam energy and number of ions per shot on the hardness value of the nitrided steels. The operation at 1 Torr had the highest beam energy as shown in the computation discussed in section 4.11. This 1 Torr pressure also yields the highest hardening result. The beam energy thus serves as a good logical explanation for the hardening effect. It is conceivable that the high beam energy level at 1 Torr somehow made it easier to implant nitrogen ions into the steel surface, thus resulting in optimum hardening. Thus, one can conclude that a higher beam energy contributes better to the effectiveness of the nitriding process. From a logical viewpoint, both the beam energy and a number of nitrogen ions must be present in order for nitriding to take place. A high beam energy without any nitrogen ions present will not result in nitriding. Similarly, a large number of nitrogen ions without sufficient beam energy to implant it into the target surface will also not result in nitriding. Both the beam energy and the nitrogen ions need to be present before nitrogen implantation can take place. What this research has shown is that, for low carbon mild steel, the point of greatest hardness improvement coincides with the point of highest beam energy.

5.2 Recommendations

From this research, it can be noted that the use of the plasma focus device for nitriding purposes has two very distinct features when compared with nitriding results using other methods. Firstly, the surface of the nitrided steel is textured with furrows and tiny overlapping pits on the surface. Secondly, the hardness effect is confined to only a small area (just a few cm^3). In other words, this method results in spot nitriding rather than blanket nitriding. However, this method is suitable for the production of textured tools where only the nose of the tool is required to be sufficiently hard. The advantage of this method is the fact that the DPF imparts a texture to the surface makes the tool suitable for usage as a textured tool in the dry machining of aluminium parts.

5.3 Future work

There has been limited experimentation to correlate the hardness improvement with the number of ion beam shots in this project. Some preliminary experimentation has indicated that the hardness increases with the number of ion beam shots. It is logical to assume that the more the shots, the greater will be the hardening effect. It is also logical to think that nothing improves indefinitely and at some point, increasing the number of ion beam shots will not result in any further increase in surface hardness. Thus, future researchers may want to pursue the following:

- (i) To determine the trend of increase in hardness with the number of shots.
- (ii) To determine an optimum number of shots for surface hardness.
- (iii) To do qualitative tests on nitriding for one step hardening-texture application on a cutting tool for the machining of aluminium, specifically tests on frictional forces and tool wear rates.

REFERENCES

- [1] Rawat, R. S., Chew, W. M., Lee, P., White, T., & Lee, S. (2003). "Deposition of Titanium Nitride Thin Films on Stainless Steel - AISI 304 Substrates Using A Plasma Focus Device." *Surface and Coatings Technology*, 173(2-3), 276-284.
- [2] Bernal, A., 2006. "Investigation on Nitriding with Emphasis in Plasma Nitriding Process, Current Technology and Equipment", *Materials Processing*, Royal Institute of Technology – KTH, Stockholm
- [3] ASM Heat Treating Society "One Minute Mentor: Plasma Nitriding", online, date accessed 23 Aug 2018. Available from: https://www.asminternational.org/web/hts/news/newswire/-/journal_content/56/10192/27077810/NEWS
- [4] Totten, G. E. & Liang, H., 2004. "Surface Modification and Mechanisms." 1 ed. New York: Marcel Dekker Inc.
- [5] Borthakur, T. K. et al., 1999. Surface "Hardening of High Carbon Steel by Plasma Focus Nitriding." *Surface Engineering*, 15(1), pp. 55-58.
- [6] Shafiq, M. et al., 2008. "Dense Plasma Focus-Assisted Nitriding of AISI-304." *Radiation Effects & Defects in Solids*, 163(9), p. 729–736.
- [7] Al-Hawat, S., Soukieh, M., Kharoub, M. A., & Al-Sadat, W. (2010). "Using Mather-type plasma focus device for surface modification of AISI304 Steel." *Vacuum*, 84, 907-912.
- [8] Gyanendra Singh Goindi, Prabir Sarkar. (2017) "Dry machining: A step towards sustainable machining-Challenges and future directions." Department of Mechanical Engineering, Indian Institute of Technology, Ropar, India.
- [9] Donguk Park. (2012) "The Occupational Exposure Limit for Fluid Aerosol Generated in Metalworking Operations: Limitations and Recommendations" *Safety and Health at Work* Volume 3, Issue 1, March 2012, Pages 1-10

- [10] E. Demirbas, M Kobya (2017) “Operating cost and treatment of metalworking fluid wastewater by chemical coagulation and electrocoagulation processes”. *Process safety and environmental protection* 105 (2017) 79-90
- [11] E. Benedicto, D. Carou, E.M. Rubio (2017) “Technical, Economic and Environmental Review of the Lubrication/Cooling Systems used in Machining Processes”. *Procedia Engineering* 184 (2017) 99-116
- [12] KK Gajrani, S Suresh, MR Sankar (2018) “Environmental friendly hard machining performance of uncoated and MoS₂ coated mechanical micro-textured tungsten carbide tools”. *Tribology International* 125 (2018) 141-155
- [13] T. Sugihara, T. Enomoto (2012) “Improving anti-adhesion in aluminium alloy cutting by micro stripe texture”. *Precision Engineering* 36 (2012) 229-237
- [14] P. Rathod, S. Aravindan, V Rao (2016) “Performance Evaluation of Novel Micro-textured Tools in Improving the Machinability of Aluminum Alloy (Al 6063)”. *Procedia Technology* 23 (2016) 296-303
- [15] T. Obikawa, A. Kamio, H Takaoka, A. Osada (2011) “Micro-texture at the coated tool face for high performance cutting”. *International Journal of Machine Tools & Manufacture* 51 (2011) 966-972
- [16] Y. Liu, L. Liu, J. Deng, R. Meng, X. Zou, F. Wu (2017) “Fabrication of micro-scale textured grooves on green ZrO₂ ceramics by pulsed laser ablation”. *Ceramics International* 43 (2017) 6519-6531
- [17] R. Sasi, K. Subbus, I.A. Palani(2017) “Performance of laser surface textured high speed steel cutting tool in machining of Al7075-T6 aerospace alloy ”. *Surface & Coatings Technology* 313 (2017) 337-346
- [18] X.L. Chen, B.Y. Dong, C.Y. Zhang, M. Wu, Z.N. Guo (2018) “Jet electrochemical machining of micro dimples with conductive mask”. *Journal of Materials Processing Tech.* 257 (2018) 101-111
- [19] P. Koshy, J. Tovey (2011) “Performance of electrical discharge textured cutting tools”. *CIRP Annals-Manufacturing Technology* 60 (2011) 153-156
- [20] M. Sedlacek, B. Podgornik, A. Ramalho, D. Cesnik (2017) “Influence of geometry and the sequence if surface texturing process on tribological properties”. *Tribology International* 115 (2017) 268-273

- [21] D. Arulkirubakaran, V. Senthilkumar (2017) "Performance of TiN and TiAlN coated micro-grooved tools during machining of Ti-6Al-4V alloy". *Int. Journal of Refractory Metals and Hard Materials* 62 (2017) 47-57
- [22] J. Kummel, D. Braun, J. Gibmeier, J. Schneider, C. Greiner, V. Schulze, A. Wanner (2015) "Study on micro texturing of uncoated cemented carbide cutting tools for wear improvement and built-up edge stabilization". *Journal of Materials Processing Technology* 215 (2015) 62-70
- [23] J. Deng, Z. Wu, Y. Lian, T. Qi, J. Cheng(2012) "Performance of carbide tools with textured rake-face filled with solid lubricants in dry cutting processes". *Int. Journal of Refractory Metals and Hard Materials* 20 (2012) 164-172
- [24] V. Sharma, P.M. Pandey(2016) "Recent advances in turning with textured cutting tools: A review". *Journal of Cleaner Production* 137 (2016) 701-715
- [25] S. Niketh, G.L. Samuel(2017) "Surface texturing for tribology enhancement and its application on drill tool for the sustainable machining of titanium alloy". *Journal of Cleaner Production* 167 (2017) 253-270
- [26] Wiesemann, K. (2012, May). "A Short Introduction to Plasma Physics", online, date accessed August 24, 2018, from http://www.aept.ruhr-uni-bochum.de/media/attachments/files/2014/09/Lecture_Notes_Senec_2012.pdf
- [27] Piel, A. (2010). "Definition of the Plasma State. In *Plasma Physics: An Introductory to Laboratory, Space, and Fusion Plasmas*" (pp. 29-43). Springer-Verlag Berlin Heidelberg.
- [28] Rawat, R. S. (2015). "Dense Plasma Focus – From Alternative Fusion Source to Versatile High Energy Density Plasma Source for Plasma Nanotechnology". *Journal of Physics: Conference Series*, 591(1).
- [29] Lee, S., & Saw, S. H. (2017) "From Beam-target to Thermonuclear Fusion in the Dense Plasma Focus pinch: Energy throughput scaling". Talk presented at the University of York on 17 Nov 2017.
- [30] Saw, S. H., Lee, P. C., Rawat, R. S., & Lee, S. (2009). "Optimizing UNU/ICTP PFF Plasma Focus for Neon Soft X-ray Operation." *IEEE Transactions on Plasma Science*, 1276-1282.
- [31] Lee, S. (2014). "Plasma Focus Radiative Model: Review of the Lee Model Code." *Journal of Fusion Energy*, 319-335.

- [32] Lee, S., & Saw, S. H. (2010). “Numerical Experiments Providing New Insights into Plasma Focus Fusion Devices.” *Energies* 3, 711-737.
- [33] AZO Materials. (2012). “AISI 1020 Low Carbon/Low Tensile Steel”, online, date accessed August 24 2018, from <http://www.azom.com/article.aspx?ArticleID=6114>
- [34] Substances and Technologies “Iron-carbon phase diagram”, online, date accessed September 17 2018. Available from: http://www.substech.com/dokuwiki/doku.php?id=iron-carbon_phase_diagram
- [35] Askeland, D. R., Fulay, P. P. & Wright, W. J., (2011). *The Science and Engineering of Materials*. 6th ed. Stamford: Cengage Learning Inc.
- [36] Herrmann, K. (2011). *Hardness testing*. 1st edition. Materials Park, Ohio: ASM International. pp.43
- [37] S.H. Saw, S. Lee. (2016) “Measurement of Radiative Collapse in 2.2 kJ PF: Achieving High Energy Density (HED) Conditions in a Small Plasma Focus” *Journal of Fusion Energy* (2016) 35:702–708 DOI 10.1007/s10894-016-0095-9
- [38] S. Lee, (2014). “Plasma Focus Radiative Model: Review of the Lee Model Code.” *Journal of Fusion Energy*, Volume 33, p. 319–335.
- [39] Shakonah, S. S., Ali, J., Rashid, N. A. & Chaudhary, K., (2014). “Determination of Ion Beam Properties In Nitrogen and Helium Using Mather Type Plasma Focus Device.” *Journal of Technology*, 71(5), pp. 47-49.
- [40] S Lee, S H Saw (2012) “Plasma focus ion beam fluence and flux- scaling with stored energy.” *Physics of Plasmas* 19, 112703 (2012);
- [41] S. Lee, S. H. Saw, (2013) “Plasma Focus Ion Beam Fluence and Flux—For Various Gases.” *Physics of Plasma*, Volume 20, pp. 062702-1 - 062702-9.
- [42] S Lee, S H Saw, P Lee and R S Rawat, “Numerical Experiments on Neon plasma focus soft x-rays scaling”, *Plasma Phys Controlled Fusion*, 51, 105013, DOI:10.1088/0741-3335/51/10/105013, (2009).

- [43] S H Saw, P C K Lee, R S Rawat and S Lee, “Optimizing UNU/ICTP PFF Plasma Focus for Neon Soft X-ray Operation”, IEEE Trans on Plasma Sci, 37, pp 1276-1282, DOI:10.1109/TPS.2009.2022167, (2009)
- [44] S Lee, Radiative Dense Plasma Focus Computation Package: RADPF, 2014
<http://www.plasmafocus.net/IPFS/modelpackage/File1RADPF.htm>
<http://www.plasmafocus.net/IPFS/modelpackage/File2Theory.pdf>
<http://www.plasmafocus.net/IPFS/modelpackage/UPF.htm>
- [45] S Lee, P Lee, S H Saw and R S Rawat, “Numerical Experiments on Plasma Focus Pinch Current Limitation”, Plasma Phys Controlled Fusion, 50, 065012, DOI:10.1088/0741-3335/50/6/065012, (2008)
- [46] S H Saw and S Lee, “Scaling Laws for Plasma Focus Machines from Numerical Experiments”, Energy and Power Engineering, pp 65-72, DOI:10.4236/epe.2010.21010, (2010)
- [47] S Lee and S H Saw, “Numerical Experiments Providing New Insights into Plasma Focus Fusion Devices”, Energies, 3, 4, pp 711-737, DOI:10.3390/en3040711, (2010)
- [48] S Lee and S H Saw, “Neutron scaling laws from numerical experiments”, J Fusion Energy, 27, pp 292–295, DOI: 10.1007/s 10894-008-9132-7, (2008)
- [49] S Lee, S H Saw, A E Abdou and H Torreblanca, “Characterizing Plasma Focus Devices-Role of Static Inductance- Instability Phase Fitted by Anomalous Resistances”, J Fusion Energy, 30, pp 277-282, DOI: 10.1007/s10894-010-9372-1, (2010)
- [50] S H Saw and S Lee, “Scaling the plasma focus for fusion energy considerations”, International Journal of Energy Research, 35, pp 81-88, DOI:10.1002/er.1758, (2011)
- [51] S H Saw, M Akel, P C K Lee, S T Ong, S N Mohamad, F D Ismail, N D Nawi, K Devi, R M Sabri, A H Baijan, J Ali and S Lee, “Magnetic Probe Measurements in INTI Plasma Focus to Determine Dependence of Axial Speed with Pressure in Neon”, J Fusion Energy, 31, pp 411–417, (2012)
- [52] M Akel M, Sh Al-Hawat and S Lee, “Pinch Current and Soft x-ray yield limitation by numerical experiments on Nitrogen Plasma Focus”, J Fusion Energy, 29, pp 94-99, DOI :10.1007/s10894-009-9238-6, (2010)

- [53] M Akel, Sh Al-Hawat, S H Saw and S Lee, “Numerical Experiments on Oxygen Soft X-Ray Emissions from Low Energy Plasma Focus Using Lee Model”, *J Fusion Energy*, 29, pp 223-231, DOI: 10.1007/s10894-009-9262-6, (2010)
- [54] S Lee, S H Saw, L Soto, S P Moo and S V Springham, “Numerical experiments on plasma focus neutron yield versus pressure compared with laboratory experiments”, *Plasma Phys Control Fusion*, 51, 075006, DOI:10.1088/0741-3335/51/7/075006, (2009)
- [55] T Y Tou, S Lee and K H Kwek, “Nonperturbing plasma-focus measurements in the run-down phase”, *IEEE Trans Plasma Sci*, 17, 2, pp 311–315, DOI: 10.1109/27.24641, (1989)
- [56] S P Chow, S Lee and B C Tan, “Current sheath studies in a co-axial plasma focus gun”, *Plasma Phys*, 8, pp21-31, DOI: 10.1017/S0022377800006905, (1972)
- [57] V A Gribkov, A Banaszak, B Bienkowska, A V Dubrovsky, I Ivanova-Stanik, L Jakubowski, L Karpinski, R A Miklaszewski, M Paduch, M J Sadowski, M Scholz, A Szydowski and K Tomaszewski, “Plasma dynamics in the PF-1000 device under full-scale energy storage: II. Fast electron and ion characteristics versus neutron emission parameters and gun optimization perspectives”, *Journal of Physics D: Applied Physics*, 40, no. 12, pp 3592–3607, DOI:10.1088/0022-3727/40/12/008, (2007)
- [58] H Herold, “Physics and technology of large plasma focus devices” *Laser and Plasma Technology: Third Tropical College on Applied Physics*, 30th May to 18 June, 1988. Pub. World Scientific, Singapore, edited by S Lee, pp 21-45, ISBN: 981-02-0168-0, (1988).
- [59] Arwinder Singh, TO Teh, Jalil Ali, SH Saw, S Lee (2018) “Suitability of using Lee Codes to fit a Mather, Phillipov and Hybrid Dense Plasma Focus Machines current waveform”. Paper presented at the International Conference on Innovation & Technopreneurship 2018 (ICIT 2018), 9 August 2018, Inti International University.
- [60] Tatsuya Sugihara, Toshiyuki Enomoto. Development of a cutting tool with a nano/micro-textured surface—Improvement of anti-adhesive effect by

- considering the texture patterns. Precision Engineering. 2009, Vol.33, No.4, p.425.
- [61] TO Teh, A Singh, Jalil Ali, SH Saw, S Lee (2018) "A study on the fabrication of a textured cutting tool using a plasma focus machine". Paper presented at the International Conference on Innovation & Technopreneurship 2018 (ICIT 2018), 9 August 2018, Inti International University.
- [62] Arwinder Singh, Teh Thiam Oun, Ng Xue Yinn, Ng Chee An, Wong Jun Wen, Saw Sor Heoh and Lee Sing (2018) "A Numerical Study on the Ion Production in the INTI International University Plasma Focus Machine using Nitrogen Gas". Thai Journal of Physics, 35 (1). pp. 1-9. ISSN 0857-1449
- [63] Arwinder Singh, S Lee, S H Saw (2017) "Effect of the Variation of Pressure on the Dynamics and Neutron Yield of Plasma Focus Machines." IEEE Transactions on Plasma Science, 45 (8). 2286 -2291. ISSN 0093-3813.
- [64] Arwinder Singh, S Lee (2017) "Numerical Experiments to Study the Variation of Pressure on India Bhabha Atomic Research Centre Plasma Focus." Jurnal Sains Nuklear Malaysia, 29 (2). pp. 1-9. ISSN 2232-0946.
- [65] Arwinder Singh, S Lee (2017) "Numerical study on the variation of pressure on India Bhabha Atomic Research Center (BARC) and Imperial College plasma focus machines." AIP Conference Proceedings, 1824 (1). ISSN 1551-7616.
- [66] Arwinder Singh, S H Saw, S Lee (2016) "Numerical Experiments Performed on the Imperial College Plasma Focus Machine: Dependence on Deuterium Pressure". Jurnal Fizik Malaysia, 38 (1). 01021-01031. ISSN 0128-0333.
- [67] S H Saw, S Lee, Rawat, Verma, Subedi, Khanal, Gautam, Shrestha, Arwinder Singh (2015) "Comparison of Measured Neutron Yield Versus Pressure Curves for FMPF-3, NX2 and NX3 Plasma Focus Machines Against Computed Results Using the Lee Model Code". Journal of Fusion Energy, 34 (3). pp. 474-479. ISSN 1572-9591.
- [68] Arwinder Singh, S Lee, S H Saw (2014) "Numerical experimentation on focusing time and neutron yield in GN1 plasma focus machine". International Journal of Modern Physics: Conference Series, 32. ISSN 2010-1945.

- [69] Arwinder Singh, S Lee, S H Saw (2014) “Numerical Experiments to Obtain the Scaling Laws for Neutron Yield on Mather-Type Plasma Focus Machines Below 500 Joules”. Kathmandu University Journal of Science, Engineering and Technology, 10 (2). pp. 34-41. ISSN 1816-8752.
- [70] S H Saw, S Lee, F Roy, P L Chong, Vengadeswaran, Sidik, Y W Leong, Arwinder Singh (2010) “In situ determination of the static inductance and resistance of a plasma focus capacitor bank”. Review of Scientific Instruments, 81 (5). ISSN 1089-7623.
- [71] S Lee and S H Saw, The Plasma Focus- Numerical Experiments, Insights and Applications, Chapter 3 (pages 113-232) in “Plasma Science and Technology for Emerging Economies – An AAAPT Experience” DOI 10.1007/978-981-10-4217-1_3 Edited by Rajdeep S Rawat, © Springer Nature Singapore Pte Ltd. (2017)
- [72] M. Rosenbluth, “Magnetohydrodynamics”, ed. by R. K. M. Landshoff, Stanford University Press, 57, 1957.
- [73] F. J. Fishman and H. Petscheck, (1962). “Flow model for large radius-ratio magnetic annular shock-tube operation”, Phys. Fluids 11, 632
- [74] T. D. Butler, I. Henins, F. C. Jahoda, J. Marshall and R. L. Morse, (1969) “Coaxial snowplow discharge”, Phys. Fluids 12, 1904).
- [75] K. V. Roberts and D. E. Potter, (1970) “Methods of Computational Physics, Academic”, New York,
- [76] A. A. Amsden, (1966) “Los Alamos Scientific Laboratory Report”, No.LA-3466
- [77] D. E. Potter, (1971) “Numerical studies of the plasma focus”, Phys. Fluids 14(9), 1911
- [78] S. V. Bazdenkov and V. V. Vikhrev, Sov. (1975). J. Plasma Phys. 1, 250
- [79] K. Behler and H. Bruhns, (1987). “Three-fluid magnetohydrodynamical simulation of plasma focus discharges”, Phys. Fluids 30(12), 3767
- [80] A. Schmidt, V. Tang and D. Welch, (2012). “Fully kinetic simulations of dense plasma focus Z-pinch devices”, Phys. Rev. Lett. 109(20), 205003

- [81] A. Schmidt, A. Link, D. Welch, J. Ellsworth, S. Falabella and V. Tang, (2014). “Comparisons of dense-plasma-focus kinetic simulations with experimental Measurements”, *Phys. Rev. E* 89 (6), 061101
- [82] A. Schmidt, A. Link, D. Welch, B.T. Meehan, V. Tang, C. Halvorson, M. May and E.C. Hagen, (2014). “Fully kinetic simulations of megajoule-scale dense plasma focus”, *Phys. Plasmas* 21, 102703
- [83] A. Schmidt, D. P. Higginson, S. Jiang, A. Link, A. Povilus, J. Sears, N. Benneth, D. V. Rose, D. R. Welch, (2015) “Kinetic simulations of dense plasma focus breakdown”. 57th Ann. Mtg. APS Division of Plasma Physics, Savannah, GA, LLNL-ABS-675188. Nov. 16–20, 2015.
- [84] J. H. González, A. Clause, H. Bruzzone and P. C. Florido, (2004) “A lumped parameter model of plasma focus”, *IEEE Trans. Plasma Sci.* 32(3), (1383)
- [85] D. Potter, (1978). “The formation of high-density z-pinchs” *Nucl. Fusion* 18(6), 813
- [86] J. H. González, F. R. Brollo and A. Clause, (2009) “Modeling of the dynamic plasma pinch in plasma focus discharges based in Von Karman approximations”, *IEEE Trans. Plasma Sci.* 37(11), 2178
- [87] M. Trunk, (1975). “Numerical parameter studies for the dense plasma focus”, *Plasma Phys.* 17(4), 237
- [88] V.S. Imshennik, N.V. Fillipov and T. I. Fillipova, (1973). “Similarity theory and increased neutron yield in a plasma focus”, *Nucl. Fusion* 13(6), 929
- [89] V. Vikhrev and V. D. Korolev, (2007). “Neutron generation from Z-pinchs”, *Plasma Phys. Rep.* 33(5), 356
- [90] E. J. Lerner, S. K. Murali and A. Haboub, (2011). “Theory and experimental program for the p-B11 fusion with the dense plasma focus”, *J. Fusion Energ.* 30, 367
- [91] S. K. H. Auluck, (2014). “Dense plasma focus: a question in search of answers, a technology in search of applications”, *Plasma Sci. Appl. Int. J. Mod. Phys. Conf. Ser.* 32, 1460315
- [92] S. Lee and S. H. Saw, (2010) “The Plasma Focus- Scaling Properties to Scaling Laws”. Joint ICTP-IAEA Workshop on Dense Magnetized Plasma and Plasma Diagnostics, 15 - 26 November 2010.

- [93] S. Lee, (1984) "Radiation in Plasma", edited by B. Namara. World Scientific, Singapore, Vol II, 978
- [94] S. Lee, (1985) "In Laser and Plasma Technology", edited by S. Lee, B.C. Tan, C.S. Wong and A.C. Chew. World Scientific, Singapore, 37, 64 and 387.
- [95] S. Lee, T. Y. Tou, S. P. Moo, M. A. Eissa, A. V. Gholap, K. H. Kwek, S. Mulyodrono, A. J. Smith, Suryadi, W. Usada and M. Zakauallah, (1998) "A simple facility for the teaching of plasma dynamics and plasma nuclear fusion", Am. J. Phys. 56, 66
- [96] S. Al-Hawat, M. Akel , S. Lee and S. H. Saw, (2012) "Model parameters vs gas pressure in two different plasma focus devices operated in argon and neon", J. Fusion Energ. 31, 13.
- [97] S. Lee, S. H. Saw, H. Hegazy, Jalil Ali, V. Damideh, N. Fatis, H. Kariri, A. Khubrani and A. Mahasi, (2014) "Some generalised characteristics of the electro dynamics of the plasma focus in its axial phase-illustrated by an application to independently determine the drive current fraction and the mass swept-up fraction", J Fusion Energ. 33, 235

LIST OF PUBLICATIONS

by Author in connection with this PhD

- 1) TO Teh, Arwinder Singh, Jalil Ali, X Y Ng, CA Ng, JW Wong, SH Saw, S Lee (2017) "A study on the surface hardness obtained by nitriding with a plasma focus machine". Paper presented at the 10th International Conference on Plasma Science and Applications (ICPSA 2017), 11 October 2017, Walailak University, Thailand. The paper has been accepted for publication in Vol 16 : Forthcoming Issue: Plasma Science and Applications, Walailak Journal of Science and Technology (WJST)
- 2) TO Teh, Arwinder Singh, Jalil Ali, SH Saw, S Lee (2018) "A study on the fabrication of a textured cutting tool using a plasma focus machine". Paper presented at the International Conference on Innovation & Technopreneurship 2018 (ICIT 2018), 9 August 2018, Inti International University.
- 3) Arwinder Singh, TO Teh, SH Saw, S Lee (2018) "Suitability of using Lee Codes to fit a Mather, Fillipov and Hybrid Dense Plasma Focus Machines current waveform". Paper presented at the International Conference on Innovation & Technopreneurship 2018 (ICIT 2018), 9 August 2018, Inti International University.
- 4) Arwinder Singh, TO Teh, SH Saw, S Lee (2018) "Numerical Experimentation on Argentina Nano Focus Machine". Paper presented at the International Conference on Innovation & Technopreneurship 2018 (ICIT 2018), 9 August 2018, Inti International University.
- 5) Arwinder Singh, TO Teh, XY Ng, CA Ng, JW Wong, SH Saw, S Lee (2018) "A numerical study on the ion production in the Inti International University Plasma focus machine using nitrogen gas". Thai Journal of Physics Vol 35 No.1 (2018) 1-9
- 6) TO Teh, Arwinder Singh, Jalil Ali, SH Saw, S Lee (2016) "Nitriding with dense plasma focus" Paper presented at the Seminar on Material Science: Superconductors (2016), 2 November 2016, Inti International University

- 7) TO Teh, Y Rengasamy, CJ Chiat, S Lee, SH Saw (2015) "Design aspects of a dense plasma focus machine". Paper presented at the Conference on Plasma Focus in series SPFE 2015, 5 November 2015, Inti International University
- 8) TO Teh, S Lee, SH Saw (2014) "Discussing the practical considerations in building a plasma focus machine." Paper presented at the Conference on Plasma Focus in series SPFE 2014, 20 June 2014, Inti International University

APPENDIX A

SURFACE HARDNESS READINGS

After plasma focus nitriding had been conducted on 20 steel samples, the surface hardness was measured with a Micro Vickers hardness tester using a 0.2 kgf indentation load. The hardness was measured at 1 mm intervals. The location of the centre of the ion beam shot was determined visually on the sample by inspecting the texture pattern on the sample surface. The texture pattern radiates out from a centre and this centre is taken as the centre of the ion beam shot.

The results of the hardness readings of all 20 test samples are presented in Tables 4.2 to 4.21.

Table A.1 Hardness readings for Sample 1

| Sample 1 | Nitrogen pressure 0.5 Torr, anode distance 40 mm Ion beam centre location: 21 mm | | | | | |
|------------------|---|-------------------------------------|-------|-------------------------------------|-------------------------------------|-------|
| | Before Nitriding: | | | After Nitriding: | | |
| Position (mm) | d ₁ (μm) | d ₂ (μm) | HV | d ₁ (μm) | d ₂ (μm) | HV |
| 1 | 47.5702 | 44.982 | 173 | 45.6662 | 45.7555 | 177.6 |
| 2 | 46.4695 | 46.1125 | 173.8 | 42.602 | 48.6412 | 178.4 |
| 3 | 48.1037 | 46.1125 | 167.2 | 43.792 | 43.9407 | 192.5 |
| 4 | 47.2132 | 44.3275 | 176.8 | 46.4695 | 44.5952 | 179.2 |
| 5 | 44.0895 | 45.2795 | 185.8 | 43.1375 | 43.673 | 196.9 |
| 6 | 46.6182 | 47.4512 | 167.9 | 45.7257 | 45.6067 | 177.6 |
| 7 | 46.648 | 47.5405 | 167.2 | 46.6182 | 45.696 | 173.8 |
| 8 | 44.5655 | 46.172 | 179.9 | 41.7392 | 42.959 | 207.3 |
| 9 | 46.41 | 45.9637 | 173.8 | 41.055 | 40.341 | 223.9 |
| 10 | 46.4992 | 45.0415 | 176.8 | 40.698 | 37.247 | 243.9 |
| 11 | 47.6297 | 45.934 | 169.3 | 39.5972 | 40.6385 | 230.7 |
| 12 | 47.4512 | 46.9455 | 166.5 | 43.1077 | 42.6317 | 202.5 |
| 13 | 46.2017 | 43.1307 | 177.6 | 37.247 | 40.936 | 242.9 |
| 14 | 45.101 | 46.053 | 178.4 | 36.9495 | 40.579 | 247.6 |
| 15 | 46.41 | 46.529 | 171.5 | 36.176 | 38.08 | 269.5 |
| 16 | 46.291 | 46.6182 | 171.5 | 39.9542 | 35.4917 | 261 |
| 17 | 48.1355 | 47.124 | 163.7 | 41.7392 | 36.9167 | 240.1 |
| 18 | 47.005 | 45.4282 | 173.8 | 39.7757 | 42.364 | 220.6 |
| 19 | 45.529 | 47.6596 | 167.2 | 39.3592 | 38.08 | 247.6 |
| 20 | 46.4695 | 47.124 | 169.3 | 45.934 | 40.103 | 200.6 |
| 21 | 48.8495 | 46.5587 | 163 | 38.6155 | 45.9042 | 207.3 |
| 22 | 47.3025 | 47.243 | 165.8 | 41.412 | 40.7872 | 219.6 |
| 23 | 47.5107 | 46.7075 | 167.2 | 42.126 | 39.9542 | 220.6 |
| 24 | 46.5885 | 45.5175 | 174.5 | 44.506 | 38.0205 | 217.4 |
| 25 | 46.648 | 46.1125 | 172.3 | 41.1442 | 38.6155 | 233 |
| 26 | 47.0347 | 46.5885 | 169.3 | 41.2037 | 38.1692 | 235.3 |
| 27 | 46.291 | 45.0415 | 177.6 | 40.6385 | 38.2882 | 238.9 |
| 28 | 44.0895 | 45.7555 | 184 | 38.1395 | 39.7162 | 245.1 |
| 29 | 45.3687 | 46.767 | 174.5 | 42.245 | 36.1165 | 242.6 |
| 30 | 44.9275 | 45.5175 | 181.5 | 39.0022 | 35.4025 | 268 |
| 31 | 46.2612 | 44.506 | 179.9 | 38.6155 | 35.7595 | 268 |

| | | | | | | |
|----------------|---------|---------|-------|---------|---------|-------|
| 32 | 46.6777 | 47.9272 | 165.8 | 41.5012 | 34.034 | 259.6 |
| 33 | 46.7372 | 45.9637 | 172.3 | 37.366 | 36.9792 | 270.9 |
| 34 | 45.57 | 45.5472 | 178.4 | 36.3545 | 36.8007 | 276.9 |
| 35 | 44.3275 | 44.2382 | 189 | 38.9427 | 37.4552 | 254.2 |
| 36 | 46.1125 | 45.0712 | 178.4 | 40.579 | 40.0732 | 228.4 |
| 37 | 46.2612 | 45.22 | 177.6 | 40.579 | 41.055 | 222.8 |
| 38 | 44.387 | 44.387 | 188.1 | 46.9752 | 41.055 | 191.6 |
| 39 | 46.291 | 46.0232 | 173.8 | 44.2085 | 45.3985 | 184.8 |
| 40 | 46.7372 | 44.9522 | 176.8 | 43.8812 | 44.5655 | 189.9 |
| 41 | 45.696 | 44.5952 | 182.3 | 41.8582 | 47.6892 | 184.8 |
| 42 | 47.4512 | 46.4612 | 168.6 | 48.1057 | 43.3457 | 177.6 |
| 43 | 45.3687 | 46.291 | 176.8 | 45.8745 | 43.911 | 184 |
| 44 | 46.9752 | 47.0942 | 167.9 | 43.554 | 45.577 | 186.5 |
| 45 | 48.7305 | 46.7372 | 163 | 42.1557 | 44.387 | 197.8 |
| 46 | 47.8082 | 46.2315 | 167.9 | 45.339 | 42.7507 | 191.6 |
| 47 | 45.6067 | 46.9455 | 173 | 47.2132 | 47.5107 | 165.1 |
| 48 | 47.0942 | 45.3092 | 173.8 | 43.673 | 50.4262 | 167.9 |
| 49 | 45.5175 | 47.1835 | 172.3 | 49.1172 | 45.3985 | 163.7 |
| 50 | 46.1125 | 45.458 | 176.8 | 46.1125 | 48.8495 | 164.4 |
| 51 | 46.767 | 47.4215 | 167.2 | 45.7555 | 49.147 | 164.4 |
| 52 | 45.0117 | 44.9225 | 183.2 | 45.4282 | 46.0232 | 177.6 |
| 53 | 48.2842 | 46.9752 | 163.7 | 47.3917 | 46.291 | 169.3 |
| 54 | 46.5587 | 44.5052 | 178.4 | 48.4677 | 46.886 | 163 |
| 55 | 47.481 | 47.1537 | 165.8 | 46.6182 | 46.8265 | 170.1 |
| 56 | 48.2545 | 45.9042 | 167.2 | 46.2017 | 44.8927 | 179.2 |
| 57 | 46.3802 | 46.529 | 171.5 | 47.719 | 47.8082 | 162.3 |
| 58 | 45.5472 | 46.6182 | 174.5 | 47.0942 | 47.6595 | 165.1 |
| 59 | 46.4695 | 43.9042 | 173.8 | 46.6486 | 45.9935 | 173 |
| 60 | 47.3917 | 46.3207 | 168.6 | 47.7487 | 47.719 | 163 |
| 61 | 44.4762 | 45.1605 | 184.8 | 47.6297 | 47.481 | 165.8 |
| 62 | 47.3917 | 45.3686 | 172.3 | 50.3667 | 46.3985 | 161.7 |
| 63 | 46.9455 | 46.3802 | 170.1 | 45.1605 | 46.1125 | 178.4 |
| 64 | 47.719 | 46.1125 | 168.6 | 43.9705 | 47.8677 | 176 |
| 65 | 44.9522 | 44.5357 | 185.6 | 44.03 | 44.5952 | 189.9 |
| 66 | 44.7142 | 43.6432 | 189.9 | 45.4282 | 47.243 | 173 |
| 67 | 45.2795 | 43.4945 | 188.1 | 46.053 | 50.3072 | 159.6 |
| 68 | 46.2612 | 46.9752 | 170.8 | 47.4512 | 46.3505 | 168.9 |
| 69 | 45.4282 | 43.8812 | 185.6 | 46.7967 | 46.3802 | 170.8 |
| Average | | | 174.1 | | | |

Table A.2 Hardness readings for Sample 2

| Sample 2 | Nitrogen pressure 0.5 Torr, anode distance 60 mm Ion beam centre location: 22 mm | | | | | |
|------------------|---|-------------------------------------|-------|-------------------------------------|-------------------------------------|-------|
| | Before Nitriding: | | | After Nitriding: | | |
| Position (mm) | d ₁ (μm) | d ₂ (μm) | HV | d ₁ (μm) | d ₂ (μm) | HV |
| 1 | 46.7075 | 45.9935 | 172.3 | 50.575 | 48.8197 | 150.2 |
| 2 | 45.458 | 45.7555 | 178.4 | 47.8082 | 50.7832 | 152.6 |
| 3 | 46.7372 | 46.886 | 169.3 | 48.7305 | 50.813 | 149.6 |
| 4 | 45.577 | 47.0347 | 173 | 46.7075 | 49.385 | 161 |
| 5 | 46.815 | 45.5157 | 173.8 | 46.5587 | 48.552 | 163.7 |
| 6 | 44.5952 | 44.8035 | 180.7 | 46.9152 | 498,907 | 158.3 |
| 7 | 47.7785 | 45.9042 | 181.5 | 45.6365 | 45.6067 | 178.4 |
| 8 | 47.7785 | 45.9637 | 168.6 | 43.5837 | 39.3592 | 215.4 |
| 9 | 44.387 | 44.1192 | 189 | 44.863 | 44.6845 | 184.8 |
| 10 | 44.863 | 43.3457 | 190.7 | 46.6777 | 45.6365 | 173.8 |
| 11 | 44.6845 | 44.4465 | 186.5 | 40.6087 | 48.8197 | 185.6 |
| 12 | 43.1077 | 44.268 | 194.2 | 46.6777 | 45.9637 | 173 |
| 13 | 43.8217 | 43.6432 | 194.2 | 44.7142 | 46.5885 | 177.6 |
| 14 | 40.7277 | 43.435 | 209.3 | 44.7737 | 40.4005 | 204.6 |
| 15 | 45.4282 | 43.9705 | 185.6 | 41.5905 | 45.8447 | 194.2 |
| 16 | 45.458 | 45.5472 | 179.2 | 40.1327 | 43.2267 | 213.3 |
| 17 | 44.387 | 44.8927 | 186.5 | 40.0137 | 42.5127 | 217.4 |
| 18 | 45.5175 | 46.3207 | 176 | 36.1462 | 46.172 | 218.5 |
| 19 | 45.4877 | 46.1422 | 176.8 | 40.698 | 36.1462 | 251.5 |
| 20 | 44.5655 | 45.9042 | 181.5 | 40.9955 | 38.1097 | 236.5 |
| 21 | 45.6067 | 47.4215 | 171.5 | 43.911 | 32.3382 | 255.5 |
| 22 | 47.7487 | 48.8495 | 159 | 35.9677 | 37.0982 | 278.4 |
| 23 | 47.3025 | 46.529 | 168.6 | 45.8745 | 39.5675 | 203.4 |
| 24 | 46.6182 | 46.767 | 170.1 | 51.2592 | 38.1692 | 185.6 |
| 25 | 47.1537 | 46.529 | 169.3 | 45.3985 | 41.0252 | 198.7 |
| 26 | 47.6595 | 48.0165 | 162.3 | 42.1557 | 40.4302 | 217.4 |
| 27 | 46.7967 | 46.6777 | 170.1 | 42.1557 | 45.8447 | 191.6 |
| 28 | 47.4215 | 49.0577 | 159.6 | 45.101 | 37.4552 | 217.4 |
| 29 | 46.9157 | 47.4215 | 166.5 | 43.3457 | 45.0415 | 189.9 |
| 30 | 46.0827 | 46.4397 | 173 | 44.3572 | 40.7575 | 204.4 |
| 31 | 47.6595 | 47.5107 | 163.7 | 41.5905 | 41.888 | 213.3 |

| | | | | | | |
|----------------|---------|---------|-------|---------|---------|-------|
| 32 | 46.053 | 47.5107 | 169.3 | 39.8352 | 40.1327 | 231.8 |
| 33 | 48.3735 | 48.8197 | 157 | 45.1307 | 43.1077 | 190.7 |
| 34 | 46.0827 | 45.1902 | 178.4 | 45.7257 | 44.3572 | 183.2 |
| 35 | 47.481 | 45.934 | 170.1 | 44.2977 | 43.1375 | 194.2 |
| 36 | 45.22 | 44.625 | 184 | 44.387 | 45.1902 | 184.8 |
| 37 | 44.5952 | 45.9042 | 181.5 | 41.412 | 43.316 | 206.3 |
| 38 | 45.2795 | 46.8265 | 174.5 | 43.1375 | 48.314 | 177.6 |
| 39 | 44.9522 | 45.0117 | 183.2 | 46.3505 | 44.8332 | 178.4 |
| 40 | 44.5952 | 45.1902 | 184 | 47.7305 | 48.4925 | 161 |
| 41 | 45.9935 | 45.934 | 175.3 | 35.358 | 45.9637 | 177.6 |
| 42 | 44.982 | 44.8332 | 184 | 43.4053 | 49.8015 | 170.8 |
| 43 | 43.435 | 43.3457 | 196.9 | 46.4695 | 47.1835 | 169.3 |
| 44 | 44.8927 | 46.3207 | 178.4 | 47.5702 | 46.4695 | 167.9 |
| 45 | 46.2017 | 45.934 | 174.5 | 47.7785 | 45.934 | 168.6 |
| 46 | 44.5655 | 45.7852 | 181.5 | 47.719 | 47.0347 | 165.8 |
| 47 | 43.911 | 44.387 | 190.7 | 48.5222 | 46.3802 | 164.4 |
| 48 | 45.577 | 47.3025 | 172.3 | 47.2727 | 46.9157 | 167.2 |
| 49 | 42.84 | 45.1307 | 191.6 | 48.076 | 47.6297 | 161.7 |
| 50 | 44.2085 | 45.1605 | 185.6 | 46.3505 | 46.41 | 172.3 |
| 51 | 46.886 | 48.4925 | 163 | 46.2315 | 47.0347 | 170.8 |
| 52 | 45.815 | 44.5357 | 181.5 | 48.4925 | 49.6527 | 153.8 |
| 53 | 44.5357 | 44.506 | 187.3 | 48.6115 | 49.1172 | 155.1 |
| 54 | 46.053 | 46.4397 | 173.8 | 46.7075 | 46.053 | 172.3 |
| 55 | 45.4282 | 46.41 | 176 | 47.0347 | 47.6 | 165.8 |
| 56 | 43.3457 | 46.4695 | 184 | 47.4215 | 47.5405 | 164.4 |
| 57 | 43.7622 | 43.792 | 193.3 | 46.3505 | 47.9272 | 167.2 |
| 58 | 43.673 | 43.911 | 193.3 | 45.696 | 46.6182 | 174.5 |
| 59 | 44.4465 | 45.9935 | 181.5 | 44.8332 | 47.124 | 175.3 |
| 60 | 43.2267 | 42.4235 | 202.5 | 47.481 | 46.8562 | 166.5 |
| 61 | 43.1375 | 43.8217 | 196 | 46.3207 | 47.9272 | 168.6 |
| 62 | 45.4282 | 45.7555 | 178.4 | 47.987 | 48.7007 | 159 |
| 63 | 42.959 | 41.531 | 208.3 | 47.987 | 48.7305 | 159 |
| 64 | 40.936 | 42.8102 | 211.3 | 48.671 | 49.861 | 152.6 |
| 65 | 44.0002 | 43.8217 | 192.5 | 48.4627 | 47.5702 | 161 |
| 66 | 43.792 | 44.7142 | 189 | 48.8197 | 47.5405 | 159.6 |
| 67 | 43.673 | 43.8812 | 193.3 | 49.3255 | 47.243 | 159 |
| 68 | 44.9522 | 47.481 | 173.8 | 46.7372 | 46.4992 | 170.8 |
| 69 | 45.815 | 48.9387 | 165.1 | 45.101 | 46.8562 | 175.3 |
| Average | | | 180.3 | | | |

Table A.3 Hardness readings for Sample 3

| Sample 3 | Nitrogen pressure 0.5 Torr, anode distance 80 mm Ion beam centre location: 21 mm | | | | | |
|------------------|---|-------------------------------------|-------|-------------------------------------|-------------------------------------|-------|
| | Before Nitriding: | | | After Nitriding: | | |
| Position (mm) | d ₁ (μm) | d ₂ (μm) | HV | d ₁ (μm) | d ₂ (μm) | HV |
| 1 | 48.7305 | 47.6892 | 159.6 | 50.337 | 49.5337 | 149 |
| 2 | 46.0827 | 46.2315 | 173.8 | 49.623 | 52.479 | 142 |
| 3 | 46.886 | 46.7075 | 169.3 | 49.742 | 46.1422 | 161.7 |
| 4 | 47.6595 | 46.172 | 168.6 | 46.1422 | 46.9455 | 171.5 |
| 5 | 46.767 | 46.4992 | 170.8 | 49.504 | 48.3437 | 155.1 |
| 6 | 46.053 | 46.767 | 172.3 | 49.504 | 46.2315 | 162.3 |
| 7 | 46.3207 | 45.815 | 174.5 | 49.3552 | 48.0165 | 156.4 |
| 8 | 46.886 | 45.7852 | 173 | 50.099 | 48.3735 | 153.2 |
| 9 | 46.8562 | 45.5472 | 173.8 | 47.2132 | 45.4282 | 173 |
| 10 | 46.4695 | 48.3735 | 165.1 | 46.9157 | 49.028 | 161 |
| 11 | 45.9042 | 46.6182 | 173 | 43.6135 | 41.9475 | 202.5 |
| 12 | 44.4167 | 44.744 | 186.5 | 45.0415 | 44.6547 | 184.8 |
| 13 | 43.4647 | 45.1902 | 189 | 41.293 | 47.8677 | 186.5 |
| 14 | 45.7555 | 44.5655 | 181.5 | 43.435 | 42.0962 | 202.5 |
| 15 | 45.7852 | 46.9157 | 172.3 | 39.1807 | 43.9047 | 214.3 |
| 16 | 45.7555 | 45.3985 | 178.4 | 43.7622 | 44.9522 | 188.1 |
| 17 | 46.4397 | 44.8927 | 177.6 | 39.0617 | 44.3572 | 213.3 |
| 18 | 47.362 | 48.1057 | 163 | 40.9955 | 41.2037 | 219.6 |
| 19 | 46.41 | 45.2795 | 176.8 | 42.8697 | 38.7345 | 222.8 |
| 20 | 47.481 | 45.3985 | 172.3 | 45.3687 | 45.0117 | 181.5 |
| 21 | 46.2017 | 45.6662 | 176.8 | 43.1672 | 49.742 | 171.5 |
| 22 | 48.6115 | 47.1537 | 161.7 | 39.8352 | 39.2997 | 236.5 |
| 23 | 47.481 | 47.9867 | 163 | 39.4187 | 39.8352 | 236.5 |
| 24 | 48.4627 | 47.243 | 161.7 | 46.3802 | 42.5722 | 187.3 |
| 25 | 48.0165 | 48.5222 | 159 | 39.1212 | 35.462 | 266.2 |
| 26 | 46.8265 | 46.0232 | 172.3 | 46.0827 | 44.268 | 181.5 |
| 27 | 46.4695 | 46.4992 | 171.5 | 43.4025 | 46.3207 | 184 |
| 28 | 49.028 | 49.0577 | 157.7 | 47.7487 | 45.0117 | 172.3 |
| 29 | 48.8197 | 49.0577 | 155.1 | 44.5052 | 40.6087 | 204.4 |
| 30 | 47.481 | 47.4512 | 164.4 | 45.1307 | 47.8082 | 171.5 |
| 31 | 46.2315 | 46.3505 | 173 | 44.7737 | 45.3985 | 182.3 |

| | | | | | | |
|----------------|---------|---------|-------|---------|---------|-------|
| 32 | 47.9272 | 47.0645 | 164.4 | 45.3985 | 46.0232 | 177.6 |
| 33 | 47.5702 | 46.0827 | 169.3 | 46.172 | 46.1125 | 174.5 |
| 34 | 47.6595 | 47.243 | 164.4 | 45.6662 | 46.5587 | 174.5 |
| 35 | 47.0645 | 47.362 | 166.5 | 46.6182 | 45.339 | 175.3 |
| 36 | 46.7372 | 45.22 | 175.3 | 45.7555 | 44.8972 | 180.7 |
| 37 | 47.3025 | 46.8265 | 167.2 | 46.0232 | 44.387 | 181.5 |
| 38 | 48.3735 | 45.7555 | 167.2 | 45.8447 | 44.3572 | 182.3 |
| 39 | 45.8447 | 46.529 | 174.5 | 45.4282 | 45.4877 | 179.2 |
| 40 | 48.4032 | 46.1422 | 165.8 | 46.8562 | 44.2382 | 179.2 |
| 41 | 47.9867 | 46.5885 | 165.8 | 45.4877 | 46.3207 | 176 |
| 42 | 45.3092 | 44.7142 | 183.2 | 46.0827 | 46.5587 | 173 |
| 43 | 45.6067 | 45.5175 | 178.4 | 45.6067 | 49.266 | 165.1 |
| 44 | 43.6135 | 43.2267 | 192.5 | 45.339 | 46.3802 | 176 |
| 45 | 45.6365 | 45.577 | 178.4 | 44.8035 | 45.4282 | 182 |
| 46 | 44.7737 | 44.268 | 187.3 | 45.4877 | 45.2795 | 179.9 |
| 47 | 46.291 | 47.5405 | 168.6 | 45.4877 | 48.79 | 167.2 |
| 48 | 45.101 | 44.4465 | 184.8 | 48.7305 | 49.1787 | 154.5 |
| 49 | 45.5175 | 43.316 | 188.1 | 46.5296 | 48.0165 | 165.8 |
| 50 | 45.339 | 44.0002 | 185.6 | 44.625 | 46.4695 | 179.2 |
| 51 | 46.7075 | 45.9637 | 173 | 45.4877 | 45.5175 | 179.2 |
| 52 | 46.8265 | 44.2977 | 178.4 | 48.195 | 47.6892 | 161.7 |
| 53 | 44.5952 | 46.2315 | 179.9 | 46.172 | 47.124 | 170.8 |
| 54 | 47.2727 | 45.696 | 171.5 | 46.6777 | 46.291 | 171.5 |
| 55 | 46.291 | 45.3985 | 176.8 | 48.433 | 47.243 | 162.3 |
| 56 | 45.9042 | 45.8745 | 176 | 48.195 | 46.767 | 164.4 |
| 57 | 45.3687 | 45.7555 | 178.4 | 47.481 | 47.6892 | 163.7 |
| 58 | 45.9935 | 45.9637 | 175.3 | 48.4032 | 48.1652 | 159 |
| 59 | 45.8745 | 48.1355 | 167.9 | 47.6 | 47.3025 | 164.4 |
| 60 | 44.2085 | 44.8927 | 186.5 | 48.314 | 47.5107 | 161.7 |
| 61 | 44.0002 | 44.149 | 190.7 | 47.0347 | 45.934 | 171.5 |
| 62 | 45.6662 | 45.1307 | 179.9 | 47.362 | 47.7487 | 163.7 |
| 63 | 49.1172 | 49.4445 | 152.6 | 48.9387 | 50.5155 | 150.7 |
| 64 | 43.5242 | 43.4052 | 196 | 48.909 | 48.195 | 157 |
| 65 | 47.8677 | 48.2543 | 160.3 | 48.0462 | 48.9685 | 157.7 |
| 66 | 47.2727 | 46.7372 | 167.9 | 47.124 | 46.8562 | 167.9 |
| 67 | 47.6 | 46.3505 | 167.9 | 49.504 | 47.957 | 156.4 |
| 68 | 45.101 | 44.6845 | 184 | 47.7487 | 48.6412 | 159.6 |
| 69 | 44.387 | 46.0232 | 181.5 | 47.8975 | 47.5107 | 163 |
| Average | | | 173.3 | | | |

Table A.4 Hardness readings for Sample 4

| Sample 4 | Nitrogen pressure 0.5 Torr, anode distance 100 mm Ion beam centre location: 24 mm | | | | | |
|------------------|--|-------------------------------------|-------|-------------------------------------|-------------------------------------|-------|
| | Before Nitriding: | | | After Nitriding: | | |
| Position (mm) | d ₁ (μm) | d ₂ (μm) | HV | d ₁ (μm) | d ₂ (μm) | HV |
| 1 | 46.6777 | 44.9225 | 176.8 | 44.2977 | 46.529 | 179.9 |
| 2 | 48.1057 | 48.314 | 159.6 | 45.7852 | 44.1192 | 183.2 |
| 3 | 49.504 | 51.3485 | 146 | 46.9752 | 46.7967 | 168.6 |
| 4 | 45.6067 | 46.4695 | 175.3 | 45.8447 | 48.1355 | 167.9 |
| 5 | 46.767 | 45.9935 | 173 | 45.3985 | 44.4465 | 184 |
| 6 | 47.9867 | 47.1835 | 163.7 | 46.4695 | 46.0827 | 173 |
| 7 | 47.838 | 46.0232 | 168.6 | 45.6067 | 46.2017 | 176 |
| 8 | 46.9752 | 47.3917 | 166.5 | 46.2315 | 45.577 | 176 |
| 9 | 48.0165 | 45.2497 | 170.8 | 45.7527 | 46.172 | 176 |
| 10 | 47.6595 | 47.124 | 165.1 | 46.1125 | 45.5175 | 176.8 |
| 11 | 45.934 | 47.4512 | 170.1 | 44.149 | 41.3227 | 203.4 |
| 12 | 45.7555 | 45.6365 | 177.6 | 45.934 | 39.7757 | 202.5 |
| 13 | 44.744 | 44.928 | 184 | 43.673 | 43.673 | 194.2 |
| 14 | 48.314 | 47.1537 | 163 | 45.0117 | 39.2997 | 208.3 |
| 15 | 46.767 | 47.2727 | 169.3 | 47.005 | 39.3295 | 198.7 |
| 16 | 44.5357 | 43.0482 | 193.3 | 47.481 | 47.3917 | 176 |
| 17 | 47.0942 | 46.529 | 169.3 | 44.268 | 42.721 | 196 |
| 18 | 47.719 | 46.1125 | 168.6 | 42.6912 | 45.1307 | 192.5 |
| 19 | 47.2727 | 47.5405 | 165.1 | 48.2545 | 47.6892 | 161 |
| 20 | 45.8447 | 46.053 | 176 | 44.3572 | 47.005 | 177.6 |
| 21 | 47.2132 | 47.4512 | 165.8 | 45.0117 | 46.0827 | 179.2 |
| 22 | 46.053 | 46.648 | 172.3 | 47.362 | 44.268 | 176.8 |
| 23 | 44.2832 | 43.4945 | 189.9 | 48.314 | 49.5932 | 154.5 |
| 24 | 47.362 | 45.9637 | 170.8 | 45.6365 | 45.6662 | 177.6 |
| 25 | 45.8745 | 46.529 | 173.8 | 46.7075 | 47.2132 | 167.9 |
| 26 | 49.2597 | 47.5107 | 158.3 | 44.625 | 47.6595 | 174.5 |
| 27 | 47.7785 | 47.3025 | 164.4 | 46.1422 | 45.5472 | 176.8 |
| 28 | 45.3985 | 46.9455 | 173.8 | 48.7305 | 49.5932 | 153.2 |
| 29 | 46.2612 | 45.9935 | 174.5 | 46.6777 | 47.7785 | 166.5 |
| 30 | 47.838 | 46.053 | 168.6 | 46.7075 | 48.8495 | 162.3 |
| 31 | 48.7305 | 44.625 | 170.1 | 42.7805 | 45.934 | 188.1 |

| | | | | | | |
|----------------|---------|---------|-------|---------|---------|-------|
| 32 | 46.886 | 46.7987 | 169.3 | 45.577 | 43.4052 | 187.3 |
| 33 | 48.7007 | 48.195 | 158.3 | 45.4282 | 44.0002 | 185.6 |
| 34 | 45.6067 | 46.2612 | 178.4 | 44.8035 | 45.3687 | 182.3 |
| 35 | 46.291 | 44.7737 | 179.2 | 45.7852 | 45.339 | 178.4 |
| 36 | 45.6662 | 45.3092 | 179.2 | 46.2612 | 46.648 | 171.5 |
| 37 | 46.3802 | 44.1787 | 180.7 | 44.268 | 48.2247 | 173.8 |
| 38 | 45.0117 | 44.7377 | 184 | 48.5817 | 47.124 | 161.7 |
| 39 | 44.4167 | 43.554 | 190.7 | 47.5107 | 47.6 | 163.7 |
| 40 | 46.5587 | 46.7372 | 170.8 | 47.0347 | 49.9502 | 157.7 |
| 41 | 46.2315 | 45.6602 | 176 | 45.9935 | 48.6412 | 165.8 |
| 42 | 47.243 | 45.339 | 173 | 47.9272 | 47.1835 | 163.7 |
| 43 | 46.648 | 45.815 | 174.5 | 43.2267 | 46.3802 | 184.8 |
| 44 | 48.076 | 47.243 | 163 | 45.6365 | 45.101 | 179.9 |
| 45 | 47.0347 | 46.2315 | 170.8 | 44.9225 | 45.9637 | 179.9 |
| 46 | 47.481 | 44.1787 | 176.8 | 45.3985 | 45.3687 | 179.9 |
| 47 | 46.172 | 46.5587 | 172.3 | 46.0232 | 48.8197 | 165.1 |
| 48 | 46.1422 | 45.1605 | 177.6 | 46.9455 | 48.4627 | 163 |
| 49 | 45.1902 | 46.0827 | 178.4 | 46.886 | 48.1355 | 164.4 |
| 50 | 46.1422 | 45.8745 | 175.3 | 45.9042 | 46.7372 | 173 |
| 51 | 46.886 | 44.744 | 176.8 | 44.625 | 46.9752 | 176.8 |
| 52 | 45.457 | 45.7852 | 178.4 | 45.3985 | 48.4032 | 168.6 |
| 53 | 46.172 | 45.6662 | 176 | 43.1872 | 47.9272 | 178.4 |
| 54 | 46.8265 | 46.9455 | 168.6 | 49.2065 | 48.4925 | 155.7 |
| 55 | 47.005 | 46.648 | 169.3 | 47.8082 | 44.7737 | 173 |
| 56 | 45.8745 | 44.6547 | 180.7 | 45.7257 | 48.6115 | 166.5 |
| 57 | 48.79 | 47.838 | 159 | 47.6 | 48.552 | 160.3 |
| 58 | 46.648 | 45.8745 | 173 | 45.7555 | 47.838 | 169.3 |
| 59 | 47.6595 | 47.4512 | 163.7 | 45.5175 | 47.4512 | 171.3 |
| 60 | 48.0462 | 46.0232 | 167.9 | 46.1422 | 49.5337 | 162.3 |
| 61 | 48.8495 | 47.124 | 161 | 45.577 | 46.4397 | 175.3 |
| 62 | 44.863 | 42.4235 | 196 | 44.744 | 46.8265 | 176.8 |
| 63 | 48.4032 | 48.6115 | 157.7 | 46.0827 | 49.6327 | 161.7 |
| 64 | 45.8745 | 45.6365 | 176.8 | 44.8927 | 47.3322 | 174.5 |
| 65 | 47.6297 | 47.6 | 163.7 | 47.4215 | 47.3025 | 165.1 |
| 66 | 43.792 | 46.4397 | 182.3 | 46.9752 | 45.9935 | 171.5 |
| 67 | 48.1355 | 47.3025 | 163 | 43.7325 | 48.2545 | 167.2 |
| 68 | 49.028 | 49.1787 | 153.8 | 44.2977 | 48.4032 | 172.3 |
| 69 | 47.4215 | 46.7967 | 167.2 | 44.5357 | 48.671 | 168.6 |
| Average | | | 171.7 | | | |

Table A.5 Hardness readings for Sample 5

| Sample 5 | Nitrogen pressure 0.5 Torr, anode distance 120 mm Ion beam centre location: 20 mm | | | | | |
|------------------|--|-------------------------------------|-------|-------------------------------------|-------------------------------------|-------|
| | Before Nitriding: | | | After Nitriding: | | |
| Position (mm) | d ₁ (μm) | d ₂ (μm) | HV | d ₁ (μm) | d ₂ (μm) | HV |
| 1 | 46.886 | 46.7075 | 169.3 | 48.762 | 46.767 | 162.3 |
| 2 | 47.0347 | 43.673 | 179.9 | 47.4512 | 43.5242 | 179.2 |
| 3 | 48.4032 | 44.2085 | 173 | 46.5885 | 46.886 | 170.1 |
| 4 | 48.1355 | 47.3025 | 163 | 45.2497 | 43.4945 | 188.1 |
| 5 | 45.3092 | 45.8447 | 178.4 | 46.3505 | 46.886 | 170.8 |
| 6 | 46.886 | 44.744 | 176.8 | 48.8792 | 47.7785 | 159 |
| 7 | 46.172 | 45.6662 | 176 | 46.172 | 47.9867 | 167.2 |
| 8 | 46.4397 | 46.41 | 172.3 | 44.5655 | 43.1872 | 192.5 |
| 9 | 46.886 | 44.5257 | 177.6 | 47.124 | 47.005 | 167.2 |
| 10 | 46.886 | 45.815 | 176.8 | 45.2795 | 43.1605 | 181.5 |
| 11 | 45.5472 | 44.03 | 184.8 | 47.3917 | 48.9982 | 159.6 |
| 12 | 45.815 | 44.982 | 179.9 | 48.9685 | 47.243 | 160.3 |
| 13 | 47.4215 | 46.7967 | 167.2 | 44.4465 | 46.4695 | 179.2 |
| 14 | 46.7967 | 46.9455 | 169.3 | 44.6845 | 44.9522 | 184.8 |
| 15 | 46.7075 | 46.4992 | 170.8 | 44.4762 | 46.4992 | 179.2 |
| 16 | 47.0056 | 44.268 | 178.4 | 45.2795 | 46.1125 | 177.6 |
| 17 | 47.4215 | 47.8082 | 163.7 | 46.2315 | 46.3802 | 173 |
| 18 | 46.529 | 46.886 | 170.1 | 45.8447 | 42.2747 | 190.7 |
| 19 | 46.7967 | 44.2977 | 179.2 | 42.959 | 45.0712 | 191.6 |
| 20 | 45.7257 | 46.2315 | 175.3 | 46.4397 | 45.0415 | 177.6 |
| 21 | 48.5222 | 48.195 | 158.3 | 46.9157 | 53.5797 | 147.2 |
| 22 | 47.005 | 46.648 | 169.3 | 46.9455 | 48.9982 | 161 |
| 23 | 47.9272 | 47.5107 | 163 | 44.4107 | 44.8035 | 186.5 |
| 24 | 47.0942 | 48.909 | 161 | 46.7967 | 45.1902 | 175.3 |
| 25 | 49.6527 | 49.8015 | 150.2 | 46.1422 | 44.982 | 178.4 |
| 26 | 45.3985 | 47.9867 | 170.1 | 47.7487 | 47.05 | 165.1 |
| 27 | 48.79 | 47.838 | 159 | 45.5175 | 47.7487 | 170.8 |
| 28 | 44.149 | 44.6845 | 188.1 | 45.7555 | 47.5702 | 170.1 |
| 29 | 45.9637 | 47.4512 | 170.1 | 47.6892 | 45.9042 | 169.3 |
| 30 | 47.5702 | 47.0645 | 165.8 | 45.458 | 47.9867 | 170.1 |
| 31 | 47.6297 | 47.6 | 163.7 | 43.911 | 43.7922 | 193.3 |

| | | | | | | |
|----------------|---------|---------|-------|---------|---------|-------|
| 32 | 47.6595 | 47.4512 | 163.7 | 44.2085 | 47.8082 | 175.3 |
| 33 | 46.767 | 46.7967 | 169.3 | 44.982 | 46.1422 | 178.4 |
| 34 | 48.4627 | 47.243 | 161.7 | 45.6365 | 45.4877 | 178.4 |
| 35 | 45.6365 | 45.577 | 178.4 | 45.101 | 44.7142 | 184 |
| 36 | 48.4032 | 48.6115 | 157.7 | 47.0347 | 46.3802 | 170.1 |
| 37 | 46.053 | 46.767 | 172.3 | 47.6892 | 47.5405 | 163.7 |
| 38 | 48.8495 | 47.124 | 161 | 46.4397 | 47.9272 | 166.5 |
| 39 | 47.4512 | 45.577 | 171.5 | 46.3505 | 48.7602 | 163.7 |
| 40 | 47.362 | 47.005 | 166.5 | 46.1422 | 47.7785 | 167.9 |
| 41 | 47.9867 | 46.5885 | 165.8 | 45.2657 | 45.1605 | 180.7 |
| 42 | 48.7602 | 48.195 | 157.7 | 45.6622 | 45.4282 | 179.2 |
| 43 | 46.291 | 47.5405 | 168.6 | 46.172 | 45.815 | 175.3 |
| 44 | 46.3802 | 45.7555 | 174.5 | 47.4512 | 46.3802 | 168.6 |
| 45 | 45.8745 | 48.1355 | 167.9 | 47.124 | 45.934 | 171.5 |
| 46 | 47.481 | 46.3505 | 168.6 | 47.3322 | 46.4992 | 168.6 |
| 47 | 48.7305 | 47.6892 | 159.6 | 46.9455 | 47.8975 | 165.1 |
| 48 | 48.5222 | 46.886 | 163 | 46.7967 | 47.0942 | 168.6 |
| 49 | 45.9042 | 46.6182 | 173 | 45.815 | 45.696 | 176.8 |
| 50 | 48.2545 | 47.5107 | 161.7 | 45.3092 | 44.8332 | 182.3 |
| 51 | 45.7852 | 46.9157 | 172.3 | 46.3505 | 45.4282 | 176 |
| 52 | 47.362 | 46.648 | 167.9 | 44.03 | 44.4762 | 189 |
| 53 | 48.6115 | 47.1537 | 161.7 | 47.005 | 48.2247 | 163.7 |
| 54 | 45.9637 | 44.9225 | 179.9 | 46.9752 | 46.8562 | 168.6 |
| 55 | 46.7372 | 45.22 | 175.3 | 47.8082 | 46.053 | 168.6 |
| 56 | 47.6595 | 46.3207 | 167.9 | 46.0827 | 46.6777 | 172.3 |
| 57 | 46.767 | 46.4992 | 170.8 | 47.2132 | 45.4877 | 172.3 |
| 58 | 47.9867 | 46.5885 | 165.8 | 47.362 | 47.5702 | 164.4 |
| 59 | 49.1172 | 49.4445 | 152.6 | 50.456 | 50.7237 | 144.9 |
| 60 | 46.8562 | 46.291 | 170.8 | 47.6297 | 49.9502 | 155.7 |
| 61 | 48.3735 | 49.028 | 156.4 | 46.9455 | 49.028 | 161 |
| 62 | 46.291 | 45.3985 | 176.8 | 46.707 | 47.4215 | 167.2 |
| 63 | 48.4627 | 47.243 | 161.7 | 46.9752 | 48.0462 | 164.4 |
| 64 | 47.9272 | 48.552 | 159.6 | 45.5175 | 47.8677 | 170.1 |
| 65 | 47.481 | 47.4512 | 164.4 | 46.3802 | 47.2132 | 169.3 |
| 66 | 49.8015 | 49.0577 | 152 | 46.2612 | 44.6845 | 179.2 |
| 67 | 46.2017 | 45.6662 | 176.8 | 44.3572 | 46.2017 | 180.7 |
| 68 | 48.0462 | 47.3917 | 163 | 48.1057 | 47.7785 | 161.7 |
| 69 | 46.7075 | 45.9637 | 173 | 46.8562 | 49.5932 | 159.6 |
| Average | | | 168.6 | | | |

Table A.6 Hardness readings for Sample 6

| Sample 6 | Nitrogen pressure 1.0 Torr, anode distance 40 mm Ion beam centre location: 21 mm | | | | | |
|------------------|---|-------------------------------------|-------|-------------------------------------|-------------------------------------|-------|
| | Before Nitriding: | | | After Nitriding: | | |
| Position (mm) | d ₁ (μm) | d ₂ (μm) | HV | d ₁ (μm) | d ₂ (μm) | HV |
| 1 | 50.1882 | 51.6162 | 143.2 | 47.3025 | 42.3937 | 184.8 |
| 2 | 49.9502 | 46.291 | 160.3 | 46.648 | 40.8467 | 194.2 |
| 3 | 45.934 | 45.458 | 177.6 | 42.9292 | 43.9705 | 196.9 |
| 4 | 44.2382 | 43.7325 | 191.6 | 43.7325 | 45.9537 | 184.8 |
| 5 | 44.5655 | 45.9042 | 181.5 | 45.9537 | 45.7852 | 176 |
| 6 | 46.7562 | 46.5587 | 170.1 | 48.79 | 40.936 | 184 |
| 7 | 44.4762 | 43.2862 | 192.5 | 43.673 | 44.9225 | 189 |
| 8 | 51.8542 | 49.4742 | 144.3 | 47.005 | 43.673 | 180.7 |
| 9 | 47.5702 | 46.6182 | 167.2 | 42.84 | 40.936 | 211.3 |
| 10 | 43.792 | 43.8515 | 193.3 | 43.911 | 41.174 | 205.3 |
| 11 | 46.9455 | 45.6365 | 173 | 40.6385 | 45.1605 | 201.5 |
| 12 | 47.4215 | 47.1835 | 165.8 | 34.9265 | 39.3295 | 269.5 |
| 13 | 49.4742 | 45.2497 | 165.1 | 38.7345 | 32.9332 | 289.4 |
| 14 | 47.2132 | 47.243 | 166.5 | 38.0205 | 38.675 | 252.8 |
| 15 | 48.9982 | 47.8677 | 158.3 | 40.9062 | 36.3842 | 248.9 |
| 16 | 48.3735 | 45.577 | 167.9 | 30.7615 | 29.869 | 404 |
| 17 | 46.8265 | 46.41 | 170.8 | 31.2077 | 37.3065 | 315.3 |
| 18 | 47.4215 | 46.3802 | 168.6 | 31.8622 | 32.0705 | 362.2 |
| 19 | 46.9157 | 46.3802 | 170.8 | 39.6567 | 32.2787 | 286.2 |
| 20 | 49.0577 | 47.124 | 160.3 | 31.5945 | 29.4822 | 398.7 |
| 21 | 47.243 | 46.3802 | 169.3 | 31.892 | 29.9285 | 388.5 |
| 22 | 48.433 | 48.3437 | 158.3 | 31.1185 | 30.226 | 393.5 |
| 23 | 46.0827 | 46.3207 | 173.8 | 33.082 | 29.393 | 381 |
| 24 | 46.0827 | 46.3207 | 173.8 | 38.1395 | 39.2105 | 247.6 |
| 25 | 47.1537 | 46.9577 | 167.9 | 33.7365 | 27.251 | 398.7 |
| 26 | 46.4695 | 46.291 | 172.3 | 35.581 | 33.8555 | 308 |
| 27 | 47.0645 | 47.0347 | 167.9 | 29.7202 | 29.036 | 429.1 |
| 28 | 47.9272 | 47.5702 | 163 | 39.9542 | 35.9677 | 256.9 |
| 29 | 46.6777 | 46.2612 | 171.5 | 43.2565 | 44.863 | 190.7 |
| 30 | 47.5702 | 47.838 | 163 | 47.3322 | 39.8352 | 195.1 |
| 31 | 45.1605 | 46.3207 | 177.6 | 43.792 | 42.6615 | 198.7 |

| | | | | | | |
|----------------|---------|---------|-------|---------|---------|-------|
| 32 | 46.9157 | 46.291 | 170.8 | 44.149 | 46.053 | 182.3 |
| 33 | 46.0827 | 46.9455 | 171.5 | 43.2565 | 43.435 | 197.8 |
| 34 | 45.4877 | 44.03 | 184.8 | 49.2362 | 45.4282 | 165.8 |
| 35 | 45.0712 | 44.9522 | 183.2 | 43.7027 | 47.243 | 179.2 |
| 36 | 44.8927 | 45.696 | 180.7 | 46.2017 | 45.22 | 177.6 |
| 37 | 46.172 | 46.7967 | 171.5 | 43.435 | 47.4512 | 179.9 |
| 38 | 45.4877 | 43.1077 | 189 | 44.149 | 47.6892 | 176 |
| 39 | 45.815 | 45.5175 | 177.6 | 46.4695 | 46.886 | 170.1 |
| 40 | 47.6892 | 47.3025 | 164.4 | 47.5107 | 45.8745 | 170.1 |
| 41 | 46.4695 | 45.0415 | 177.6 | 48.076 | 47.6 | 162.3 |
| 42 | 46.8265 | 44.2382 | 179.2 | 51.051 | 39.2402 | 182.3 |
| 43 | 46.41 | 46.3027 | 172.3 | 47.481 | 45.9637 | 170.1 |
| 44 | 46.4397 | 46.9355 | 170.1 | 46.7967 | 46.3505 | 170.8 |
| 45 | 47.5702 | 46.886 | 166.5 | 47.2132 | 47.719 | 164.4 |
| 46 | 47.3025 | 47.124 | 166.5 | 46.8562 | 45.6067 | 173.8 |
| 47 | 49.266 | 47.4215 | 159 | 48.8197 | 48.2247 | 157.7 |
| 48 | 44.4465 | 43.0482 | 194.2 | 48.195 | 47.4512 | 162.3 |
| 49 | 46.4695 | 45.101 | 176.8 | 45.8745 | 46.6777 | 173 |
| 50 | 46.7075 | 47.3917 | 167.9 | 46.648 | 47.362 | 167.9 |
| 51 | 44.5655 | 46.767 | 177.6 | 48.0462 | 47.243 | 163.7 |
| 52 | 46.5587 | 47.243 | 168.6 | 46.2612 | 47.6892 | 167.9 |
| 53 | 47.3917 | 47.837 | 163.7 | 48.7602 | 47.719 | 159.6 |
| 54 | 45.22 | 45.815 | 179.2 | 45.9935 | 45.6662 | 176.8 |
| 55 | 47.2132 | 45.934 | 170.8 | 47.719 | 48.671 | 159.6 |
| 56 | 45.2795 | 45.3687 | 180.7 | 47.3025 | 46.529 | 168.6 |
| 57 | 46.1125 | 48.552 | 165.8 | 47.362 | 46.8265 | 167.2 |
| 58 | 47.6595 | 45.4877 | 170.8 | 48.1652 | 49.4445 | 155.7 |
| 59 | 47.243 | 47.1835 | 166.5 | 46.6777 | 45.5472 | 174.5 |
| 60 | 43.1077 | 47.1835 | 182.3 | 47.3025 | 46.7372 | 167.9 |
| 61 | 44.3275 | 44.4167 | 188.1 | 42.126 | 44.149 | 199.7 |
| 62 | 45.1307 | 44.9225 | 183.2 | 41.8582 | 44.7737 | 197.8 |
| 63 | 48.433 | 48.195 | 159 | 48.5817 | 47.0942 | 162.3 |
| 64 | 44.863 | 45.2795 | 182.3 | 43.7622 | 43.2862 | 196 |
| 65 | 43.5242 | 43.911 | 194 | 45.5472 | 48.552 | 167.9 |
| 66 | 46.172 | 46.886 | 171.5 | 45.8447 | 45.696 | 176.8 |
| 67 | 45.0415 | 46.1125 | 178.4 | 44.863 | 46.6182 | 177.6 |
| 68 | 45.9637 | 46.1125 | 175.3 | 47.1537 | 45.6662 | 172.3 |
| 69 | 42.483 | 45.9637 | 189.9 | 42.483 | 45.9637 | 189.9 |
| Average | | | 172.7 | | | |

Table A.7 Hardness readings for Sample 7

| Sample 7 | Nitrogen pressure 1.0 Torr, anode distance 60 mm Ion beam centre location: 20 mm | | | | | |
|------------------|---|-------------------------------------|-------|-------------------------------------|-------------------------------------|-------|
| | Before Nitriding: | | | After Nitriding: | | |
| Position (mm) | d ₁ (μm) | d ₂ (μm) | HV | d ₁ (μm) | d ₂ (μm) | HV |
| 1 | 47.9867 | 44.0597 | 175.3 | 45.0712 | 47.5405 | 173 |
| 2 | 39.984 | 50.813 | 179.9 | 45.7257 | 44.6845 | 181.5 |
| 3 | 47.1537 | 45.3092 | 173.8 | 46.1422 | 44.8927 | 179.2 |
| 4 | 46.4992 | 40.9955 | 194.2 | 47.481 | 42.245 | 184 |
| 5 | 46.8562 | 46.4397 | 170.8 | 46.3505 | 47.0942 | 170.1 |
| 6 | 49.742 | 45.6662 | 163 | 48.1355 | 46.886 | 164.4 |
| 7 | 46.7167 | 45.7852 | 173 | 46.8265 | 45.2497 | 175.3 |
| 8 | 45.7852 | 47.7487 | 169.3 | 44.5952 | 51.8243 | 159.6 |
| 9 | 46.2017 | 44.4167 | 180.7 | 44.3572 | 46.172 | 180.7 |
| 10 | 47.719 | 50.0097 | 155.1 | 44.4762 | 48.2247 | 172.3 |
| 11 | 48.7305 | 46.0827 | 165.1 | 43.673 | 42.8697 | 197.8 |
| 12 | 45.9042 | 46.8265 | 172.3 | 42.3937 | 43.3755 | 201.5 |
| 13 | 45.2792 | 44.1787 | 185.6 | 46.053 | 51.527 | 155.7 |
| 14 | 47.6 | 45.4877 | 171.5 | 43.8812 | 47.005 | 179.9 |
| 15 | 44.5952 | 44.8927 | 185.6 | 44.149 | 44.9225 | 187.3 |
| 16 | 47.124 | 47.2132 | 166.5 | 45.5175 | 43.2565 | 188.1 |
| 17 | 45.101 | 45.4282 | 180.7 | 40.2815 | 42.0367 | 218.5 |
| 18 | 47.8677 | 46.4397 | 166.5 | 41.293 | 41.2335 | 217.4 |
| 19 | 46.2017 | 45.934 | 174.5 | 39.7757 | 38.318 | 243.9 |
| 20 | 46.41 | 44.3572 | 179.9 | 36.5032 | 37.0982 | 273.9 |
| 21 | 48.7967 | 48.671 | 163 | 36.6222 | 43.3755 | 231.8 |
| 22 | 46.886 | 45.3687 | 174.5 | 41.1442 | 37.0982 | 242.6 |
| 23 | 48.4925 | 43.673 | 174.5 | 36.2057 | 35.7 | 286.2 |
| 24 | 44.0895 | 44.149 | 190.7 | 40.3942 | 37.6064 | 242.6 |
| 25 | 44.5357 | 42.9887 | 193.3 | 35.6107 | 35.2835 | 294.3 |
| 26 | 45.8447 | 45.696 | 176.8 | 36.5627 | 38.3477 | 263.8 |
| 27 | 46.6182 | 44.1192 | 179.9 | 43.9705 | 40.0435 | 210.3 |
| 28 | 46.41 | 43.3735 | 184 | 42.6062 | 39.7162 | 218.5 |
| 29 | 45.9637 | 44.863 | 179.9 | 39.3592 | 41.769 | 225 |
| 30 | 45.7852 | 45.3092 | 179.2 | 40.6385 | 40.1327 | 226.1 |
| 31 | 45.4282 | 44.6547 | 183 | 42.9887 | 46.7075 | 184.8 |

| | | | | | | |
|----------------|---------|---------|-------|---------|---------|-------|
| 32 | 47.0347 | 42.1855 | 186.5 | 44.625 | 42.9887 | 193.3 |
| 33 | 47.1835 | 48.79 | 161 | 47.005 | 44.5952 | 176.8 |
| 34 | 46.7967 | 46.5885 | 170.1 | 43.2565 | 44.03 | 195.1 |
| 35 | 45.0415 | 45.9637 | 179.2 | 47.838 | 48.6412 | 159.6 |
| 36 | 46.8265 | 45.9637 | 172.3 | 46.4992 | 47.3322 | 168.6 |
| 37 | 48.076 | 44.1787 | 174.5 | 45.1902 | 47.5107 | 172.3 |
| 38 | 45.8745 | 44.6547 | 180.7 | 44.0002 | 43.0185 | 196 |
| 39 | 46.41 | 46.3505 | 172.3 | 44.506 | 46.9455 | 177.6 |
| 40 | 46.4992 | 44.5952 | 179.2 | 46.172 | 47.6297 | 168.6 |
| 41 | 46.5885 | 48.076 | 165.8 | 46.767 | 45.6365 | 173.8 |
| 42 | 45.4887 | 44.9522 | 181.5 | 44.4167 | 46.648 | 179.2 |
| 43 | 46.4992 | 46.2612 | 172.3 | 44.5655 | 42.602 | 195.1 |
| 44 | 46.8562 | 45.8745 | 172.3 | 44.0895 | 44.2977 | 189.9 |
| 45 | 46.7372 | 45.6365 | 170.1 | 46.1422 | 41.1145 | 195.1 |
| 46 | 45.2497 | 44.1192 | 185.6 | 43.4647 | 46.648 | 182.3 |
| 47 | 46.6182 | 45.101 | 176 | 43.5242 | 44.5357 | 191.6 |
| 48 | 46.053 | 44.506 | 180.7 | 45.4282 | 42.6912 | 190.7 |
| 49 | 46.1125 | 45.0117 | 178.4 | 44.8927 | 43.8515 | 188.1 |
| 50 | 47.5405 | 44.03 | 176.8 | 45.4282 | 46.0232 | 177.6 |
| 51 | 46.1422 | 45.4248 | 176.8 | 45.22 | 46.4397 | 176.8 |
| 52 | 46.3505 | 45.6622 | 175.3 | 43.2565 | 43.4647 | 196.9 |
| 53 | 45.9042 | 46.053 | 175.3 | 40.7872 | 39.8055 | 228.4 |
| 54 | 44.8972 | 44.6845 | 184.8 | 43.8217 | 44.149 | 191.6 |
| 55 | 45.815 | 46.4397 | 174.5 | 44.8927 | 43.792 | 189 |
| 56 | 46.053 | 45.8477 | 176 | 42.4235 | 43.792 | 199.7 |
| 57 | 45.1902 | 45.9935 | 178.4 | 43.3457 | 40.579 | 210.3 |
| 58 | 47.5104 | 47.5405 | 164.4 | 43.9407 | 42.007 | 200.6 |
| 59 | 45.4282 | 45.1307 | 181.5 | 44.0002 | 41.5607 | 202.5 |
| 60 | 46.9455 | 45.7852 | 172.3 | 43.8812 | 44.3572 | 190.7 |
| 61 | 47.4215 | 47.2727 | 165.8 | 42.126 | 44.5955 | 197.8 |
| 62 | 46.7075 | 46.2612 | 171.5 | 42.5722 | 43.5837 | 199.7 |
| 63 | 47.2132 | 45.3092 | 173.8 | 42.0665 | 40.341 | 218.5 |
| 64 | 45.4877 | 44.7142 | 182.3 | 41.8582 | 42.7507 | 207.3 |
| 65 | 45.6662 | 42.8995 | 189 | 44.1192 | 46.4397 | 180.7 |
| 66 | 47.243 | 47.0347 | 167.2 | 43.5837 | 44.6845 | 190.7 |
| 67 | 46.0827 | 45.101 | 178.4 | 42.1855 | 45.934 | 190.7 |
| 68 | 46.7075 | 46.0827 | 172.3 | 46.7967 | 47.4215 | 167.2 |
| 69 | 48.9387 | 47.5702 | 159 | 47.243 | 47.0347 | 167.2 |
| Average | | | 175.6 | | | |

Table A.8 Hardness readings for Sample 8

| Sample 8 | Nitrogen pressure 1.0 Torr, anode distance 80 mm Ion beam centre location: 20 mm | | | | | |
|---------------|---|---------------------|-------|---------------------|---------------------|-------|
| | Before Nitriding: | | | After Nitriding: | | |
| Position (mm) | d ₁ (μm) | d ₂ (μm) | HV | d ₁ (μm) | d ₂ (μm) | HV |
| 1 | 45.1016 | 45.8447 | 179.2 | 47.5107 | 42.7507 | 182.3 |
| 2 | 44.4465 | 42.7507 | 195.1 | 46.3802 | 47.0645 | 170.1 |
| 3 | 43.911 | 42.9887 | 196.9 | 45.0712 | 50.6642 | 161.7 |
| 4 | 44.982 | 44.0597 | 187.3 | 45.2497 | 45.5175 | 179.9 |
| 5 | 44.8322 | 44.4167 | 186.5 | 46.172 | 49.266 | 163 |
| 6 | 43.3755 | 43.2565 | 197.8 | 47.2727 | 47.1537 | 166.5 |
| 7 | 45.5662 | 45.1605 | 179.9 | 45.3687 | 49.1767 | 165.8 |
| 8 | 47.3322 | 46.648 | 167.9 | 45.6067 | 44.7737 | 181.5 |
| 9 | 47.3322 | 45.7257 | 171.5 | 46.5885 | 45.1605 | 176 |
| 10 | 43.1672 | 43.1077 | 199.7 | 47.0645 | 48.314 | 163 |
| 11 | 46.5885 | 45.9637 | 173 | 46.2612 | 48.6115 | 165.1 |
| 12 | 46.6777 | 47.243 | 167.9 | 47.0645 | 41.531 | 189 |
| 13 | 49.1172 | 48.6412 | 155.1 | 48.9387 | 49.9502 | 152 |
| 14 | 47.5702 | 46.8562 | 166.5 | 49.5932 | 48.1652 | 155.1 |
| 15 | 48.3735 | 48.433 | 158.3 | 48.7007 | 48.2842 | 157.7 |
| 16 | 47.5405 | 46.9752 | 165.8 | 49.3255 | 49.742 | 151.4 |
| 17 | 47.3322 | 47.4512 | 165.1 | 41.055 | 45.815 | 196.9 |
| 18 | 48.3437 | 46.9157 | 163.7 | 46.8562 | 45.9637 | 172.3 |
| 19 | 46.2612 | 46.053 | 173.8 | 44.1192 | 40.4302 | 207.3 |
| 20 | 45.2497 | 46.4992 | 176 | 40.8467 | 40.9657 | 221.7 |
| 21 | 44.4167 | 45.577 | 183.2 | 38.08 | 38.5262 | 252.8 |
| 22 | 46.6777 | 46.1422 | 172.3 | 42.7507 | 40.46 | 214.3 |
| 23 | 44.5357 | 46.6182 | 178.4 | 38.5857 | 37.9907 | 252.8 |
| 24 | 45.815 | 47.1835 | 171.5 | 39.8352 | 41.412 | 225 |
| 25 | 46.0827 | 46.2315 | 173.8 | 42.0962 | 36.3545 | 241.4 |
| 26 | 48.195 | 47.2132 | 163 | 37.1875 | 38.7047 | 258.2 |
| 27 | 45.1902 | 44.3572 | 184.8 | 40.379 | 39.746 | 230.7 |
| 28 | 47.1835 | 45.9637 | 170.8 | 44.506 | 38.4072 | 215.4 |
| 29 | 45.0117 | 44.8332 | 184 | 42.84 | 39.627 | 218.4 |
| 30 | 47.5702 | 45.4877 | 171.5 | 45.22 | 37.5445 | 216.4 |
| 31 | 44.7737 | 46.1422 | 179.2 | 39.508 | 45.1902 | 207.3 |
| 32 | 43.8812 | 42.8697 | 196.9 | 43.792 | 45.9042 | 184.8 |

| | | | | | | |
|----------------|---------|---------|-------|---------|---------|-------|
| 33 | 46.2612 | 45.6662 | 175.3 | 44.577 | 44.5357 | 182.3 |
| 34 | 46.7697 | 46.5587 | 170.1 | 44.3275 | 45.22 | 184.8 |
| 35 | 48.0462 | 46.41 | 166.5 | 42.5425 | 45.0712 | 193.3 |
| 36 | 44.149 | 47.3322 | 177.6 | 39.508 | 42.602 | 219.6 |
| 37 | 45.9935 | 47.0645 | 171.5 | 44.268 | 45.7555 | 183.2 |
| 38 | 46.9752 | 46.1422 | 170.8 | 45.577 | 45.8447 | 177.6 |
| 39 | 45.1307 | 44.9225 | 183.2 | 43.9407 | 39.8352 | 211.3 |
| 40 | 44.8927 | 45.3985 | 183.2 | 44.0002 | 42.5425 | 197.8 |
| 41 | 42.8102 | 44.5952 | 194.2 | 46.2612 | 44.0002 | 182.3 |
| 42 | 47.838 | 46.7967 | 165.8 | 45.6365 | 45.22 | 179.9 |
| 43 | 45.4282 | 46.2017 | 176.8 | 44.2382 | 44.6845 | 187.3 |
| 44 | 45.4877 | 44.1787 | 184.8 | 43.2565 | 45.7555 | 187.3 |
| 45 | 45.9935 | 44.7737 | 179.9 | 44.4167 | 42.7805 | 195.1 |
| 46 | 46.1422 | 46.9157 | 171.5 | 44.625 | 43.6135 | 190.7 |
| 47 | 46.7372 | 46.9752 | 168.6 | 46.1123 | 46.4992 | 173 |
| 48 | 44.8035 | 44.0895 | 188.1 | 45.3092 | 46.1125 | 177.6 |
| 49 | 43.6135 | 44.5357 | 190.7 | 42.9887 | 43.3755 | 198.7 |
| 50 | 46.0232 | 44.1787 | 182.3 | 42.7805 | 45.2795 | 191.6 |
| 51 | 46.7372 | 45.0117 | 176 | 44.7142 | 44.1787 | 188.1 |
| 52 | 43.8515 | 45.4877 | 185.6 | 42.721 | 44.863 | 193.3 |
| 53 | 46.41 | 44.5952 | 179.2 | 43.911 | 44.268 | 190.7 |
| 54 | 44.863 | 45.2795 | 182.3 | 47.1835 | 41.0252 | 190.7 |
| 55 | 46.172 | 46.886 | 171.5 | 43.7027 | 45.934 | 184.8 |
| 56 | 42.4532 | 48.1355 | 180.7 | 45.815 | 52.122 | 154.5 |
| 57 | 46.2017 | 44.9522 | 178.4 | 45.339 | 45.5175 | 179.9 |
| 58 | 45.4282 | 44.5655 | 183.2 | 47.3322 | 48.0165 | 163 |
| 59 | 45.6365 | 47.8975 | 169.3 | 47.2132 | 46.6182 | 168.6 |
| 60 | 45.9637 | 47.0942 | 171.5 | 45.3092 | 48.3437 | 169.3 |
| 61 | 43.7027 | 43.8515 | 193.3 | 44.268 | 46.9455 | 178.4 |
| 62 | 47.8677 | 47.4512 | 163 | 42.3937 | 47.6297 | 183.2 |
| 63 | 46.5587 | 47.5107 | 167.9 | 45.7852 | 46.0827 | 176 |
| 64 | 48.7602 | 47.0942 | 161.7 | 47.1537 | 46.7075 | 168.6 |
| 65 | 44.5647 | 45.1307 | 184 | 46.023 | 46.529 | 173 |
| 66 | 44.9522 | 45.934 | 179.9 | 45.934 | 45.4877 | 177.6 |
| 67 | 45.9935 | 45.2795 | 178.4 | 44.625 | 46.0827 | 179.9 |
| 68 | 45.9637 | 45.101 | 179.2 | 44.3275 | 45.9042 | 182.3 |
| 69 | 46.9752 | 44.5357 | 176.8 | 45.22 | 44.8927 | 182.3 |
| Average | | | 177.1 | | | |

Table A.9 Hardness readings for Sample 9

| Sample 9 | Nitrogen pressure 1.0 Torr, anode distance 100 mm Ion beam centre location: 19 mm | | | | | |
|---------------|--|---------------------|-------|---------------------|---------------------|-------|
| | Before Nitriding: | | | After Nitriding: | | |
| Position (mm) | d ₁ (μm) | d ₂ (μm) | HV | d ₁ (μm) | d ₂ (μm) | HV |
| 1 | 45.2497 | 43.5837 | 188.1 | 46.7372 | 47.3025 | 167.9 |
| 2 | 44.2382 | 43.5242 | 192.5 | 43.1375 | 44.6845 | 192.5 |
| 3 | 46.6777 | 44.9225 | 176.8 | 47.4512 | 43.7622 | 178.4 |
| 4 | 45.7555 | 45.22 | 179.2 | 47.0347 | 46.2612 | 170.8 |
| 5 | 46.3802 | 45.7555 | 174.5 | 43.8812 | 46.6777 | 180.7 |
| 6 | 46.6182 | 45.8745 | 173.8 | 48.6412 | 46.3207 | 164.4 |
| 7 | 45.0117 | 44.4762 | 185.6 | 47.3372 | 46.9455 | 167.2 |
| 8 | 46.053 | 43.4945 | 184.8 | 45.8745 | 45.0712 | 179.2 |
| 9 | 43.1077 | 42.1557 | 204.4 | 46.053 | 43.6432 | 184.8 |
| 10 | 46.2612 | 45.815 | 175.3 | 45.1902 | 45.0117 | 182.3 |
| 11 | 45.3505 | 46.291 | 173 | 47.8975 | 45.4877 | 170.1 |
| 12 | 46.0827 | 46.3505 | 173.8 | 45.7852 | 45.6662 | 177.6 |
| 13 | 44.4167 | 43.8812 | 190.7 | 47.4512 | 40.1327 | 193.3 |
| 14 | 46.9455 | 44.4465 | 177.6 | 48.6412 | 45.339 | 167.9 |
| 15 | 44.863 | 46.3207 | 178.4 | 43.5242 | 42.0962 | 202.5 |
| 16 | 46.1422 | 45.0117 | 178.4 | 41.65 | 43.0185 | 207.5 |
| 17 | 43.078 | 45.7257 | 188.1 | 43.6135 | 43.911 | 193.3 |
| 18 | 46.8265 | 46.3505 | 170.8 | 44.8927 | 46.4992 | 177.6 |
| 19 | 46.648 | 45.4282 | 175.3 | 43.4052 | 41.7095 | 205.3 |
| 20 | 45.8745 | 44.149 | 183.2 | 41.1145 | 45.1902 | 198.7 |
| 21 | 43.7805 | 43.1375 | 197.6 | 41.3525 | 43.1672 | 207.3 |
| 22 | 46.3505 | 47.3917 | 168.6 | 46.648 | 42.8697 | 184.8 |
| 23 | 42.5722 | 45.3985 | 191.6 | 45.4282 | 41.293 | 196.9 |
| 24 | 44.5357 | 45.0712 | 184.8 | 46.767 | 45.1902 | 175.3 |
| 25 | 42.2152 | 43.1375 | 203.4 | 47.5702 | 45.7257 | 170.8 |
| 26 | 46.1422 | 46.172 | 173.8 | 45.5175 | 43.673 | 186.5 |
| 27 | 43.5837 | 44.0597 | 193.3 | 43.9407 | 43.0482 | 196 |
| 28 | 43.554 | 44.863 | 189.9 | 42.8102 | 44.2085 | 196 |
| 29 | 43.911 | 45.7852 | 184.8 | 45.6365 | 45.5175 | 178.4 |
| 30 | 44.4167 | 44.0002 | 189.9 | 44.9522 | 42.6912 | 193.3 |
| 31 | 44.1787 | 45.4877 | 184.8 | 46.3207 | 45.0712 | 177.6 |
| 32 | 46.1125 | 44.4167 | 180.7 | 43.9407 | 43.1077 | 196 |

| | | | | | | |
|----------------|---------|---------|-------|---------|---------|-------|
| 33 | 43.0665 | 43.0665 | 199.3 | 42.8102 | 43.1672 | 200.6 |
| 34 | 43.078 | 44.625 | 192.5 | 45.339 | 43.2565 | 189 |
| 35 | 42.126 | 43.673 | 201.5 | 45.7257 | 43.5242 | 186.5 |
| 36 | 41.5012 | 43.435 | 205.3 | 45.577 | 46.172 | 176 |
| 37 | 42.4532 | 42.2747 | 206.3 | 44.8927 | 47.9867 | 172.3 |
| 38 | 44.8332 | 44.9225 | 184 | 47.7487 | 44.6845 | 173.8 |
| 39 | 44.2085 | 44.9225 | 186.5 | 45.3092 | 44.2977 | 184.8 |
| 40 | 44.0895 | 43.4647 | 193.3 | 43.4945 | 45.3092 | 188.1 |
| 41 | 43.435 | 45.6067 | 187.3 | 44.8332 | 42.6317 | 194.2 |
| 42 | 44.8927 | 45.101 | 183.2 | 42.4532 | 45.3687 | 192.5 |
| 43 | 42.8697 | 44.8035 | 193.3 | 45.0117 | 44.5357 | 184.8 |
| 44 | 44.4167 | 43.7622 | 190.7 | 46.2017 | 44.5655 | 181.5 |
| 45 | 45.1605 | 43.8515 | 187.3 | 46.7555 | 45.7555 | 173.8 |
| 46 | 46.1422 | 45.8745 | 175.3 | 46.3802 | 45.0117 | 177.6 |
| 47 | 43.673 | 44.3275 | 191.6 | 44.863 | 45.0415 | 183.2 |
| 48 | 44.8332 | 46.4992 | 177.6 | 45.4877 | 44.7737 | 182.3 |
| 49 | 44.5655 | 44.0002 | 189 | 45.4877 | 42.6912 | 191.6 |
| 50 | 45.8745 | 46.8265 | 172.3 | 44.863 | 45.696 | 180.7 |
| 51 | 45.577 | 46.648 | 174.5 | 46.9752 | 45.339 | 173.8 |
| 52 | 45.696 | 46.767 | 173.8 | 46.4397 | 45.3092 | 176 |
| 53 | 45.2497 | 45.3687 | 180.7 | 46.8265 | 45.7555 | 173 |
| 54 | 46.3505 | 44.9225 | 178.4 | 47.2132 | 45.8447 | 171.5 |
| 55 | 43.5242 | 46.3505 | 184 | 45.7257 | 44.6845 | 181.5 |
| 56 | 45.1902 | 47.719 | 171.5 | 45.1307 | 45.9042 | 179.2 |
| 57 | 44.268 | 43.435 | 192.5 | 45.4877 | 47.3025 | 172.3 |
| 58 | 46.3505 | 47.5405 | 168.6 | 46.9157 | 45.0415 | 175.3 |
| 59 | 42.8697 | 43.0482 | 200.6 | 45.3985 | 44.0002 | 185.6 |
| 60 | 44.4762 | 44.03 | 189 | 46.9157 | 46.767 | 169.3 |
| 61 | 42.8102 | 45.3985 | 190.7 | 50.099 | 45.458 | 162.3 |
| 62 | 44.744 | 44.928 | 184 | 47.4512 | 46.7967 | 167.2 |
| 63 | 43.792 | 44.7142 | 189 | 47.6 | 46.2612 | 168.6 |
| 64 | 45.815 | 44.5357 | 181.5 | 47.1835 | 45.22 | 173.8 |
| 65 | 43.7027 | 44.6845 | 189.9 | 48.0165 | 46.6777 | 165.8 |
| 66 | 43.673 | 43.911 | 193.3 | 46.3207 | 47.2727 | 169.3 |
| 67 | 43.435 | 43.0482 | 198.7 | 47.9272 | 46.7075 | 165.8 |
| 68 | 44.5655 | 45.7852 | 181.5 | 45.6365 | 47.005 | 173 |
| 69 | 44.2085 | 45.1605 | 185.6 | 47.8082 | 47.2132 | 164.4 |
| Average | | | 185.4 | | | |

Table A.10 Hardness readings for Sample 10

| Sample 10 | Nitrogen pressure 1.0 Torr, anode distance 120 mm Ion beam centre location: 20 mm | | | | | |
|------------------|--|-------------------------------------|-------|-------------------------------------|-------------------------------------|-------|
| | Before Nitriding: | | | After Nitriding: | | |
| Position (mm) | d ₁ (μm) | d ₂ (μm) | HV | d ₁ (μm) | d ₂ (μm) | HV |
| 1 | 45.3897 | 45.4877 | 179.9 | 46.3505 | 43.4945 | 184 |
| 2 | 45.4877 | 44.863 | 181.5 | 46.0232 | 41.9177 | 191.6 |
| 3 | 46.767 | 46.0232 | 172.3 | 44.625 | 42.5127 | 195.1 |
| 4 | 44.7142 | 42.9292 | 193.3 | 44.4167 | 46.4965 | 179.9 |
| 5 | 45.1902 | 45.5472 | 179.9 | 44.8927 | 45.2795 | 182.3 |
| 6 | 45.9637 | 46.6182 | 173 | 45.934 | 40.2517 | 199.7 |
| 7 | 45.1307 | 42.7507 | 192.5 | 45.4282 | 41.6202 | 196 |
| 8 | 46.3207 | 43.6432 | 183.2 | 45.8447 | 44.3572 | 182.3 |
| 9 | 45.5175 | 44.03 | 184.8 | 44.8927 | 45.458 | 181.5 |
| 10 | 44.4167 | 45.0415 | 185.6 | 45.9935 | 42.6615 | 189 |
| 11 | 46.3802 | 44.4762 | 179.9 | 45.5175 | 43.0185 | 189 |
| 12 | 44.5952 | 47.0645 | 176.8 | 43.1375 | 46.7372 | 184 |
| 13 | 45.4282 | 42.3937 | 192.5 | 46.3207 | 43.1077 | 185.6 |
| 14 | 45.3985 | 44.625 | 184 | 45.3092 | 44.2382 | 184.8 |
| 15 | 44.982 | 43.4647 | 189.9 | 43.9407 | 42.2747 | 199.7 |
| 16 | 45.5175 | 44.7737 | 182.3 | 44.8927 | 46.291 | 178.4 |
| 17 | 46.6777 | 45.3092 | 175.3 | 44.7142 | 45.9935 | 179.9 |
| 18 | 43.6432 | 44.268 | 191.6 | 46.3207 | 43.8217 | 182.3 |
| 19 | 45.1307 | 45.1307 | 182.3 | 38.6155 | 43.1672 | 221.7 |
| 20 | 45.4877 | 46.1422 | 176.8 | 42.245 | 41.293 | 212.3 |
| 21 | 45.5472 | 44.7737 | 181.5 | 41.7987 | 42.8697 | 206.3 |
| 22 | 43.1077 | 44.4762 | 193.3 | 46.1125 | 44.4167 | 180.7 |
| 23 | 44.4465 | 43.673 | 190.7 | 46.2017 | 42.9887 | 186.5 |
| 24 | 44.8927 | 43.1672 | 191.6 | 43.9407 | 43.5837 | 193.3 |
| 25 | 44.4167 | 43.673 | 191.6 | 46.0232 | 46.2315 | 174.5 |
| 26 | 43.554 | 43.1077 | 198.7 | 44.9225 | 44.7737 | 184.8 |
| 27 | 43.9402 | 45.101 | 187.3 | 45.2497 | 43.4025 | 189 |
| 28 | 44.625 | 42.0665 | 197.8 | 45.6067 | 44.8332 | 181.5 |
| 29 | 44.268 | 43.9705 | 190.7 | 44.1787 | 43.1375 | 194.2 |
| 30 | 44.3572 | 43.911 | 190.7 | 45.339 | 44.5952 | 183.2 |
| 31 | 43.1077 | 44.5655 | 193.3 | 45.7257 | 44.4762 | 182.3 |
| 32 | 44.2085 | 43.435 | 193.3 | 44.0002 | 43.1077 | 195.1 |

| | | | | | | |
|----------------|---------|---------|-------|---------|---------|-------|
| 33 | 44.03 | 44.5357 | 189 | 46.3505 | 45.1605 | 176.8 |
| 34 | 45.101 | 45.1605 | 182.3 | 44.1192 | 44.3572 | 189.9 |
| 35 | 44.0895 | 43.9407 | 191.6 | 43.316 | 43.0482 | 198.7 |
| 36 | 45.0712 | 45.815 | 179.9 | 46.291 | 44.6547 | 179.2 |
| 37 | 43.8812 | 45.0117 | 188.1 | 44.7142 | 43.6135 | 189.9 |
| 38 | 44.2085 | 43.8515 | 191.6 | 45.339 | 44.5655 | 183.2 |
| 39 | 44.149 | 44.863 | 187.3 | 45.458 | 44.5655 | 183.2 |
| 40 | 45.3092 | 45.101 | 181.5 | 44.625 | 44.625 | 186.5 |
| 41 | 44.1192 | 43.5837 | 192.5 | 47.243 | 45.0415 | 174.5 |
| 42 | 43.0185 | 43.7027 | 196.9 | 44.7142 | 45.7852 | 181.5 |
| 43 | 44.268 | 42.8697 | 195.1 | 44.03 | 43.435 | 194.2 |
| 44 | 42.721 | 43.554 | 198.7 | 46.767 | 43.6432 | 181.5 |
| 45 | 44.2382 | 42.8102 | 196 | 44.03 | 44.506 | 189 |
| 46 | 45.6365 | 42.3045 | 191.6 | 45.7555 | 43.792 | 184.8 |
| 47 | 44.5357 | 46.2612 | 179.9 | 43.9407 | 44.8035 | 188.1 |
| 48 | 45.3525 | 41.3525 | 195.1 | 43.435 | 44.1787 | 193.3 |
| 49 | 44.982 | 45.22 | 182.3 | 45.0117 | 44.149 | 186.5 |
| 50 | 46.2017 | 44.625 | 179.9 | 45.6365 | 43.2267 | 188.1 |
| 51 | 44.9225 | 45.9637 | 179.9 | 45.1307 | 45.339 | 181.5 |
| 52 | 45.9042 | 46.7967 | 173 | 45.2497 | 45.458 | 179.9 |
| 53 | 45.0712 | 45.577 | 180.7 | 46.41 | 44.149 | 180.7 |
| 54 | 47.1833 | 44.2382 | 177.6 | 43.5242 | 44.3275 | 192.5 |
| 55 | 46.4992 | 45.22 | 176 | 45.2497 | 45.0415 | 183.2 |
| 56 | 44.4762 | 45.7555 | 182.3 | 45.7852 | 44.03 | 184 |
| 57 | 45.5472 | 46.2612 | 176 | 46.4695 | 44.0895 | 180.7 |
| 58 | 46.41 | 46.5587 | 171.5 | 44.03 | 43.4945 | 193.3 |
| 59 | 44.03 | 42.5425 | 197.8 | 44.7142 | 43.2565 | 191.6 |
| 60 | 44.2382 | 43.5242 | 192.5 | 43.4647 | 43.2267 | 197.8 |
| 61 | 44.744 | 45.1902 | 183.2 | 45.2795 | 45.3985 | 180.7 |
| 62 | 45.1902 | 47.005 | 174.5 | 46.5587 | 44.4465 | 179.2 |
| 63 | 44.4465 | 45.7257 | 182.3 | 47.5702 | 45.8745 | 170.1 |
| 64 | 48.433 | 49.3255 | 153.8 | 45.3092 | 44.4465 | 184 |
| 65 | 43.673 | 43.2267 | 198.9 | 45.7852 | 45.101 | 179.9 |
| 66 | 44.387 | 42.0367 | 198.7 | 44.3572 | 43.4945 | 192.5 |
| 67 | 45.6067 | 44.387 | 183.2 | 42.2152 | 47.005 | 186.5 |
| 68 | 44.5357 | 44.8035 | 185.6 | 44.506 | 44.6845 | 186.5 |
| 69 | 43.2862 | 44.3572 | 193.3 | 46.7075 | 44.506 | 178.4 |
| Average | | | 185.8 | | | |

Table A.11 Hardness readings for Sample 11

| Sample 11 | Nitrogen pressure 1.5 Torr, anode distance 40 mm Ion beam centre location: 25 mm | | | | | |
|------------------|---|-------------------------------------|-------|-------------------------------------|-------------------------------------|-------|
| | Before Nitriding: | | | After Nitriding: | | |
| Position (mm) | d ₁ (μm) | d ₂ (μm) | HV | d ₁ (μm) | d ₂ (μm) | HV |
| 1 | 44.8035 | 46.2315 | 179.2 | 48.79 | 43.554 | 173.8 |
| 2 | 46.9455 | 42.6615 | 184.8 | 41.769 | 48.2842 | 183.2 |
| 3 | 42.84 | 42.5127 | 203.4 | 43.0185 | 46.0232 | 187.3 |
| 4 | 42.6615 | 44.8035 | 195.1 | 44.3275 | 42.7507 | 196 |
| 5 | 43.0185 | 43.2565 | 199.7 | 45.0712 | 45.5472 | 180.7 |
| 6 | 45.0117 | 45.6662 | 180.7 | 43.0185 | 44.0895 | 195.1 |
| 7 | 43.911 | 43.5837 | 194.2 | 44.982 | 44.625 | 184.8 |
| 8 | 43.7027 | 44.744 | 189.9 | 43.6135 | 44.863 | 189.9 |
| 9 | 46.767 | 45.339 | 174.5 | 45.6662 | 43.4052 | 187.3 |
| 10 | 44.2977 | 43.3755 | 193.3 | 43.1672 | 45.8745 | 187.3 |
| 11 | 46.2017 | 47.6 | 168.6 | 43.9407 | 46.5587 | 181.5 |
| 12 | 45.1902 | 45.8745 | 179.2 | 45.1902 | 45.0415 | 182.3 |
| 13 | 46.3207 | 46.529 | 172.3 | 45.458 | 45.9935 | 177.6 |
| 14 | 46.172 | 44.8332 | 179.2 | 46.7075 | 45.815 | 173 |
| 15 | 47.124 | 44.6845 | 176 | 42.5424 | 47.005 | 184.8 |
| 16 | 46.172 | 44.268 | 181.5 | 42.0665 | 49.504 | 176.8 |
| 17 | 45.6067 | 44.0597 | 184.8 | 43.7622 | 47.5107 | 178.4 |
| 18 | 44.03 | 43.4845 | 193.3 | 39.508 | 38.7642 | 242.6 |
| 19 | 47.3917 | 47.3917 | 165.1 | 41.531 | 39.9245 | 223.9 |
| 20 | 45.3092 | 45.339 | 180.7 | 31.6242 | 49.028 | 228.4 |
| 21 | 45.1605 | 46.0232 | 178.4 | 35.9975 | 39.984 | 256.9 |
| 22 | 45.3905 | 43.1375 | 189 | 26.9535 | 35.819 | 376.2 |
| 23 | 46.5587 | 46.9157 | 170.1 | 28.322 | 32.725 | 398.7 |
| 24 | 45.7257 | 45.1902 | 179.2 | 36.89 | 29.5715 | 336.5 |
| 25 | 45.4877 | 45.1605 | 180.7 | 33.8257 | 33.796 | 324.7 |
| 26 | 44.8332 | 44.4167 | 186.5 | 25.4065 | 39.9245 | 346.9 |
| 27 | 45.6365 | 44.9225 | 180.7 | 39.627 | 39.0915 | 238.9 |
| 28 | 43.2267 | 44.2382 | 194.2 | 41.65 | 33.1117 | 265.2 |
| 29 | 44.0597 | 45.1902 | 186.5 | 35.9677 | 42.959 | 237.7 |
| 30 | 45.2795 | 44.03 | 185.6 | 44.4167 | 26.7155 | 292.7 |
| 31 | 46.2612 | 45.7555 | 175.3 | 37.961 | 36.6222 | 266.6 |
| 32 | 46.2612 | 46.7075 | 171.5 | 39.508 | 38.556 | 243.9 |

| | | | | | | |
|----------------|---------|---------|-------|---------|---------|-------|
| 33 | 43.435 | 46.41 | 184 | 40.0435 | 40.4005 | 229.5 |
| 34 | 45.934 | 45.815 | 176 | 43.435 | 38.437 | 221.7 |
| 35 | 44.7737 | 46.4397 | 178.4 | 41.2037 | 42.126 | 213.3 |
| 36 | 45.6067 | 47.124 | 172.3 | 43.792 | 45.101 | 188.1 |
| 37 | 46.172 | 47.3025 | 170.1 | 41.5607 | 42.959 | 207.3 |
| 38 | 46.7967 | 49.2957 | 161 | 44.0895 | 40.103 | 209.3 |
| 39 | 46.1123 | 49.861 | 161 | 45.3985 | 44.7142 | 182.3 |
| 40 | 44.5357 | 42.602 | 195.1 | 45.7257 | 49.861 | 162.3 |
| 41 | 45.7257 | 46.4397 | 174.5 | 49.2065 | 44.03 | 170.8 |
| 42 | 45.9042 | 46.9157 | 172.3 | 45.696 | 47.7785 | 170.1 |
| 43 | 45.6067 | 44.625 | 182.3 | 45.22 | 44.387 | 184.8 |
| 44 | 47.243 | 45.458 | 172.3 | 46.6777 | 39.508 | 199.7 |
| 45 | 44.625 | 45.7852 | 181.5 | 42.8995 | 44.625 | 193.3 |
| 46 | 45.0117 | 45.696 | 179.9 | 40.5492 | 42.5127 | 215.4 |
| 47 | 44.7737 | 42.8102 | 193.3 | 44.3572 | 42.483 | 196.9 |
| 48 | 46.5587 | 44.387 | 179.2 | 43.6432 | 45.3092 | 187.3 |
| 49 | 47.0347 | 46.7967 | 168.6 | 44.5952 | 42.9887 | 193.3 |
| 50 | 43.9407 | 44.8332 | 188.1 | 41.8285 | 42.721 | 207.3 |
| 51 | 45.7257 | 48.314 | 167.9 | 43.7325 | 42.3045 | 200.6 |
| 52 | 44.8927 | 44.982 | 184 | 44.7142 | 44.625 | 185.6 |
| 53 | 46.2612 | 45.1902 | 177.6 | 45.934 | 44.2085 | 182.3 |
| 54 | 44.5357 | 45.0415 | 184.8 | 44.8332 | 46.4397 | 178.4 |
| 55 | 45.6662 | 44.03 | 184.8 | 44.4167 | 47.3322 | 176 |
| 56 | 47.7487 | 46.4992 | 167.2 | 42.959 | 45.7555 | 188.1 |
| 57 | 44.6547 | 43.435 | 191.6 | 44.7142 | 46.5587 | 178.4 |
| 58 | 45.458 | 46.2612 | 176 | 45.934 | 45.22 | 178.4 |
| 59 | 45.6067 | 46.3207 | 175.3 | 44.4762 | 46.0827 | 180.7 |
| 60 | 45.5472 | 46.422 | 176.8 | 46.3505 | 45.577 | 175.3 |
| 61 | 44.625 | 46.3207 | 179.2 | 44.3572 | 45.5175 | 184 |
| 62 | 46.1422 | 44.7142 | 179.9 | 43.911 | 46.291 | 182.3 |
| 63 | 44.8035 | 45.9042 | 179.9 | 43.2267 | 44.625 | 192.5 |
| 64 | 46.767 | 46.2017 | 171.5 | 45.7257 | 47.6 | 170.1 |
| 65 | 44.5952 | 45.1302 | 184 | 42.602 | 46.767 | 185.6 |
| 66 | 46.0232 | 47.0347 | 173 | 41.9475 | 44.625 | 197.8 |
| 67 | 45.7852 | 47.6 | 170.1 | 46.2612 | 44.9522 | 178.4 |
| 68 | 46.3505 | 45.8447 | 174.5 | 43.2267 | 45.22 | 189.9 |
| 69 | 47.2132 | 47.6297 | 165.1 | 44.625 | 45.3985 | 183.2 |
| Average | | | 179.8 | | | |

Table A.12 Hardness readings for Sample 12

| Sample 12 | Nitrogen pressure 1.5 Torr, anode distance 60 mm Ion beam centre location: 19 mm | | | | | |
|------------------|---|-------------------------------------|-------|-------------------------------------|-------------------------------------|-------|
| | Before Nitriding: | | | After Nitriding: | | |
| Position (mm) | d ₁ (μm) | d ₂ (μm) | HV | d ₁ (μm) | d ₂ (μm) | HV |
| 1 | 47.3025 | 45.4877 | 172.3 | 43.792 | 44.2085 | 191.6 |
| 2 | 46.1422 | 44.4762 | 180.7 | 44.982 | 46.3802 | 177.6 |
| 3 | 47.2132 | 45.8447 | 171.5 | 44.5952 | 45.0712 | 184.8 |
| 4 | 44.2382 | 47.9272 | 174.5 | 44.1192 | 43.6432 | 192.5 |
| 5 | 46.1472 | 42.6615 | 188.1 | 45.0712 | 45.5472 | 180.7 |
| 6 | 44.3655 | 45.4282 | 183.2 | 47.6596 | 48.0165 | 162.3 |
| 7 | 47.957 | 46.767 | 165.1 | 44.8332 | 46.1125 | 179.2 |
| 8 | 45.8745 | 45.3985 | 178.4 | 45.1902 | 46.9455 | 174.5 |
| 9 | 46.3802 | 45.7555 | 174.5 | 43.1672 | 44.4167 | 193.3 |
| 10 | 46.7372 | 46.291 | 171.5 | 45.0712 | 46.3505 | 177.6 |
| 11 | 45.6662 | 44.863 | 180.6 | 45.9637 | 39.3295 | 204.4 |
| 12 | 47.0942 | 44.625 | 176 | 39.865 | 47.243 | 195.1 |
| 13 | 43.197 | 46.886 | 183.2 | 36.6817 | 44.0002 | 228.4 |
| 14 | 47.1537 | 46.053 | 170.8 | 44.8332 | 43.2267 | 191.6 |
| 15 | 47.8677 | 48.1057 | 161 | 43.4052 | 43.435 | 196.9 |
| 16 | 42.126 | 50.0327 | 167.2 | 45.3092 | 42.6317 | 191.6 |
| 17 | 49.147 | 46.0232 | 163.7 | 35.9082 | 38.1692 | 270.9 |
| 18 | 45.339 | 44.0306 | 185.6 | 35.8785 | 35.6107 | 291 |
| 19 | 44.5655 | 51.289 | 161.7 | 35.938 | 48.9685 | 205.3 |
| 20 | 46.1422 | 45.1307 | 178.4 | 43.0185 | 36.2355 | 236.5 |
| 21 | 46.2017 | 48.4627 | 165.8 | 43.0185 | 43.2862 | 198.7 |
| 22 | 46.7372 | 42.364 | 186.5 | 46.6777 | 36.3842 | 215.4 |
| 23 | 46.886 | 45.0415 | 175.3 | 36.3842 | 35.5512 | 286.2 |
| 24 | 45.934 | 44.6845 | 180.7 | 41.5607 | 41.2632 | 216.4 |
| 25 | 47.362 | 43.9705 | 177.6 | 43.6432 | 46.4695 | 182.3 |
| 26 | 48.1355 | 46.3207 | 166.5 | 44.5655 | 41.7392 | 198.7 |
| 27 | 46.886 | 46.5885 | 170.1 | 44.2085 | 43.0185 | 195.1 |
| 28 | 47.838 | 48.8495 | 159 | 46.3207 | 44.4465 | 179.9 |
| 29 | 45.22 | 45.934 | 178.4 | 47.243 | 43.5837 | 179.9 |
| 30 | 49.504 | 45.339 | 165.1 | 47.5702 | 45.3687 | 171.5 |
| 31 | 47.7785 | 46.7969 | 165.8 | 46.767 | 44.3275 | 179.2 |
| 32 | 46.2315 | 45.2795 | 176.8 | 46.7372 | 47.3917 | 167.2 |

| | | | | | | |
|----------------|---------|---------|-------|---------|---------|-------|
| 33 | 48.5502 | 44.8035 | 170.1 | 45.0415 | 52.0922 | 157 |
| 34 | 43.197 | 50.8427 | 167.9 | 48.2842 | 47.005 | 163.7 |
| 35 | 47.3917 | 44.5655 | 175.3 | 46.8562 | 47.0942 | 167.9 |
| 36 | 47.3917 | 45.8745 | 170.8 | 49.028 | 41.5012 | 180.7 |
| 37 | 46.4397 | 44.0002 | 181.5 | 46.6182 | 45.9637 | 173 |
| 38 | 45.1605 | 45.9935 | 178.4 | 48.1057 | 44.506 | 173 |
| 39 | 44.9225 | 46.4695 | 177.6 | 46.4397 | 49.2362 | 162.3 |
| 40 | 48.909 | 43.1077 | 175.3 | 43.4647 | 45.815 | 186.5 |
| 41 | 49.6825 | 45.815 | 163 | 45.1307 | 44.2085 | 185.6 |
| 42 | 45.577 | 48.671 | 167.2 | 45.339 | 49.147 | 166.5 |
| 43 | 44.4465 | 44.6547 | 186.5 | 45.577 | 50.5452 | 160.3 |
| 44 | 45.0415 | 45.3985 | 181.5 | 43.2267 | 46.529 | 184 |
| 45 | 48.0165 | 47.362 | 163 | 43.7325 | 42.5722 | 198.7 |
| 46 | 46.7075 | 44.3275 | 179.2 | 42.5722 | 44.387 | 196 |
| 47 | 48.195 | 47.0645 | 163.7 | 43.4647 | 44.982 | 189.9 |
| 48 | 46.648 | 45.3687 | 175.3 | 45.3985 | 43.6135 | 187.3 |
| 49 | 44.6845 | 43.4945 | 190.7 | 44.9522 | 43.2267 | 190.7 |
| 50 | 45.4282 | 47.481 | 171.5 | 43.3755 | 45.1307 | 189 |
| 51 | 47.0645 | 44.5952 | 176.8 | 45.2497 | 45.5472 | 179.9 |
| 52 | 47.6297 | 46.6777 | 166.5 | 43.3457 | 47.3322 | 180.7 |
| 53 | 46.9752 | 48.8197 | 161.7 | 46.4992 | 43.4945 | 183.2 |
| 54 | 45.2795 | 46.7967 | 175.3 | 45.2497 | 42.8995 | 190.7 |
| 55 | 45.3687 | 43.8515 | 186.5 | 44.3572 | 45.101 | 185.6 |
| 56 | 45.22 | 46.172 | 177.6 | 44.387 | 42.364 | 196.9 |
| 57 | 47.8062 | 47.0942 | 164.4 | 45.22 | 44.3572 | 184.8 |
| 58 | 46.3207 | 47.1537 | 170.1 | 44.625 | 43.673 | 190.7 |
| 59 | 44.4465 | 42.2747 | 196.9 | 42.5425 | 44.0002 | 197.8 |
| 60 | 46.4695 | 45.1605 | 176.8 | 45.4877 | 44.7142 | 182.3 |
| 61 | 47.9272 | 46.5885 | 165.8 | 45.2795 | 44.2382 | 184.8 |
| 62 | 46.9455 | 47.124 | 167.9 | 42.8102 | 46.529 | 185.6 |
| 63 | 45.7257 | 46.1125 | 176 | 48.4627 | 46.7372 | 163.7 |
| 64 | 45.7257 | 46.2315 | 175.3 | 43.792 | 45.577 | 185.6 |
| 65 | 44.8035 | 45.101 | 183.2 | 44.03 | 43.2267 | 195.1 |
| 66 | 46.3207 | 46.7967 | 170.8 | 43.4052 | 45.696 | 186.5 |
| 67 | 43.9705 | 44.8035 | 188.1 | 44.625 | 42.84 | 194.2 |
| 68 | 46.291 | 46.6777 | 171.5 | 41.769 | 43.1077 | 206.3 |
| 69 | 46.291 | 47.362 | 169.3 | 44.5952 | 41.888 | 198.7 |
| Average | | | 174.1 | | | |

Table A.13 Hardness readings for Sample 13

| Sample 13 | Nitrogen pressure 1.5 Torr, anode distance 80 mm Ion beam centre location: 22 mm | | | | | |
|------------------|---|-------------------------------------|-------|-------------------------------------|-------------------------------------|-------|
| | Before Nitriding: | | | After Nitriding: | | |
| Position (mm) | d ₁ (μm) | d ₂ (μm) | HV | d ₁ (μm) | d ₂ (μm) | HV |
| 1 | 47.243 | 45.4877 | 172.3 | 45.9637 | 44.0895 | 183.2 |
| 2 | 44.4762 | 41.8582 | 198.7 | 44.268 | 45.6067 | 184 |
| 3 | 46.7967 | 45.9935 | 172.3 | 46.3802 | 45.696 | 175.3 |
| 4 | 45.458 | 45.1307 | 180.7 | 45.9042 | 46.2612 | 174.5 |
| 5 | 45.0712 | 45.7257 | 179.9 | 45.0117 | 48.2842 | 170.8 |
| 6 | 46.648 | 46.9157 | 169.3 | 45.6662 | 46.8265 | 173.8 |
| 7 | 45.2497 | 43.3457 | 189 | 46.4992 | 46.3207 | 172.3 |
| 8 | 43.5242 | 43.078 | 197.8 | 45.815 | 45.1902 | 179.2 |
| 9 | 45.815 | 46.767 | 173 | 45.815 | 45.934 | 176 |
| 10 | 43.8217 | 43.7027 | 193.3 | 45.1605 | 44.982 | 182.3 |
| 11 | 45.6662 | 45.2497 | 179.9 | 44.1787 | 43.554 | 192.5 |
| 12 | 45.5472 | 42.6912 | 190.7 | 45.2795 | 44.9225 | 182.3 |
| 13 | 46.172 | 43.6135 | 184 | 44.1787 | 45.4877 | 184.8 |
| 14 | 44.2085 | 44.9522 | 186.5 | 44.0597 | 46.4397 | 181.5 |
| 15 | 46.2615 | 43.4025 | 184.8 | 44.8035 | 44.8332 | 184.8 |
| 16 | 46.1422 | 47.8082 | 167.9 | 43.5837 | 41.412 | 205.3 |
| 17 | 46.172 | 44.9225 | 179.2 | 44.3275 | 41.412 | 201.5 |
| 18 | 44.387 | 44.3275 | 188.1 | 46.3207 | 41.0847 | 193.3 |
| 19 | 47.7785 | 43.3755 | 178.4 | 42.364 | 41.1145 | 213.3 |
| 20 | 46.7967 | 41.65 | 189.9 | 44.7737 | 40.222 | 205.3 |
| 21 | 44.4167 | 45.4877 | 183.2 | 44.2085 | 42.126 | 198.7 |
| 22 | 45.934 | 44.744 | 180.7 | 38.5262 | 46.9157 | 203.4 |
| 23 | 46.2017 | 44.8332 | 179.2 | 40.1922 | 44.149 | 208.3 |
| 24 | 44.2085 | 42.2747 | 198.7 | 43.078 | 42.5425 | 202.5 |
| 25 | 45.458 | 46.291 | 176 | 43.792 | 42.721 | 197.8 |
| 26 | 46.0827 | 46.41 | 173.8 | 45.815 | 39.4187 | 204.4 |
| 27 | 46.529 | 45.22 | 176 | 45.1902 | 45.6662 | 179.9 |
| 28 | 44.5655 | 44.03 | 189 | 44.03 | 43.792 | 192.5 |
| 29 | 44.7142 | 45.1902 | 183.2 | 45.0415 | 44.149 | 186.5 |
| 30 | 45.0415 | 43.673 | 188.1 | 47.3322 | 41.888 | 186.5 |
| 31 | 46.2017 | 44.5952 | 179.9 | 45.101 | 45.3092 | 181.5 |
| 32 | 45.339 | 43.7325 | 187.3 | 40.0732 | 45.0712 | 204.4 |

| | | | | | | |
|----------------|---------|---------|-------|---------|---------|-------|
| 33 | 45.577 | 44.4167 | 183.2 | 45.6662 | 44.625 | 182.3 |
| 34 | 46.2612 | 44.6845 | 179.2 | 45.0117 | 45.101 | 182.3 |
| 35 | 47.362 | 45.9935 | 170.1 | 46.4695 | 45.9935 | 173.8 |
| 36 | 44.5357 | 44.0597 | 189 | 44.5952 | 46.9157 | 176.8 |
| 37 | 45.1307 | 44.0895 | 186.5 | 44.9225 | 46.3505 | 178.4 |
| 38 | 45.8447 | 43.7325 | 184.8 | 44.0895 | 43.5837 | 193.3 |
| 39 | 45.1902 | 45.1605 | 181.5 | 44.03 | 48.2545 | 173.8 |
| 40 | 45.7257 | 42.6615 | 189.9 | 47.6 | 47.2727 | 165.1 |
| 41 | 47.3322 | 45.7555 | 171.5 | 46.7273 | 45.3985 | 174.5 |
| 42 | 45.4282 | 44.6845 | 182.3 | 43.9407 | 44.4167 | 189.9 |
| 43 | 45.2497 | 44.2382 | 185.6 | 46.2315 | 46.2017 | 173.8 |
| 44 | 43.5837 | 45.0712 | 189 | 45.0415 | 44.4465 | 185.6 |
| 45 | 46.3027 | 46.6067 | 175.3 | 45.3687 | 46.291 | 176.8 |
| 46 | 47.3322 | 46.2017 | 169.3 | 44.4167 | 44.2085 | 189 |
| 47 | 45.6067 | 46.291 | 176 | 46.8562 | 45.6662 | 173 |
| 48 | 44.4167 | 44.5357 | 187.3 | 45.8745 | 44.5655 | 181.5 |
| 49 | 45.22 | 44.2977 | 184.8 | 45.9935 | 46.886 | 172.3 |
| 50 | 44.5952 | 45.1902 | 184 | 46.4397 | 44.5655 | 179.2 |
| 51 | 45.934 | 44.7737 | 179.9 | 45.22 | 44.4465 | 184.8 |
| 52 | 46.2017 | 45.22 | 177.6 | 45.0712 | 44.149 | 186.5 |
| 53 | 45.22 | 46.5885 | 176 | 46.3802 | 47.3322 | 168.6 |
| 54 | 45.934 | 45.1902 | 178.4 | 46.4492 | 45.6365 | 174.5 |
| 55 | 45.5472 | 45.1902 | 179.9 | 46.8562 | 44.625 | 177.6 |
| 56 | 46.0232 | 46.2017 | 174.5 | 47.005 | 46.3802 | 170.1 |
| 57 | 46.767 | 47.1835 | 167.9 | 46.9455 | 46.3505 | 170.8 |
| 58 | 45.339 | 45.1902 | 180.7 | 45.5175 | 45.1605 | 180.7 |
| 59 | 44.7737 | 46.5587 | 177.6 | 46.291 | 47.9272 | 167.2 |
| 60 | 45.4877 | 44.9225 | 181.5 | 46.6182 | 45.101 | 176 |
| 61 | 45.8447 | 45.4877 | 177.6 | 45.3092 | 44.0597 | 185.6 |
| 62 | 48.6115 | 46.41 | 164.4 | 45.9935 | 46.0827 | 175.3 |
| 63 | 46.291 | 46.6182 | 171.5 | 47.6297 | 47.005 | 165.8 |
| 64 | 45.458 | 43.673 | 186.5 | 45.7852 | 46.3207 | 174.5 |
| 65 | 43.435 | 45.3687 | 188.1 | 47.0942 | 46.053 | 170.8 |
| 66 | 46.2315 | 46.4695 | 172.3 | 46.291 | 45.577 | 176 |
| 67 | 44.8927 | 46.291 | 178.4 | 46.3505 | 45.5175 | 176 |
| 68 | 47.1835 | 47.3025 | 166.5 | 45.8447 | 47.124 | 171.5 |
| 69 | 45.5472 | 43.7325 | 186.5 | 45.22 | 43.8217 | 187.3 |
| Average | | | 181.0 | | | |

Table A.14 Hardness readings for Sample 14

| Sample 14 | Nitrogen pressure 1.5 Torr, anode distance 100 mm Ion beam centre location: 22 mm | | | | | |
|------------------|--|-------------------------------------|-------|-------------------------------------|-------------------------------------|-------|
| | Before Nitriding: | | | After Nitriding: | | |
| Position (mm) | d ₁ (μm) | d ₂ (μm) | HV | d ₁ (μm) | d ₂ (μm) | HV |
| 1 | 47.243 | 43.9705 | 178.4 | 47.0347 | 47.4215 | 166.5 |
| 2 | 45.9637 | 43.435 | 185.6 | 47.6595 | 43.7622 | 177.6 |
| 3 | 42.5425 | 44.8332 | 194.2 | 45.6067 | 44.744 | 181.5 |
| 4 | 44.2977 | 45.22 | 184.8 | 45.696 | 43.6432 | 185.6 |
| 5 | 43.435 | 43.7027 | 195.1 | 45.4877 | 46.5587 | 175.3 |
| 6 | 42.84 | 47.243 | 183.2 | 46.053 | 46.5587 | 173 |
| 7 | 42.721 | 44.8035 | 193.3 | 46.886 | 45.7257 | 173 |
| 8 | 43.197 | 45.696 | 188.1 | 45.0415 | 41.2037 | 199.7 |
| 9 | 43.4052 | 42.6615 | 200.6 | 48.9982 | 47.1537 | 160.3 |
| 10 | 45.9637 | 43.6432 | 184.8 | 45.0712 | 45.8745 | 179.2 |
| 11 | 44.5655 | 43.316 | 192.5 | 44.3572 | 43.7622 | 190.7 |
| 12 | 44.0002 | 45.1902 | 186.5 | 44.8927 | 43.4647 | 189.9 |
| 13 | 44.149 | 42.245 | 198.7 | 46.7967 | 45.8745 | 173 |
| 14 | 43.0482 | 44.1102 | 195.1 | 45.4282 | 43.3457 | 188.1 |
| 15 | 42.9887 | 44.7142 | 192.5 | 42.7805 | 41.8582 | 207.3 |
| 16 | 43.3755 | 43.5242 | 196.9 | 42.959 | 43.5837 | 197.8 |
| 17 | 44.5357 | 45.6067 | 182.3 | 42.5722 | 43.1672 | 201.5 |
| 18 | 41.9177 | 43.4052 | 203.4 | 44.625 | 45.458 | 183.2 |
| 19 | 44.6547 | 45.2487 | 183.2 | 42.7507 | 42.3937 | 204.4 |
| 20 | 42.6912 | 43.0185 | 201.5 | 47.005 | 43.673 | 180.7 |
| 21 | 42.602 | 43.316 | 200.6 | 44.1787 | 46.2017 | 181.5 |
| 22 | 43.197 | 44.9225 | 190.7 | 46.41 | 46.4695 | 172.3 |
| 23 | 43.197 | 43.6432 | 196.9 | 43.7027 | 43.8812 | 193.3 |
| 24 | 44.8035 | 44.149 | 187.3 | 42.7507 | 40.1327 | 216.4 |
| 25 | 45.815 | 44.4465 | 182.3 | 41.412 | 42.126 | 212.3 |
| 26 | 46.41 | 45.22 | 176.8 | 43.1672 | 43.6135 | 196.9 |
| 27 | 42.8995 | 42.5425 | 203.4 | 41.2037 | 40.2815 | 223.9 |
| 28 | 44.2977 | 44.625 | 187.3 | 46.5587 | 41.9177 | 189.9 |
| 29 | 43.078 | 44.149 | 195.1 | 38.4072 | 44.2382 | 217.4 |
| 30 | 44.387 | 45.696 | 183.2 | 43.435 | 44.7737 | 190.7 |
| 31 | 41.5905 | 44.5655 | 199.7 | 46.5587 | 42.6615 | 186.5 |
| 32 | 43.4052 | 44.4167 | 192.5 | 42.245 | 43.8812 | 199.7 |

| | | | | | | |
|----------------|---------|---------|-------|---------|---------|-------|
| 33 | 42.5722 | 44.268 | 196.9 | 44.6547 | 41.9475 | 197.8 |
| 34 | 45.815 | 43.197 | 187.3 | 44.6845 | 43.316 | 191.6 |
| 35 | 42.5127 | 45.3687 | 192.5 | 45.3687 | 43.7325 | 186.5 |
| 36 | 43.2862 | 43.197 | 198.7 | 42.3937 | 43.078 | 203.4 |
| 37 | 44.1787 | 44.1787 | 189.9 | 44.5952 | 43.3457 | 191.6 |
| 38 | 41.9457 | 44.268 | 199.7 | 43.2267 | 44.1787 | 194.2 |
| 39 | 43.9705 | 43.4647 | 194.2 | 43.1077 | 45.0117 | 190.7 |
| 40 | 43.7325 | 44.3275 | 191.6 | 44.3572 | 43.554 | 191.6 |
| 41 | 43.792 | 44.625 | 189.9 | 44.2977 | 45.9935 | 182.3 |
| 42 | 43.3755 | 44.6845 | 191.6 | 44.1192 | 43.3457 | 194.2 |
| 43 | 42.7507 | 45.4877 | 190.7 | 48.2545 | 44.03 | 174.5 |
| 44 | 42.3937 | 43.9705 | 198.7 | 45.4877 | 44.5952 | 183.2 |
| 45 | 43.9705 | 45.101 | 187.3 | 47.1835 | 43.7027 | 179.9 |
| 46 | 43.911 | 43.554 | 194.2 | 45.7257 | 44.8332 | 180.7 |
| 47 | 45.0712 | 46.5587 | 176.8 | 44.1787 | 42.483 | 197.8 |
| 48 | 45.339 | 45.1902 | 180.7 | 44.4762 | 43.3755 | 192.5 |
| 49 | 47.6 | 46.0827 | 169.3 | 45.696 | 45.4877 | 178.4 |
| 50 | 42.5722 | 43.5837 | 199.7 | 44.4167 | 44.7142 | 186.5 |
| 51 | 43.2862 | 43.8217 | 195.1 | 45.6662 | 44.0597 | 184 |
| 52 | 44.2085 | 46.648 | 179.9 | 44.6547 | 44.0002 | 189 |
| 53 | 45.22 | 46.4992 | 176 | 45.6067 | 45.9935 | 176.8 |
| 54 | 43.1375 | 42.2152 | 203.4 | 44.387 | 48.0462 | 173.8 |
| 55 | 45.0415 | 44.4762 | 194.8 | 44.744 | 44.3572 | 186.5 |
| 56 | 42.8995 | 41.5607 | 208.3 | 46.886 | 43.4052 | 182.3 |
| 57 | 42.4235 | 44.148 | 197.8 | 43.8812 | 44.4167 | 190.7 |
| 58 | 44.2977 | 45.8745 | 182.3 | 44.5357 | 42.1557 | 197.8 |
| 59 | 44.5952 | 44.4762 | 187.3 | 44.0002 | 43.197 | 195.1 |
| 60 | 42.4235 | 45.339 | 192.5 | 44.506 | 43.8515 | 189.9 |
| 61 | 43.8217 | 46.2612 | 183.2 | 42.9887 | 44.268 | 195.1 |
| 62 | 43.7325 | 45.3092 | 187.3 | 44.9522 | 44.2977 | 186.5 |
| 63 | 42.84 | 44.0895 | 196 | 45.22 | 45.9935 | 178.4 |
| 64 | 42.721 | 43.8217 | 197.8 | 44.2977 | 42.483 | 196.9 |
| 65 | 42.721 | 44.1192 | 196.9 | 48.7007 | 45.6365 | 166.5 |
| 66 | 44.9522 | 46.1422 | 179.2 | 46.172 | 45.934 | 174.5 |
| 67 | 45.0415 | 44.9522 | 183.2 | 47.4512 | 47.4215 | 165.1 |
| 68 | 45.5472 | 44.9522 | 181.5 | 45.5472 | 44.9522 | 181.5 |
| 69 | 43.3755 | 44.5952 | 191.6 | 48.3735 | 47.6 | 161 |
| Average | | | 190.7 | | | |

Table A.15 Hardness readings for Sample 15

| Sample 15 | Nitrogen pressure 1.5 Torr, anode distance 120 mm Ion beam centre location: 22 mm | | | | | |
|------------------|--|-------------------------------------|-------|-------------------------------------|-------------------------------------|-------|
| | Before Nitriding: | | | After Nitriding: | | |
| Position (mm) | d ₁ (μm) | d ₂ (μm) | HV | d ₁ (μm) | d ₂ (μm) | HV |
| 1 | 44.744 | 44.7142 | 185.6 | 44.982 | 47.3025 | 174.5 |
| 2 | 45.0712 | 47.7785 | 172.3 | 43.2267 | 47.3025 | 180.7 |
| 3 | 45.6365 | 44.982 | 180.7 | 43.9407 | 43.554 | 194.2 |
| 4 | 47.4215 | 45.934 | 170.1 | 41.174 | 44.0002 | 204.4 |
| 5 | 46.648 | 47.2727 | 167.9 | 44.5655 | 44.8035 | 185.6 |
| 6 | 45.339 | 44.0002 | 185.6 | 44.3275 | 45.2795 | 184.8 |
| 7 | 46.291 | 44.03 | 181.5 | 46.2017 | 48.2842 | 166.5 |
| 8 | 48.3735 | 44.2382 | 173 | 45.0117 | 47.0347 | 175.3 |
| 9 | 45.577 | 44.625 | 182.3 | 45.9637 | 46.9455 | 171.5 |
| 10 | 46.588 | 44.863 | 177.6 | 44.149 | 43.6432 | 192.5 |
| 11 | 44.4167 | 43.6432 | 191.6 | 45.1307 | 46.2612 | 177.6 |
| 12 | 47.8975 | 46.3505 | 167.2 | 45.339 | 43.9705 | 185.6 |
| 13 | 46.0827 | 45.3092 | 177 | 44.982 | 46.9455 | 175.3 |
| 14 | 47.4215 | 44.3572 | 176 | 45.4877 | 44.8332 | 181.5 |
| 15 | 47.183 | 42.4532 | 184.8 | 45.7852 | 46.6182 | 173.8 |
| 16 | 47.9867 | 44.2382 | 174.5 | 47.5405 | 46.1125 | 169.3 |
| 17 | 48.433 | 43.8515 | 174.5 | 46.5587 | 45.22 | 176 |
| 18 | 46.767 | 46.2612 | 171.5 | 45.3985 | 47.4512 | 172.3 |
| 19 | 45.0415 | 42.602 | 193.3 | 46.9455 | 46.3505 | 170.8 |
| 20 | 45.339 | 44.8332 | 182.3 | 46.4397 | 46.3505 | 172.3 |
| 21 | 44.4167 | 46.4695 | 179.9 | 46.0232 | 45.1307 | 178.4 |
| 22 | 44.387 | 42.8697 | 190.1 | 45.4282 | 46.3207 | 176 |
| 23 | 48.2842 | 44.8332 | 170.8 | 44.8035 | 46.41 | 178.4 |
| 24 | 43.1672 | 44.9522 | 190.7 | 44.5655 | 43.8515 | 189.9 |
| 25 | 42.3342 | 48.8792 | 178.4 | 45.3985 | 45.339 | 179.9 |
| 26 | 46.6182 | 44.6251 | 178.4 | 45.3985 | 44.8035 | 182.3 |
| 27 | 46.6182 | 42.0962 | 188.1 | 46.41 | 45.6067 | 175.3 |
| 28 | 44.1192 | 46.0827 | 182.3 | 45.9935 | 48.3735 | 166.5 |
| 29 | 48.2842 | 44.8332 | 170.8 | 43.435 | 44.387 | 192.5 |
| 30 | 46.529 | 46.291 | 172.3 | 44.982 | 47.1537 | 174.5 |
| 31 | 47.3917 | 45.9935 | 170.1 | 46.4992 | 46.5885 | 171.5 |
| 32 | 46.7372 | 49.0875 | 161.7 | 46.4397 | 46.8265 | 170.8 |

| | | | | | | |
|----------------|---------|---------|-------|---------|---------|-------|
| 33 | 46.2017 | 45.2497 | 177.6 | 45.9637 | 45.6662 | 176.8 |
| 34 | 45.22 | 44.3275 | 184.8 | 46.2017 | 46.053 | 174.5 |
| 35 | 45.815 | 47.6 | 170.1 | 45.696 | 45.2795 | 179.2 |
| 36 | 44.4465 | 46.1125 | 180.7 | 44.1192 | 44.982 | 186.5 |
| 37 | 48.8792 | 44.268 | 170.8 | 42.8995 | 43.435 | 198.7 |
| 38 | 47.3322 | 48.9685 | 159.6 | 45.7257 | 44.4465 | 182.3 |
| 39 | 46.3802 | 47.005 | 170.1 | 42.0665 | 42.1855 | 209.3 |
| 40 | 44.6845 | 45.934 | 180.7 | 40.103 | 43.7027 | 211.3 |
| 41 | 44.744 | 46.3802 | 178.4 | 43.2656 | 43.316 | 197.8 |
| 42 | 46.5587 | 46.648 | 170.8 | 43.4647 | 44.2085 | 193.3 |
| 43 | 48.5222 | 47.481 | 161 | 42.9887 | 42.1557 | 204.4 |
| 44 | 45.934 | 48.195 | 167.9 | 40.341 | 39.8352 | 230.7 |
| 45 | 47.4512 | 46.7075 | 167.2 | 43.6135 | 44.2282 | 192.5 |
| 46 | 46.2315 | 43.0185 | 186.5 | 42.483 | 42.6615 | 204.4 |
| 47 | 45.9042 | 45.101 | 179.2 | 42.0665 | 43.4647 | 202.5 |
| 48 | 45.696 | 44.149 | 184 | 42.959 | 44.2977 | 195.1 |
| 49 | 46.7372 | 45.101 | 176 | 41.531 | 41.2305 | 216.4 |
| 50 | 47.5702 | 46.1125 | 169.3 | 44.8035 | 44.0895 | 188.1 |
| 51 | 47.719 | 46.648 | 166.5 | 44.149 | 44.9522 | 186.5 |
| 52 | 46.648 | 44.5952 | 178.4 | 41.9475 | 41.4715 | 213.3 |
| 53 | 45.339 | 44.6547 | 183.2 | 43.8515 | 45.815 | 184.8 |
| 54 | 46.1125 | 44.8332 | 179.2 | 45.8745 | 44.3275 | 182.3 |
| 55 | 46.4992 | 45.7257 | 174.5 | 44.387 | 41.055 | 203.4 |
| 56 | 47.957 | 45.0415 | 171.5 | 45.0117 | 44.506 | 184.8 |
| 57 | 47.9272 | 46.1125 | 167.9 | 46.41 | 44.2977 | 179.9 |
| 58 | 46.053 | 46.7372 | 172.3 | 44.8332 | 45.6365 | 181.5 |
| 59 | 48.1057 | 46.4695 | 165.8 | 43.7325 | 43.0482 | 196.9 |
| 60 | 47.005 | 47.0942 | 167.9 | 42.3045 | 43.4945 | 201.5 |
| 61 | 46.0232 | 46.4397 | 173.8 | 44.2085 | 43.3937 | 197.8 |
| 62 | 46.6777 | 46.291 | 171.5 | 43.8575 | 44.5357 | 189.9 |
| 63 | 48.0165 | 47.6892 | 161.7 | 43.8515 | 43.792 | 193.3 |
| 64 | 44.7142 | 45.3985 | 182.3 | 42.7507 | 42.8995 | 202.5 |
| 65 | 45.8447 | 45.7852 | 176.8 | 42.364 | 41.5905 | 210.3 |
| 66 | 47.6892 | 46.5885 | 167.2 | 42.6317 | 42.1855 | 206.3 |
| 67 | 45.4877 | 46.2612 | 176 | 42.4532 | 40.8467 | 214.3 |
| 68 | 47.4512 | 47.7487 | 163.7 | 42.5425 | 42.0367 | 207.3 |
| 69 | 46.7075 | 45.339 | 175.3 | 40.103 | 40.4005 | 218.4 |
| Average | | | 175.6 | | | |

Table A.16 Hardness readings for Sample 16

| Sample 16 | Nitrogen pressure 2.0 Torr, anode distance 40 mm Ion beam centre location: 22 mm | | | | | |
|------------------|---|-------------------------------------|-------|-------------------------------------|-------------------------------------|-------|
| | Before Nitriding: | | | After Nitriding: | | |
| Position (mm) | d ₁ (μm) | d ₂ (μm) | HV | d ₁ (μm) | d ₂ (μm) | HV |
| 1 | 45.7852 | 47.6297 | 170.1 | 46.8265 | 47.9272 | 165.1 |
| 2 | 47.1835 | 47.1537 | 166.5 | 46.3505 | 51.2295 | 155.7 |
| 3 | 46.0827 | 49.8907 | 161 | 48.3437 | 49.9502 | 153.8 |
| 4 | 45.4877 | 48.1355 | 169.3 | 45.8745 | 48.671 | 165.8 |
| 5 | 46.648 | 47.5405 | 167.2 | 43.1077 | 44.4465 | 193.3 |
| 6 | 46.172 | 46.291 | 173.8 | 45.6067 | 45.5472 | 178.4 |
| 7 | 47.0645 | 46.4695 | 169.3 | 42.245 | 46.4695 | 188.1 |
| 8 | 45.1902 | 44.625 | 184 | 47.8677 | 47.957 | 161.7 |
| 9 | 45.458 | 49.5932 | 164.4 | 45.696 | 41.6797 | 194.2 |
| 10 | 48.314 | 44.268 | 173 | 46.053 | 44.9225 | 179.2 |
| 11 | 45.9042 | 45.696 | 176.8 | 50.2775 | 41.0847 | 177.6 |
| 12 | 47.3322 | 46.4992 | 168.6 | 44.6845 | 45.9637 | 180.7 |
| 13 | 46.172 | 48.9982 | 163.7 | 46.8562 | 43.2862 | 182.3 |
| 14 | 47.3322 | 46.2812 | 169.3 | 44.03 | 44.744 | 188.1 |
| 15 | 45.577 | 46.1125 | 176.8 | 31.2375 | 44.03 | 262.4 |
| 16 | 45.3092 | 49.2362 | 165.8 | 42.8697 | 38.794 | 222.8 |
| 17 | 45.7257 | 49.4445 | 163.7 | 35.6405 | 38.675 | 268 |
| 18 | 46.7075 | 45.5175 | 174.5 | 38.2585 | 41.3525 | 234.1 |
| 19 | 43.8515 | 49.5635 | 170.1 | 37.1577 | 39.8947 | 250.2 |
| 20 | 44.863 | 48.909 | 168.6 | 40.5195 | 42.1855 | 216.4 |
| 21 | 46.648 | 47.1537 | 168.6 | 34.7182 | 39.3592 | 270.9 |
| 22 | 45.5472 | 46.2017 | 176 | 41.5905 | 42.2152 | 211.3 |
| 23 | 46.9455 | 45.9042 | 172.3 | 40.1625 | 38.9427 | 236.5 |
| 24 | 46.1422 | 45.4282 | 176.8 | 40.4897 | 41.9177 | 218.5 |
| 25 | 43.0482 | 46.1125 | 186.5 | 36.6222 | 36.0272 | 281.5 |
| 26 | 45.458 | 46.9455 | 173.8 | 40.936 | 35.105 | 256.9 |
| 27 | 46.6777 | 45.5175 | 174.5 | 35.1645 | 40.4005 | 259.6 |
| 28 | 45.9042 | 44.982 | 179.9 | 36.8305 | 40.8765 | 245.1 |
| 29 | 45.3092 | 46.1125 | 177.6 | 41.5012 | 46.767 | 190.7 |
| 30 | 43.554 | 46.886 | 181.5 | 42.0665 | 42.9887 | 205.3 |
| 31 | 43.673 | 47.719 | 177.6 | 43.9705 | 46.1125 | 183.2 |
| 32 | 46.8562 | 45.4877 | 173.8 | 39.5675 | 43.4052 | 215.4 |

| | | | | | | |
|----------------|---------|---------|-------|---------|---------|-------|
| 33 | 44.8332 | 46.291 | 178.4 | 45.0415 | 50.1585 | 163.7 |
| 34 | 45.1605 | 43.673 | 188.1 | 47.719 | 46.7967 | 165.8 |
| 35 | 45.0117 | 44.268 | 186.5 | 43.673 | 44.9225 | 189 |
| 36 | 44.9522 | 45.5175 | 181.5 | 45.101 | 47.124 | 174.5 |
| 37 | 46.3207 | 46.648 | 171.5 | 46.4695 | 48.0165 | 166.5 |
| 38 | 46.6182 | 45.7555 | 173.8 | 46.7967 | 48.4032 | 163.7 |
| 39 | 44.744 | 43.9705 | 188.1 | 46.8265 | 47.5702 | 166.5 |
| 40 | 45.339 | 46.7372 | 175.3 | 47.2132 | 49.3255 | 159 |
| 41 | 45.7555 | 46.648 | 173.8 | 47.6892 | 45.2795 | 171.5 |
| 42 | 43.792 | 45.577 | 185.6 | 45.9637 | 48.9982 | 164.4 |
| 43 | 46.9157 | 45.7852 | 172.3 | 46.8265 | 46.291 | 170.8 |
| 44 | 46.172 | 45.339 | 176.8 | 46.3207 | 47.957 | 167.2 |
| 45 | 45.696 | 46.8265 | 173 | 46.2315 | 48.5222 | 165.1 |
| 46 | 46.2612 | 44.863 | 178.4 | 46.2017 | 46.9455 | 170.8 |
| 47 | 45.8447 | 43.7622 | 184.8 | 46.3207 | 50.8725 | 157 |
| 48 | 46.5587 | 44.625 | 178.4 | 45.3092 | 46.886 | 174.5 |
| 49 | 46.1125 | 46.1125 | 174.5 | 44.7737 | 48.3437 | 170.8 |
| 50 | 45.22 | 48.4925 | 168.6 | 44.5655 | 47.8677 | 173.8 |
| 51 | 45.6067 | 44.506 | 182.3 | 46.291 | 44.8927 | 178.4 |
| 52 | 44.2085 | 46.2612 | 181.5 | 45.3092 | 51.517 | 158.3 |
| 53 | 46.9157 | 44.982 | 176 | 46.8562 | 47.0645 | 167.9 |
| 54 | 45.7852 | 46.648 | 173.8 | 46.529 | 43.8515 | 181.5 |
| 55 | 45.696 | 48.9685 | 165.8 | 45.3687 | 45.3985 | 179.9 |
| 56 | 44.5655 | 48.671 | 170.8 | 46.3505 | 43.9407 | 182.3 |
| 57 | 45.6365 | 45.0712 | 179.9 | 45.3687 | 45.6365 | 179.2 |
| 58 | 44.863 | 45.2795 | 182.3 | 43.1375 | 44.6547 | 192.5 |
| 59 | 44.6547 | 43.7325 | 189.9 | 45.22 | 41.9177 | 195.1 |
| 60 | 45.4282 | 45.8745 | 177.6 | 44.6547 | 44.2085 | 188.1 |
| 61 | 45.6365 | 46.8563 | 173.8 | 41.8285 | 45.7257 | 193.3 |
| 62 | 46.767 | 45.9935 | 172.3 | 44.8927 | 44.387 | 186.5 |
| 63 | 46.291 | 48.7305 | 164.4 | 46.0232 | 43.8812 | 183.2 |
| 64 | 47.2132 | 47.1537 | 166.5 | 44.149 | 45.6365 | 184 |
| 65 | 45.9637 | 49.3552 | 163 | 44.9225 | 45.3092 | 182.3 |
| 66 | 44.744 | 46.648 | 177.6 | 43.554 | 44.1192 | 193.3 |
| 67 | 44.5357 | 46.4695 | 179.2 | 43.911 | 47.362 | 178.4 |
| 68 | 45.696 | 47.2727 | 171.5 | 43.554 | 44.9522 | 189.9 |
| 69 | 42.483 | 43.911 | 198.7 | 44.4762 | 44.3275 | 188.1 |
| Average | | | 175.0 | | | |

Table A.17 Hardness readings for Sample 17

| Sample 17 | Nitrogen pressure 2.0 Torr, anode distance 60 mm Ion beam centre location: 24 mm | | | | | |
|------------------|---|------------------------------|-------|------------------------------|------------------------------|-------|
| | Before Nitriding: | | | After Nitriding: | | |
| Position (mm) | d ₁ (μ m) | d ₂ (μ m) | HV | d ₁ (μ m) | d ₂ (μ m) | HV |
| 1 | 44.5655 | 46.767 | 177.6 | 44.5357 | 45.5175 | 183.2 |
| 2 | 44.0002 | 44.3572 | 189.9 | 47.0942 | 46.886 | 167.9 |
| 3 | 44.7737 | 44.3572 | 186.5 | 45.101 | 42.3937 | 194.2 |
| 4 | 45.5175 | 43.1672 | 189 | 44.4167 | 44.9522 | 185.6 |
| 5 | 44.4762 | 45.6662 | 182.3 | 46.41 | 44.4167 | 179.9 |
| 6 | 46.053 | 44.7737 | 179.9 | 47.1537 | 43.5242 | 180.7 |
| 7 | 46.6182 | 44.7142 | 177.6 | 44.8035 | 46.9157 | 176 |
| 8 | 45.3687 | 46.0827 | 177.6 | 44.863 | 45.6967 | 181.5 |
| 9 | 45.0712 | 43.0482 | 190.7 | 43.9407 | 46.4397 | 181.5 |
| 10 | 46.4695 | 44.6547 | 178.4 | 48.7602 | 47.3917 | 160.3 |
| 11 | 44.1192 | 43.911 | 191.6 | 48.1355 | 45.2795 | 170.1 |
| 12 | 46.2612 | 51.6162 | 191.6 | 47.2777 | 47.3917 | 165.8 |
| 13 | 44.6845 | 46.2315 | 179.2 | 44.8332 | 43.9407 | 188.1 |
| 14 | 44.3275 | 44.3572 | 189 | 46.3207 | 44.5952 | 179.2 |
| 15 | 43.9705 | 44.268 | 190.7 | 42.4235 | 43.3457 | 201.5 |
| 16 | 47.3322 | 44.7142 | 175.3 | 46.648 | 44.0002 | 180.7 |
| 17 | 43.4052 | 42.8995 | 198.7 | 43.554 | 42.5127 | 200.6 |
| 18 | 44.7142 | 44.0895 | 188.1 | 40.1922 | 40.222 | 229.5 |
| 19 | 45.9935 | 44.8927 | 179.9 | 42.8697 | 43.5242 | 198.7 |
| 20 | 44.0895 | 45.5175 | 184.8 | 40.9062 | 42.007 | 215.4 |
| 21 | 45.815 | 43.911 | 184 | 43.1077 | 46.7372 | 184 |
| 22 | 45.339 | 44.982 | 181.5 | 52.3005 | 41.055 | 170.1 |
| 23 | 45.101 | 44.6845 | 184 | 43.1077 | 46.7372 | 184 |
| 24 | 44.0895 | 44.0895 | 190.7 | 52.3005 | 41.055 | 170.1 |
| 25 | 43.911 | 45.4282 | 185.6 | 39.8947 | 54.2342 | 167.2 |
| 26 | 43.078 | 43.2267 | 198.7 | 43.4945 | 47.5702 | 179.2 |
| 27 | 43.7325 | 46.2315 | 183.2 | 45.577 | 39.8352 | 203.4 |
| 28 | 44.0895 | 42.8995 | 196 | 44.2977 | 43.8217 | 190.7 |
| 29 | 45.8745 | 47.481 | 170.1 | 47.124 | 39.0617 | 199.7 |
| 30 | 46.9752 | 48.1355 | 163.7 | 43.2267 | 41.888 | 204.4 |
| 31 | 48.9982 | 48.8495 | 155.1 | 45.2497 | 38.437 | 212.3 |
| 32 | 46.529 | 45.7555 | 174.5 | 43.8515 | 42.9887 | 196.9 |

| | | | | | | |
|----------------|---------|---------|-------|---------|---------|-------|
| 33 | 44.8035 | 45.9042 | 179.9 | 41.6797 | 44.6547 | 198.7 |
| 34 | 43.554 | 45.4877 | 187.3 | 45.8447 | 45.5175 | 177.6 |
| 35 | 44.9522 | 46.4695 | 177.6 | 43.8217 | 46.0827 | 183.2 |
| 36 | 44.0002 | 44.5655 | 189 | 49.6825 | 48.9982 | 152.6 |
| 37 | 45.934 | 46.4695 | 173.8 | 46.7372 | 45.815 | 173 |
| 38 | 44.0597 | 44.8332 | 188.1 | 47.124 | 46.5885 | 168.6 |
| 39 | 46.4695 | 45.9042 | 173.8 | 44.9522 | 48.195 | 170.8 |
| 40 | 46.8265 | 47.5702 | 166.5 | 46.5885 | 45.1605 | 176 |
| 41 | 44.1787 | 45.101 | 186.5 | 45.2795 | 46.7075 | 175.3 |
| 42 | 43.554 | 43.1077 | 197.8 | 46.2315 | 47.3025 | 169.3 |
| 43 | 44.7737 | 42.5425 | 194.2 | 45.22 | 45.6662 | 179.9 |
| 44 | 45.1605 | 44.0895 | 186.5 | 47.5405 | 46.5587 | 167.9 |
| 45 | 43.2862 | 44.7737 | 190.7 | 45.934 | 45.3985 | 177.6 |
| 46 | 43.8515 | 44.387 | 190.7 | 44.506 | 46.6777 | 178.4 |
| 47 | 43.7325 | 43.7622 | 194.2 | 46.3802 | 46.053 | 173.8 |
| 48 | 46.1125 | 45.458 | 176.8 | 49.2065 | 48.7602 | 154.5 |
| 49 | 44.7142 | 43.435 | 190.7 | 45.1307 | 45.458 | 180.7 |
| 50 | 44.6547 | 45.3985 | 183.2 | 47.838 | 44.982 | 172.3 |
| 51 | 44.863 | 45.7555 | 180.7 | 46.291 | 45.1605 | 177.6 |
| 52 | 45.22 | 44.6547 | 184 | 44.8035 | 45.101 | 183.2 |
| 53 | 46.41 | 47.8677 | 167.2 | 44.744 | 45.1902 | 183.2 |
| 54 | 43.7622 | 44.387 | 190.7 | 45.7852 | 44.625 | 181.5 |
| 55 | 44.982 | 44.6845 | 184.8 | 48.195 | 45.5175 | 168.6 |
| 56 | 44.8035 | 44.4167 | 186.5 | 45.0712 | 48.076 | 170.8 |
| 57 | 44.9522 | 44.4762 | 185.6 | 48.2247 | 45.7257 | 167.9 |
| 58 | 46.8265 | 46.8562 | 169.3 | 45.9935 | 44.0895 | 183.2 |
| 59 | 46.886 | 45.9935 | 172.3 | 45.3985 | 45.1605 | 180.7 |
| 60 | 43.1375 | 43.0185 | 199.7 | 45.815 | 45.934 | 176 |
| 61 | 43.5837 | 43.4845 | 196 | 45.3092 | 45.815 | 178.4 |
| 62 | 43.3755 | 44.0895 | 194.2 | 46.172 | 44.4762 | 180.7 |
| 63 | 43.792 | 43.3457 | 195.1 | 46.41 | 45.0117 | 177.6 |
| 64 | 44.387 | 44.863 | 186.5 | 44.5952 | 44.5655 | 186.5 |
| 65 | 45.7555 | 45.22 | 179.2 | 45.9637 | 45.0712 | 179.2 |
| 66 | 45.9637 | 45.7555 | 176 | 43.435 | 45.577 | 187.3 |
| 67 | 44.4167 | 43.8217 | 190.7 | 45.3687 | 44.0002 | 185.6 |
| 68 | 45.6365 | 45.577 | 178.4 | 43.435 | 45.0415 | 189.9 |
| 69 | 46.053 | 46.7075 | 172.3 | 47.243 | 43.792 | 179.2 |
| Average | | | 183.8 | | | |

Table A.18 Hardness readings for Sample 18

| Sample 18 | Nitrogen pressure 2.0 Torr, anode distance 80 mm Ion beam centre location: 22 mm | | | | | |
|------------------|---|------------------------------|-------|------------------------------|------------------------------|-------|
| | Before Nitriding: | | | After Nitriding: | | |
| Position (mm) | d ₁ (μ m) | d ₂ (μ m) | HV | d ₁ (μ m) | d ₂ (μ m) | HV |
| 1 | 45.8447 | 47.5405 | 170.1 | 43.8217 | 44.744 | 189 |
| 2 | 47.957 | 48.671 | 159 | 47.8082 | 47.1835 | 164.4 |
| 3 | 46.0827 | 47.4215 | 169.3 | 44.8332 | 45.4877 | 181.5 |
| 4 | 46.8265 | 45.458 | 174.5 | 47.4512 | 45.815 | 170.8 |
| 5 | 47.362 | 45.6365 | 171.5 | 45.22 | 46.0827 | 177.6 |
| 6 | 46.3802 | 46.0232 | 173.8 | 47.9272 | 49.98 | 154.5 |
| 7 | 47.5405 | 45.3092 | 172.3 | 45.9637 | 47.3025 | 170.8 |
| 8 | 46.291 | 47.243 | 169.3 | 47.957 | 47.0942 | 164.4 |
| 9 | 46.5885 | 44.0002 | 180.7 | 45.696 | 42.9292 | 189 |
| 10 | 46.0827 | 47.243 | 170.1 | 46.172 | 45.7852 | 175.3 |
| 11 | 46.2017 | 44.149 | 181.5 | 46.529 | 45.458 | 175.3 |
| 12 | 46.41 | 43.3755 | 184 | 43.3755 | 45.934 | 185.6 |
| 13 | 47.5702 | 47.4512 | 164.4 | 46.4992 | 49.0577 | 162.3 |
| 14 | 46.8265 | 46.0232 | 172.3 | 48.7305 | 49.7717 | 152.6 |
| 15 | 46.3802 | 45.3985 | 176 | 47.005 | 44.1192 | 178.4 |
| 16 | 47.4512 | 46.41 | 168.6 | 42.9596 | 48.314 | 165.8 |
| 17 | 42.5127 | 46.6182 | 186.5 | 46.9157 | 46.1125 | 171.5 |
| 18 | 46.0827 | 42.9887 | 187.3 | 45.6365 | 44.5655 | 182.3 |
| 19 | 45.6662 | 48.314 | 168.6 | 44.982 | 44.4465 | 185.6 |
| 20 | 46.5885 | 48.1355 | 165.1 | 43.316 | 46.767 | 183.2 |
| 21 | 47.3025 | 46.1125 | 170.1 | 43.2565 | 44.0895 | 194.2 |
| 22 | 48.7305 | 46.2315 | 164.4 | 47.838 | 44.0597 | 176 |
| 23 | 45.815 | 48.5817 | 166.5 | 43.5837 | 43.6432 | 195.1 |
| 24 | 45.339 | 47.124 | 173.8 | 45.8447 | 45.458 | 177.6 |
| 25 | 45.3687 | 47.4215 | 172.3 | 45.5222 | 47.005 | 162.3 |
| 26 | 45.5175 | 45.577 | 179.2 | 46.291 | 44.863 | 178.4 |
| 27 | 45.458 | 46.4695 | 175.3 | 48.909 | 43.9407 | 172.3 |
| 28 | 46.2315 | 44.9225 | 178.4 | 47.0645 | 47.481 | 165.8 |
| 29 | 45.815 | 48.0165 | 168.6 | 48.2545 | 49.0875 | 156.4 |
| 30 | 44.8035 | 50.5452 | 163 | 48.9685 | 47.4215 | 159.6 |
| 31 | 47.243 | 45.9935 | 170.8 | 46.9752 | 45.9935 | 171.5 |
| 32 | 46.8562 | 45.22 | 175.3 | 47.838 | 48.4627 | 159.6 |

| | | | | | | |
|----------------|---------|---------|-------|---------|---------|-------|
| 33 | 45.577 | 44.9522 | 180.7 | 49.028 | 48.671 | 155.7 |
| 34 | 47.471 | 44.8927 | 173.8 | 48.7602 | 48.2247 | 157.7 |
| 35 | 46.0232 | 45.1307 | 178.4 | 46.9455 | 47.362 | 166.5 |
| 36 | 44.4762 | 43.316 | 192.5 | 48.7662 | 48.5817 | 156.4 |
| 37 | 46.3207 | 43.8217 | 182.3 | 47.481 | 46.172 | 169.3 |
| 38 | 45.577 | 44.4167 | 183.2 | 46.2315 | 46.7372 | 171.5 |
| 39 | 45.2497 | 47.8975 | 170.8 | 45.5472 | 47.6287 | 170.8 |
| 40 | 46.3505 | 48.0462 | 166.5 | 47.8082 | 43.8515 | 176.8 |
| 41 | 44.744 | 44.0895 | 188.1 | 48.195 | 45.101 | 170.8 |
| 42 | 43.2862 | 44.7142 | 191.6 | 47.7487 | 46.9157 | 165.8 |
| 43 | 45.7257 | 47.243 | 171.5 | 46.3207 | 45.7555 | 175.3 |
| 44 | 48.2545 | 46.7967 | 164.4 | 47.1835 | 44.8332 | 175.3 |
| 45 | 47.0942 | 45.815 | 171.5 | 48.1355 | 44.2685 | 173.8 |
| 46 | 46.2315 | 45.6365 | 176 | 47.6297 | 44.9225 | 173.8 |
| 47 | 46.1125 | 45.6365 | 176 | 46.767 | 43.4167 | 178.4 |
| 48 | 46.052 | 45.3985 | 177.6 | 47.7487 | 49.98 | 155.1 |
| 49 | 46.886 | 46.8265 | 168.6 | 44.982 | 45.0712 | 183.2 |
| 50 | 47.9272 | 46.648 | 165.8 | 45.458 | 45.22 | 180.7 |
| 51 | 47.124 | 46.8265 | 167.9 | 47.243 | 45.577 | 172.3 |
| 52 | 47.6595 | 46.4695 | 167.2 | 43.7325 | 47.481 | 178.4 |
| 53 | 47.3917 | 48.314 | 161.7 | 46.767 | 44.982 | 176 |
| 54 | 46.1422 | 45.8745 | 175.3 | 47.1835 | 46.291 | 170.1 |
| 55 | 44.5952 | 42.3045 | 196.9 | 44.4465 | 46.3207 | 179.9 |
| 56 | 47.8082 | 48.4032 | 160.3 | 46.291 | 44.4465 | 179.9 |
| 57 | 45.3985 | 47.362 | 172.3 | 42.959 | 47.3025 | 182.3 |
| 58 | 47.0645 | 48.0165 | 164.4 | 45.1902 | 44.8332 | 183.2 |
| 59 | 47.362 | 47.1835 | 165.8 | 46.5587 | 44.149 | 179.9 |
| 60 | 45.339 | 46.053 | 177.6 | 45.1307 | 44.1192 | 186.5 |
| 61 | 48.1652 | 48.6115 | 158.3 | 46.41 | 44.0895 | 181.5 |
| 62 | 45.9637 | 47.6 | 169.3 | 45.9637 | 45.1902 | 178.4 |
| 63 | 49.7717 | 47.6 | 156.4 | 46.4397 | 45.3687 | 176 |
| 64 | 45.6365 | 45.0712 | 179.9 | 46.9455 | 42.8102 | 184 |
| 65 | 46.4397 | 46.2612 | 172.3 | 47.005 | 44.625 | 176.8 |
| 66 | 43.673 | 45.5175 | 186.5 | 45.6662 | 48.9685 | 165.8 |
| 67 | 48.0165 | 46.7075 | 165.1 | 44.5655 | 46.172 | 179.9 |
| 68 | 46.4695 | 47.0347 | 169.3 | 45.9042 | 46.4397 | 173.8 |
| 69 | 48.79 | 47.6892 | 159.6 | 47.3025 | 41.2037 | 189 |
| Average | | | 172.9 | | | |

Table A.19 Hardness readings for Sample 19

| Sample 19 | Nitrogen pressure 2.0 Torr, anode distance 100 mm Ion beam centre location: 22 mm | | | | | |
|------------------|--|------------------------------|-------|------------------------------|------------------------------|-------|
| | Before Nitriding: | | | After Nitriding: | | |
| Position (mm) | d ₁ (μ m) | d ₂ (μ m) | HV | d ₁ (μ m) | d ₂ (μ m) | HV |
| 1 | 45.458 | 44.0002 | 185.6 | 45.6662 | 46.3207 | 175.3 |
| 2 | 45.1307 | 44.0597 | 186.5 | 46.3207 | 44.8035 | 178.4 |
| 3 | 43.3457 | 42.84 | 199.7 | 44.387 | 43.2267 | 193.3 |
| 4 | 43.078 | 43.8217 | 196.9 | 43.9407 | 44.5357 | 189.9 |
| 5 | 44.1787 | 44.7737 | 187.3 | 48.195 | 46.3207 | 165.8 |
| 6 | 46.2017 | 44.625 | 179.9 | 44.5357 | 44.506 | 187.3 |
| 7 | 44.2382 | 46.1125 | 181.5 | 46.529 | 47.0347 | 169.3 |
| 8 | 43.2562 | 44.863 | 190.7 | 49.6527 | 45.339 | 164.4 |
| 9 | 44.982 | 43.078 | 191.6 | 45.5472 | 46.886 | 178.8 |
| 10 | 43.6432 | 44.268 | 191.6 | 45.1307 | 45.0415 | 182.3 |
| 11 | 43.1077 | 43.5242 | 197.8 | 48.195 | 43.9705 | 174.5 |
| 12 | 44.3275 | 42.2747 | 197.8 | 48.8197 | 46.2315 | 164.4 |
| 13 | 45.696 | 44.0597 | 184 | 49.504 | 44.6547 | 167.2 |
| 14 | 45.0415 | 42.7507 | 192.5 | 46.4992 | 44.8927 | 177.6 |
| 15 | 43.7325 | 41.9177 | 202.5 | 46.41 | 45.339 | 176 |
| 16 | 43.8217 | 44.982 | 188.1 | 48.7602 | 42.2747 | 178.4 |
| 17 | 44.3572 | 43.8515 | 190.7 | 45.101 | 48.433 | 169.3 |
| 18 | 42.8995 | 43.8217 | 196.9 | 41.7987 | 44.3572 | 199.7 |
| 19 | 43.673 | 45.5175 | 186.5 | 48.433 | 43.1672 | 176.8 |
| 20 | 43.7622 | 44.8332 | 189 | 45.339 | 45.7852 | 178.4 |
| 21 | 42.6317 | 44.268 | 196.9 | 46.0877 | 47.7487 | 168.6 |
| 22 | 43.792 | 43.7622 | 193.3 | 45.6067 | 46.529 | 174.5 |
| 23 | 43.8515 | 43.9407 | 192.5 | 44.9225 | 49.385 | 166.5 |
| 24 | 44.7142 | 42.5425 | 195.1 | 50.9022 | 43.3457 | 167.2 |
| 25 | 43.5242 | 42.364 | 201.5 | 46.3802 | 48.5817 | 164.4 |
| 26 | 44.387 | 42.9292 | 194.2 | 44.8927 | 45.934 | 179.9 |
| 27 | 43.7622 | 44.5952 | 189.9 | 48.433 | 47.6297 | 161 |
| 28 | 44.744 | 44.2977 | 187.3 | 46.4695 | 49.742 | 160.3 |
| 29 | 40.5492 | 45.0712 | 202.5 | 48.6412 | 47.0942 | 161.7 |
| 30 | 43.5242 | 43.5837 | 195.1 | 46.5587 | 48.5817 | 163.7 |
| 31 | 40.222 | 48.552 | 188.1 | 52.9252 | 44.744 | 155.7 |
| 32 | 41.7392 | 44.387 | 199.7 | 51.884 | 46.5885 | 153.2 |

| | | | | | | |
|----------------|---------|---------|-------|---------|---------|-------|
| 33 | 42.6912 | 43.9407 | 197.8 | 48.1652 | 44.5357 | 172.3 |
| 34 | 43.316 | 42.959 | 199.7 | 48.2247 | 44.625 | 172.3 |
| 35 | 44.6845 | 44.2977 | 187.3 | 44.2977 | 45.9637 | 182.3 |
| 36 | 44.4762 | 43.2267 | 192.5 | 46.5587 | 42.8697 | 185.6 |
| 37 | 44.7737 | 42.0962 | 196.9 | 47.3025 | 45.7555 | 171.5 |
| 38 | 41.8888 | 45.1902 | 196 | 46.291 | 48.9387 | 163.7 |
| 39 | 45.0712 | 43.6432 | 188.1 | 42.364 | 45.9042 | 190.7 |
| 40 | 45.2497 | 42.126 | 194.2 | 46.7372 | 47.6297 | 166.5 |
| 41 | 43.6432 | 43.0482 | 197.8 | 44.0597 | 44.8927 | 182.3 |
| 42 | 43.3755 | 42.3045 | 202.5 | 43.5837 | 48.7007 | 174.5 |
| 43 | 43.2267 | 42.2747 | 202.5 | 46.6182 | 47.5405 | 167.2 |
| 44 | 43.2862 | 44.4167 | 192.5 | 43.7027 | 43.1375 | 196.9 |
| 45 | 43.3457 | 44.268 | 193.3 | 45.696 | 45.934 | 176.8 |
| 46 | 43.7622 | 43.8812 | 193.3 | 44.3572 | 45.1902 | 184.8 |
| 47 | 41.7987 | 44.5357 | 198.7 | 45.7257 | 48.671 | 166.5 |
| 48 | 43.8217 | 44.4167 | 190.7 | 44.5655 | 44.7737 | 185.6 |
| 49 | 43.1077 | 44.149 | 195.1 | 44.2382 | 46.1125 | 182.3 |
| 50 | 42.721 | 43.316 | 200.6 | 45.0117 | 44.2085 | 186.5 |
| 51 | 43.9705 | 44.1787 | 190.7 | 45.3687 | 44.625 | 183.2 |
| 52 | 43.3755 | 44.506 | 192.5 | 45.3687 | 45.1605 | 180.7 |
| 53 | 42.5127 | 43.673 | 199.7 | 47.4215 | 46.7372 | 167.2 |
| 54 | 41.5905 | 43.8812 | 203.4 | 46.5587 | 45.696 | 174.5 |
| 55 | 42.9887 | 44.268 | 195.1 | 44.9225 | 44.982 | 183.2 |
| 56 | 42.6615 | 45.3687 | 191.6 | 43.7325 | 45.22 | 187.3 |
| 57 | 44.1192 | 43.1077 | 195.1 | 46.8265 | 46.2315 | 171.5 |
| 58 | 42.8995 | 42.721 | 202.5 | 45.9935 | 44.863 | 179.9 |
| 59 | 41.6797 | 43.8217 | 202.5 | 45.696 | 43.6135 | 185.6 |
| 60 | 42.0665 | 43.792 | 201.5 | 49.3552 | 49.2957 | 152.6 |
| 61 | 43.673 | 43.078 | 196.9 | 43.8217 | 44.8035 | 189 |
| 62 | 43.0185 | 43.2862 | 198.7 | 46.5885 | 47.3322 | 167.9 |
| 63 | 43.5837 | 45.339 | 187.3 | 45.0415 | 45.3687 | 181.5 |
| 64 | 42.7507 | 42.9292 | 202.5 | 46.9157 | 45.2497 | 174.5 |
| 65 | 45.2497 | 47.362 | 173 | 49.504 | 49.4445 | 151.4 |
| 66 | 45.1307 | 45.3092 | 181.5 | 47.4512 | 45.815 | 170.8 |
| 67 | 45.577 | 45.9042 | 177.6 | 44.6845 | 46.2612 | 176.2 |
| 68 | 44.3275 | 43.673 | 191.6 | 45.815 | 46.172 | 175.3 |
| 69 | 46.4397 | 46.886 | 170.1 | 46.5587 | 47.1537 | 168.6 |
| Average | | | 193.1 | | | |

Table A.20 Hardness readings for Sample 20

| Sample 20 | Nitrogen pressure 2.0 Torr, anode distance 120 mm Ion beam centre location: 23 mm | | | | | |
|------------------|--|-------------------------------------|-------|-------------------------------------|-------------------------------------|-------|
| | Before Nitriding: | | | After Nitriding: | | |
| Position (mm) | d ₁ (μm) | d ₂ (μm) | HV | d ₁ (μm) | d ₂ (μm) | HV |
| 1 | 45.2795 | 44.7142 | 183.1 | 52.003 | 48.0462 | 148.4 |
| 2 | 43.1375 | 45.7852 | 187.3 | 46.5587 | 45.1902 | 176 |
| 3 | 43.2862 | 23.8515 | 195.1 | 45.9637 | 47.2436 | 170.8 |
| 4 | 45.22 | 45.1307 | 181.5 | 45.6365 | 44.0597 | 184.8 |
| 5 | 44.625 | 44.4465 | 187.3 | 46.053 | 45.3092 | 177.6 |
| 6 | 43.7027 | 43.1672 | 196.9 | 48.4627 | 44.03 | 173.8 |
| 7 | 43.7622 | 44.2382 | 191.6 | 43.6135 | 44.0002 | 193.3 |
| 8 | 43.2267 | 44.4762 | 192.5 | 46.4992 | 44.3275 | 179.9 |
| 9 | 45.3687 | 43.7072 | 187.3 | 46.529 | 46.9752 | 169.3 |
| 10 | 43.9705 | 45.3092 | 186.5 | 46.1422 | 46.2017 | 173.8 |
| 11 | 43.2267 | 44.8927 | 190.7 | 46.7372 | 45.9042 | 173 |
| 12 | 44.149 | 43.8515 | 191.6 | 42.0367 | 45.1902 | 195.1 |
| 13 | 44.0895 | 42.6615 | 196.9 | 47.838 | 42.602 | 181.5 |
| 14 | 45.9042 | 45.8745 | 176 | 48.5817 | 44.0895 | 173 |
| 15 | 44.7737 | 43.3457 | 190.7 | 46.41 | 48.6412 | 163.7 |
| 16 | 44.0002 | 44.0895 | 191.6 | 48.4627 | 48.8197 | 157 |
| 17 | 43.8812 | 44.268 | 190.7 | 42.6317 | 51.6162 | 167.2 |
| 18 | 43.2267 | 42.3342 | 202.5 | 46.0827 | 45.6662 | 176 |
| 19 | 44.625 | 44.3572 | 187.3 | 49.4445 | 44.744 | 167.2 |
| 20 | 43.1375 | 45.8745 | 189 | 47.957 | 43.7325 | 176.8 |
| 21 | 43.7027 | 42.6912 | 198.7 | 44.2977 | 46.648 | 179.2 |
| 22 | 42.9887 | 42.4532 | 203.4 | 44.268 | 44.4167 | 189 |
| 23 | 44.194 | 45.0117 | 186.5 | 46.648 | 46.7967 | 170.1 |
| 24 | 45.22 | 44.5952 | 184 | 46.2315 | 49.385 | 162.3 |
| 25 | 45.5472 | 44.0002 | 184.8 | 45.7852 | 46.9157 | 172.3 |
| 26 | 44.4762 | 45.0415 | 184.8 | 48.1057 | 48.076 | 160.3 |
| 27 | 44.4167 | 45.2795 | 184.8 | 47.5107 | 47.3322 | 165.1 |
| 28 | 42.5452 | 43.792 | 198.7 | 46.648 | 46.3497 | 171.5 |
| 29 | 46.1125 | 44.8332 | 179.2 | 45.458 | 47.838 | 170.8 |
| 30 | 42.721 | 43.4945 | 199.7 | 48.8495 | 48.314 | 157 |
| 31 | 44.6845 | 41.9117 | 197.8 | 46.8562 | 46.9157 | 168.6 |
| 32 | 43.4052 | 42.7507 | 199.7 | 44.8332 | 45.7852 | 180.7 |

| | | | | | | |
|----------------|---------|---------|-------|---------|---------|-------|
| 33 | 42.0962 | 43.435 | 202.5 | 47.5405 | 44.1787 | 176 |
| 34 | 43.8515 | 43.8217 | 193.3 | 45.458 | 45.5472 | 179.2 |
| 35 | 42.6615 | 43.7622 | 198.7 | 44.8332 | 49.8015 | 165.8 |
| 36 | 42.9292 | 42.7805 | 201.5 | 48.9387 | 47.957 | 158.3 |
| 37 | 42.6615 | 43.4647 | 199.7 | 49.6527 | 44.4465 | 167.9 |
| 38 | 43.197 | 43.3755 | 197.8 | 16.3207 | 48.1355 | 166.5 |
| 39 | 44.863 | 42.5425 | 194.2 | 48.4627 | 48.3437 | 158.3 |
| 40 | 42.8697 | 43.435 | 198.7 | 44.2977 | 45.2497 | 184.8 |
| 41 | 41.2632 | 44.625 | 201.5 | 44.03 | 46.529 | 180.7 |
| 42 | 42.3045 | 44.149 | 198.7 | 45.5472 | 44.8035 | 181.5 |
| 43 | 43.0482 | 44.6547 | 192.5 | 15.2497 | 45.3985 | 179.9 |
| 44 | 47.124 | 48.7602 | 161.7 | 50.456 | 51.2295 | 143.7 |
| 45 | 46.6182 | 43.9705 | 180.7 | 44.4465 | 46.3802 | 179.9 |
| 46 | 48.5222 | 44.2085 | 172.3 | 44.03 | 43.0482 | 196 |
| 47 | 45.6662 | 43.8812 | 184.8 | 44.8035 | 44.7737 | 184 |
| 48 | 43.9407 | 42.6615 | 197.8 | 43.9407 | 44.4167 | 189.9 |
| 49 | 43.5242 | 41.888 | 203.4 | 45.3687 | 44.5952 | 183.2 |
| 50 | 42.721 | 43.8217 | 197.8 | 44.4762 | 45.7555 | 182.3 |
| 51 | 43.673 | 42.3045 | 200.6 | 46.8265 | 44.3572 | 178.4 |
| 52 | 42.7805 | 47.5107 | 182.3 | 43.673 | 45.8447 | 184.8 |
| 53 | 44.7737 | 44.5357 | 185.6 | 46.4397 | 44.5357 | 179.2 |
| 54 | 44.0002 | 43.911 | 191.6 | 44.0002 | 44.7737 | 188.1 |
| 55 | 45.0415 | 44.1192 | 186.5 | 46.7075 | 47.362 | 167.9 |
| 56 | 45.0117 | 43.4052 | 189.9 | 47.243 | 45.7555 | 171.5 |
| 57 | 44.9522 | 45.1902 | 182.3 | 44.5655 | 43.2565 | 192.5 |
| 58 | 44.6845 | 45.9935 | 180.7 | 46.1125 | 45.696 | 176 |
| 59 | 46.1125 | 44.2085 | 181.5 | 45.6365 | 43.2862 | 187.3 |
| 60 | 45.6365 | 44.5952 | 182.3 | 45.6067 | 46.648 | 174.5 |
| 61 | 43.2267 | 43.7027 | 196 | 46.5885 | 51.3187 | 154.5 |
| 62 | 43.9407 | 42.7507 | 197.8 | 45.2497 | 46.291 | 177.6 |
| 63 | 44.0002 | 43.8812 | 192.5 | 46.1422 | 48.1652 | 166.5 |
| 64 | 47.2132 | 45.815 | 171.5 | 48.1057 | 45.696 | 168.6 |
| 65 | 45.1307 | 44.6547 | 184 | 45.339 | 45.0712 | 181.5 |
| 66 | 44.2977 | 44.8035 | 186.5 | 42.4532 | 46.1422 | 189 |
| 67 | 42.9292 | 42.9887 | 200.6 | 47.5107 | 46.6182 | 167.2 |
| 68 | 45.0117 | 46.41 | 177.6 | 46.053 | 44.744 | 179.9 |
| 69 | 45.6365 | 46.7372 | 173.8 | 44.863 | 45.4877 | 181.5 |
| Average | | | 190.1 | | | |

APPENDIX B

STANDARD OPERATING PROCEDURES FOR DPF

The DPF machine operates on a very high voltage and therefore, in the interest of safety, safe standard operating procedures need to be followed. The procedures have been developed for the firing in nitrogen gas. Nevertheless, they can also be adapted for the firing in other gases.

The firing can be very loud and thus the ears need to be protected. One should use earmuffs or earplugs during the firing of the ion beam. The steps below show the standard operating procedures. Italicized words enclosed by apostrophes (“.....”) must be spoken out loudly to warn people in the laboratory about the progress of the experiment.

B.1 Standard Operating Procedure prior to firing

1. Ensure the vacuum chamber of the DPF is totally closed.
2. Adjust the axial distance between substrate and the anode to the desired distance.
3. Evacuate the chamber of DPF by turning on the vacuum pump valve fully anticlockwise to pump out nitrogen gas and air mixture.
4. Close the vacuum pump valve clockwise after 2 minutes.
5. Fill the chamber with nitrogen gas to about 10 Torr by controlling the valve at the nitrogen gas cylinder.
6. Evacuate the chamber again until the capsule pressure gauge reading is 0 Torr.
7. Repeat step 5 and 6 two more times. The machine is now ready for firing.

B.2 Standard Operating Procedure for firing

1. Fill the chamber with nitrogen gas to about 10 Torr.
2. Switch on the vacuum pump and evacuate the chamber by operating the vacuum pump valve until desired pressure is reached.
3. Close the vacuum pump valve and switch off the vacuum pump. Ensure that no one is near the DPF.

4. Lift the shorting bar on the DPF to disconnect the earth ground connection.
(*“Shorting Bar Up!”*)
5. Put on earmuffs. Then turn on the main switch at the charger.
(*“Main Switch On!”*)
6. Turn on the high voltage switch at the charger.
(*“High Voltage On!”*)
7. Turn the dial of the variac fully open to charge the capacitor.
(*“Charging!”*)
8. Increase voltage to 12kV (or 22 μ A on the dial gauge).
(*Track the current verbally: “Five... Ten... Fifteen... Twenty...”*)
9. Once the 22 μ A level is reached, quickly turn the dial down.
10. Press the triggering switch to fire the shot.
(*“Three... Two... One... Fire!”*)
11. Switch off the high voltage switch on charger.
(*“High Voltage Off!”*)
12. Allow time for the current to return to zero. Then set down the shorting bar on the DPF to the ground connection.
(*“Shorting Bar Down!”*)
13. Recording the data on oscilloscope using computer.
14. Evacuate the chamber by turning on the vacuum pump.
15. Allow 5 minutes for the device to cool before firing the next shot.

B.3 Standard Operating Procedure for waveform capture

1. Press the Single Sequence button on the Tektronix recorder before firing the shot.
2. Record the waveform with the software in the computer after firing the shot.
3. Save the .csv (Comma-Separated Values) file by clicking (Waveform Data Capture > Get Data > Save as .csv). This file will save the numerical data of the waveform.
4. Save the .jpg (Joint Photographic Group) file by clicking (Screen Capture > Get Screen > Save as .jpg). This file will save the image of the waveform.